Appendix A
Literature Review

Appendix A4:FLECHT-SEASET 161 Rod Unblocked Bundle Tests

Dates When Tests Were Performed 1981-1982

References:

R6 Loftus, M. J., et al," PWR FLECHT-SEASET Unblocked Bundle Forced and Gravity Reflood Task Data Report," NUREG/CR-1532, September 1981.

R7 Lee, N. ,Wong, S., Yeh, H.C., and L.E. Hochreiter, "PWR FLECHT-SEASET Unblocked Bundle Forced and Gravity Task, Data Evaluation and Analysis Report", NUREG/CR-2256, February 1982.

R8 Wong, S. and L.E. Hochreiter, "PWR FLECHT-SEASET Analysis of Unblocked Bundle Steam-Cooling and Boil-off Tests", NUREG/CR-1533, May 1981.

Availability of Data:

Plots and tables of selected data are given in R6 for each of the tests. These tests are similar to the Low Flooding Rate Cosine Tests excepting that the rod array used in the FLECHT-SEASET tests used the newer 17x17 array while the Low Flooding Rate Cosine and Skewed Power Tests used the older 15x15 rod array. There are selected tests which were analyzed in detail in Reference 2 particularly test 31504, which is a 40 psia, 1 in/sec constant reflood test. There was additional instrumentation on the test bundle which permitted more accurate mass and energy balances for the two-phase dispersed flow region of the bundle. There were also several high-speed movies of the different tests taken as the 3, 6, and 9 windows. The drop diameter and droplet velocities were obtained and are given in R7. A heat transfer correlation was developed as a function of the distance from the quench front for both the 15x15 and 17x17 rod bundle geometry.

The raw data in engineering units is available from the Nuclear Regulatory Commission Data Bank for selected tests. All the data exists at Westinghouse on Microfiche, including the analyzed data. The analyzed data and the row data in engineering units also exists at Westinghouse in storage on older computer tapes. It is not clear at this time if the data can be assessed.

Test Facility Description, Types of Tests

The FLECHT-SEASET Unblocked Bundle tests were the first publicly available reflood experiments on the newer 17x17 fuel array which was adopted by the utilities in the 1980's. This fuel array used fuel rod of approximately 0.374-inches on a square pitch of 0.496-inches. The experiments used a 1.66 chopped cosine power shape which was the same as the FLECHT Low Flooding Rate Cosine Tests. The tests were used to help confirm the conservatism in the Appendix K rule as well as to be used for reflood safety analysis computer code assessment. Two of the experiments were also used as US Standard Problem 9 in which different parties predicted two FLECHT-SEASET unblocked bundle reflood transients. The unblocked bundle tests were also used as a basis for determining the effects of flow blockage within the rod bundle which simulated the ballooning and bursting of the Zircaloy cladding.

The majority of the tests were separate effects constant and or variable reflood tests. There were also limited gravity reflood scoping experiments as well. In addition, there were boil-off and steam cooling tests performed as well as given in R8.

The 161 rod bundle unblocked bundle did have problems with the electrical heater rod. The new smaller diameter rods, with smaller inside wall thermocouples, proved to be less reliable then the previous larger (0.422-inch diameter) rods. Several of the heater rod thermocouples failed in the initial transient tests such that the bundle instrumentation became degraded. Consequently, the 161 rod bundle was rebuilt by replacing heater rods approximately one-half way into the testing program. Those individuals using the test data must verify the proper channel and rod location since new rods were used in several different locations. The full channel list for all tests is given in R6.

The 161 bundle also used the thin wall circular housing so as to minimize the housing radiation heat sink effects as well as the housing heat release effects. Figure A-4.1 shows the cross-section of the rod bundle and Figure A-4.2 shows the facility flow diagram. The majority of these tests were conducted with a uniform radial power profile for ease of analysis, as well as obtaining a statistical distribution for the hot spot temperatures and heat transfer coefficient.

The 161 bundle was much more heavily instrumented as compared to the previous FLECHT test bundles. Most of the heater rods were instrumented and would have eight thermocouples per rod. Rods were located in symmetric positions such that complete coverage over the bundle length was achieved. The differential pressure cells were located one foot apart as in the skewed bundle tests and the data was used to determine the mass balance as well as for the average void fraction over the given cell span. There was no specific thermocouple placement relative to the grids, and the spacer grids were not instrumented, however, the axial placement was sufficiently fine that the data does indicate the heat transfer improvements caused by the spacer grids. The FLECHT egg-crate spacers grids were used and are the same as those used in previous FLECHT tests. One of the objectives of the 161 tests was to provide improved data for the development and validation of safety analysis computer codes. To this end, there were additional aspirating steam probes added to the guide tube thimbles. Some of the steam probes aspirated the flow out the bottom of the bundle while other probes aspirated out the top of the bundle. It was discovered that the bottom probes would not indicate the true steam temperature since they were more easily wetted during the transient. The probes which are regarded as unreliable are given in R6.

The range of conditions which were examined were similar to the Low Flooding Rate FLECHT tests and included:

Constant flooding rates	0.45 - 6.1 inches/sec
Upper Plenum Pressure	20 - 60 psia
Initial clad temperature at peak location	494. - 2045 ^{0}F
Initial peak power at peak location	0.40 - 1.0 kw/ft
Radial power distribution similar to FLECHT tests	uniform - FLECHT
Inlet liquid temperature	124 - 257 ^{0}F
Variable flooding rate tests	6.36 inches/sec for 5 sec; 0.82 inches/sec onward
	6.53 inches/sec for 5 sec; 0.98 inches/sec for 25 sec; 0.62 inches/sec onward
Gravity injection tests	5.8 inches/sec for 15 sec; 0.785 inches/sec onward

There were other tests performed such as hot and cold channel tests to examine the effects of liquid entrainment, repeat tests to verify that the bundle was performing in a repeatable manner overlap tests with the previously performed 15x15 cosine experiments and steam cooling tests. The steam cooling tests are given in Reference 3 and investigated the steam cooling in the bundle over a Reynolds number range of approximately 1500 to 25000. The test matrix for this test series is given as Table A-4.1, along with the measured peak cladding temperatures,

There were a significant number of power cycles performed on the test bundle which led to heater rod distortion at the end of the test program. An analysis was performed to determine

when the effects of distortion became evident in the data. This analysis is given in Reference 1 and should be consulted when modeling the tests from this program such that only valid data is used
High-speed movies were taken for a number of tests at the three, six, and nine-foot windows with camera speeds up to 2000 frames/sec. The movie data was reduced and analyzed to obtain droplet size and velocity data which was then compared to values from the literature as well as calculations. It was found that a log-normal distribution fit the droplet diameter data reasonably well while there was no real correlation of the droplet velocity with the droplet diameter or any other parameter.

An empirical reflood heat transfer correlation was developed from the 161-rod bundle experiments. The heat transfer correlation was a function of the distance above the quench front as well as the bundle initial conditions of power, pressure, flooding rate, inlet subcooling, and initial power. This correlation was used to predict the heat transfer above the quench. In addition, a quench front correlation was also developed such that given a set of system conditions, the dispersed flow film boiling heat transfer above the quench front in the PCT region could be predicted. The correlation was also used the older 15x15 FLECHT Low Flooding Rate Cosine and Skewed Power test data for developing the correlation.

The unique area that the 161-rod bundle tests addressed was the analysis of the test data above the quench front in the film-boiling region. The analysis methods which were first developed as part of the FLECHT Low Flooding Rate Test Series were expanded upon in the FLECHT-SEASET program. There was increased instrumentation for axial vapor temperature measurements along the test bundle which could then be used with the exit flow measurements to calculate the local actual quality in the test bundle, from an energy balance, such that the local liquid and vapor velocities could be determined. From the calculations of the vapor flows, velocities, and temperatures, the local vapor Reynolds number could be calculated such that a convective heat transfer could be predicted from different single-phase correlations. The effects of the vapor superheat on the calculated Reynolds number were significant since superheated steam flows at 50 ft/sec could result in a Reynolds number in the laminar regime. The results from the energy balance were also used with the high-speed movie from the analysis of the droplet data to calculate the void fraction in the flow. The measured void fraction from the differential pressure cells is not as accurate in the highly dispersed flow regime when the flow has very little liquid content.

The wall heat flux was also decomposed using a six-node radiation heat transfer network such that the radiation heat transfer from the inner hot rods, outer cold rods, guide tube thimbles, housing, droplets, and vapor could be calculated. Once the radiation component of the hot rods was calculated, the convective-dispersed flow film boiling portion of the rod heat transfer could be determined by subtracting the calculated radiation heat transfer from the measured total heat transfer which was calculated from an inverse conduction calculation using the heater rod thermocouple and local power. The convective-dispersed flow film boiling heat transfer was also compared to the single phase heat transfer one would predict using the same vapor Reynolds number, wall temperature and vapor temperature conditions. As with the FLECHT tests, the convective dispersed flow heat transfer data gave much higher values of the Nusselt number when compared to the Nusselt number calculated form the same conditions for a single-phase vapor. The interpretation of this difference is that the droplets are acting to enhance the heat transfer in the flow by acting as additional turbulence promoters, as well as temperature sinks which change the local bulk temperature profile. The comparisons indicate that the droplet effects are the greatest at the lowest vapor Reynolds numbers where the natural turbulence in the flow is the smallest. Therefore, the drops could be promoting increased turbulence in the flow which provides for increased heat transfer. It was also observed that as the liquid content of the flow increased, the difference between the convective dispersed flow film boiling heat transfer and the predicted single phase heat transfer also increased.

The 161-bundle tests also clearly showed that two different two-phase regions exist above the quench front. A lower void fraction, liquid rich froth or transition region, exits at and just above the quench front for the forced flooding tests. The length of this region depends on the flooding rate value relative to the quench velocity. The larger the flooding rates relative to the quench velocity (which is conduction controlled), the longer the froth region. The froth region was observed and appears as liquid ligaments which are sheared into increasingly smaller droplets from the steam flow generated at the quench front and the higher wall temperature in the quench front region. The vapor shearing effects generate the entrained droplets which then provide cooling at the upper elevations of the test bundle in the non-equilibrium dispersed flow film-boiling regime.

Conclusions

The FLECHT-SEASET 161 unblocked bundle experiments represent the best reflood experiments which were performed. It was recognized in the test planning that data was needed for advanced reflood computer code development such that an effort was made to obtain additional local condition heat transfer and fluid flow condition data in addition to the total heater rod heat transfer data for an empirical correlation. The mass balances on the tests were generally very good such that the data can be used with confidence, however, one must be careful of the vapor measurements as indicated earlier since some of the steam probes did not function as desired. Also because of heater rod problems, the bundle was rebuilt so that channel designation relative to specific heater rods may have changed. These changes are documented in the reports such that the user can correctly obtain the data for a given test.

The analysis for the test data is the most complete of all the FLECHT test series. One test 31504 was analyzed in detail with several plots given in the reports which can be used for computer code validation. There is also an amount of very good droplet size and velocity information which can also be used for computer code validation. If all the data is used for the validation, not just the heater rod temperatures, one can more realistically assess a computer code reflood heat transfer model since the test measurements include the rod surface temperature, vapor temperature, drop size, drop velocity as well as the local quality, void fraction, and heat flux split between radiation heat transfer and convective dispersed flow film boiling heat transfer.

Two of the FLECHT-SEASET tests were used as US Standard Problem 9 for the purposes of code validation. It is strongly recommended that these data be used for validating the NRC merged code.

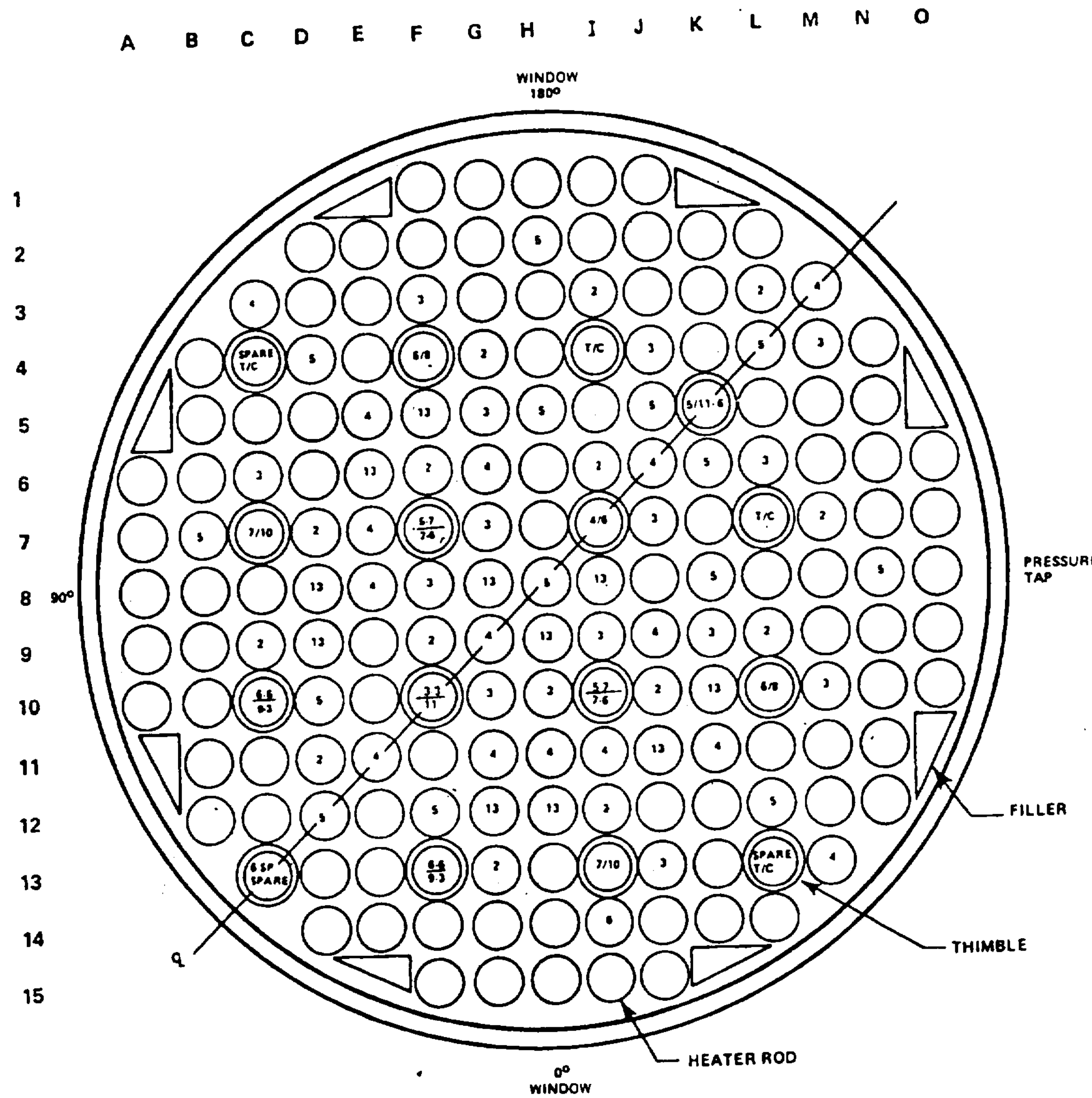

BUNDLE STATISTICS

HOUSING INSIDE DIAMETER	194.0 mm (7.625 in.)
HOUSING WALL THICKNESS	5.08 mm (0.200 in.)
ROD DIAMETER	9.50 mm (0.374 in.)
THIMBLE DIAMETER	12.0 mm (0.474 in.)
ROD PITCH	12.6 mm (0.496 in.)
CROSS-SECTIONAL FLOW AREA	15571 mm^2 (24.136 $in.^2$)
FILLER DIMENSIONS	18.8 x 8.43 mm (0.741 x 0.332 in.)
161 HEATER RODS	— —
16 THIMBLES	— —
8 FILLERS	— —

Figure A4-1. FLECHT-SEASET Rod Bundle Cross Section

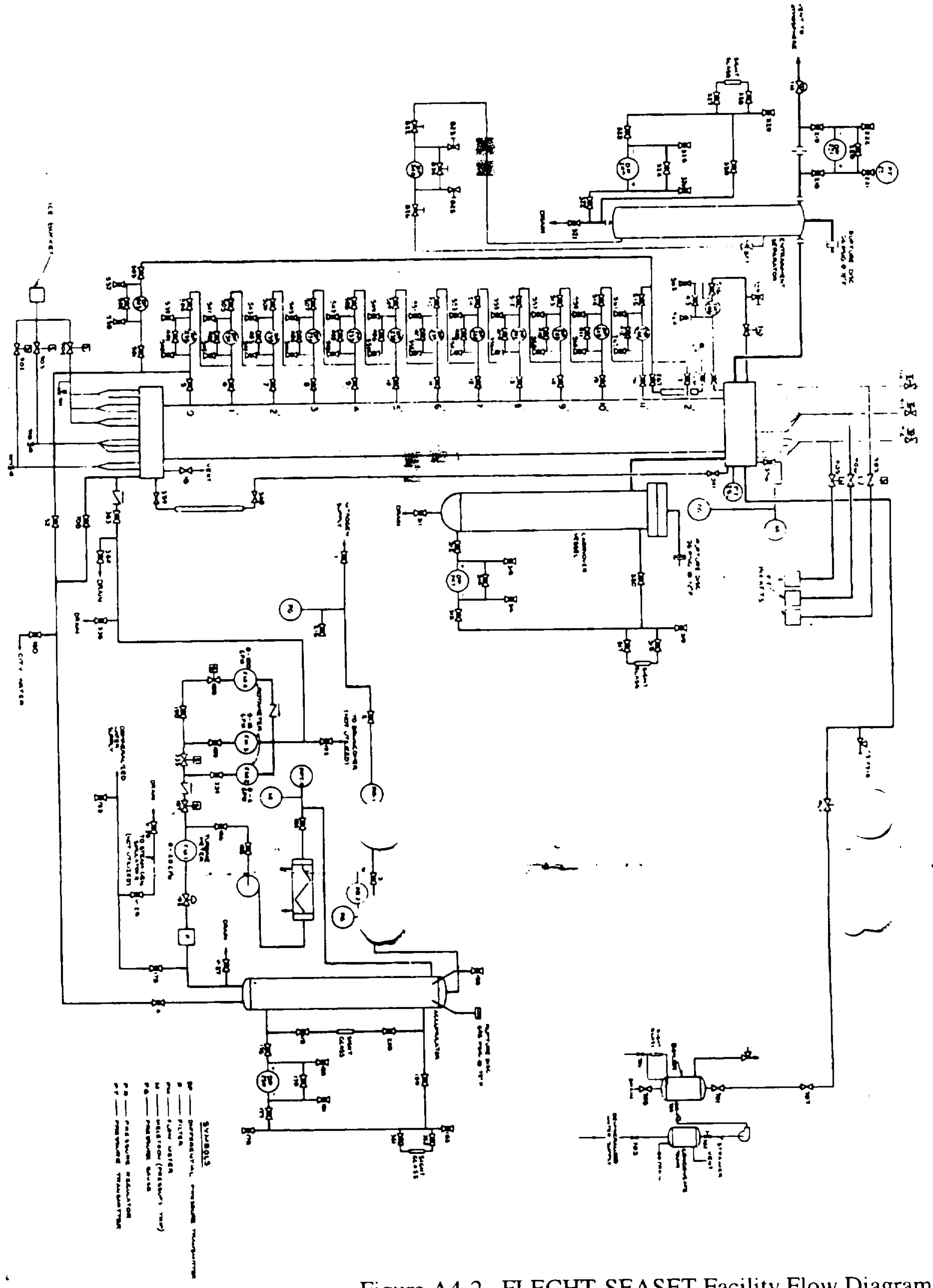

Figure A4-2. FLECHT-SEASET Facility Flow Diagram

Table A4-1

FLECHT SEASET UNBLOCKED BUNDLE REFLOOD TEST DATA SUMMARY

Test No.	Run No.	Actual Test Conditions: Upper Plenum Pressure [MPa (psia)]	Rod Initial T_{clad} at 1.83m (72 in.) [°C(°F)]	Rod Peak Power [kw/m (kw/ft)]	Flooding Rate [mm/sec (in./sec)]	Coolant Temperature [°C(°F)]	Radial Power Distribution	Results: Hottest Rod T/C and Elevation [m(in.)]	Initial Temperature [°C(°F)]	Maximum Temperature [°C(°F)]	Temperature Rise [°C(°F)]	Turn-around Time (sec)	Quench Time (sec)	Bundle Quench Time (sec)	Disconnected Rod Location
CONSTANT FLOODING RATE															
1	31701	0.28 (40)	872 (1601)	2.3 (0.70)	155 (6.1)	53 (127)	Uniform	9I-1.78(70)	893 (1640)	923 (1694)	30 (54)	5	55	114	4G, 5G
2	31302	0.28 (40)	869 (1597)	2.3 (0.69)	76.5 (3.01)	52 (126)	Uniform	8E-1.70(67)	889 (1631)	932 (1710)	43 (79)	8	124	262	4G, 5G, 6J, 11G
3	31203	0.28 (40)	872 (1601)	2.3 (0.70)	38.4 (1.51)	52 (126)	Uniform	9L-1.93(76)	870 (1597)	1037 (1898)	167 (301)	63	246	435	4G, 5G
	33903	0.28 (40)	881 (1619)	2.3 (0.70)	40.1 (1.58)	52 (125)	Uniform	7K-1.98(78)	868 (1594)	1048 (1919)	180 (325)	68	220	335	4G, 5G, 11I, 11J, 11K, 12IJK, 13JK
	34103	0.28 (40)	885 (1626)	2.4 (0.74)	38.1 (1.50)	51 (123)	Uniform	7K-1.98(78)	872 (1601)	1089 (1992)	217 (391)	71	241	381	4G, 5G, 11IJK, 12IJK, 13JK
4	31504	0.28 (40)	863 (1585)	2.3 (0.70)	24 (0.97)	51 (123)	Uniform	8K-1.98(78)	820 (1507)	1150 (2101)	330 (593)	130	325	594	4G, 5G
	35304[a]	0.28 (40)	915 (1679)	2.4 (0.74)	25.9 (1.02)	51 (124)	Uniform	9F-1.93(76)	797 (1467)	1230 (2246)	433 (779)	125	249	499	4G, 5G, 11IJK, 12IJK, 13JK,
5	31805	0.28 (40)	871 (1600)	2.3 (0.70)	21 (0.81)	51 (124)	Uniform	11K-1.98(78)	851 (1563)	1232 (2250)	381 (687)	134	419	691	4G, 5G
6	34006	0.27 (39)	882 (1620)	1.3 (0.40)	15 (0.59)	51 (124)	Uniform	7K-1.98(78)	864 (1587)	1163 (2126)	299 (539)	175	327	566	4G, 5G, 11IJK, 12IJK, 13JK
7	34907[a,b]	0.28 (40)	897 (1648)	1.4 (0.42)	11 (0.45) 76 (3.0)	51 (123)	Uniform	9F-1.98(78)	836 (1538)	1230 (2246)	394 (708)	203	326	385	4G, 5G, 11IJK, 12IJK, 13JK
	35807[a]	0.28 (40)	886 (1628)	0.89(0.27)	10 (0.41)	50 (121)	Uniform	9F-1.88(74)	849 (1560)	1182 (2160)	333 (600)	217	368	734	4G, 5G, 11IJK, 12IJK, 13JK
PRESSURE AT CONSTANT FLOODING RATE															
8	31108	0.13 (19)	871 (1600)	2.3 (0.70)	79.0 (3.11)	33 (91)	Uniform	9I-1.78(70)	884 (1624)	938 (1720)	54 (96)	10	156	364	4G, 5G
9	34209	0.14 (20)	889 (1636)	2.4 (0.72)	27.2 (1.07)	32 (90)	Uniform	7K-1.98(78)	854 (1570)	1161 (2121)	307 (551)	127	427	701	4G, 5G, 11IJK, 12IJK, 13JK

a. Significant rod bundle distortion occurred between 1.52 and 2.27 m (60 and 90 in.)

b. Scrammed at 279 seconds becuase of high rod temperature

Table A4-1 (cont.)

FLECHT SEASET UNBLOCKED BUNDLE REFLOOD TEST DATA SUMMARY

		As-Run Test Conditions						Results							
Test No.	Run No.	Upper Plenum Pressure [MPa (psia)]	Rod Initial T_{clad} at 1.83m (72 in.) [°C(°F)]	Rod Peak Power [kw/m (kw/ft)]	Flooding Rate [mm/sec (in./sec)]	Coolant Temperature [°C(°F)]	Radial Power Distribution	Hottest Rod T/C and Elevation [m(in.)]	Initial Temperature [°C(°F)]	Maximum Temperature [°C(°F)]	Temperature Rise [°C(°F)]	Turn-around Time (sec)	Quench Time (sec)	Bundle Quench Time (sec)	Disconnected Rod Location
10	34610	0.14 (20)	892 (1637)	1.4 (0.42)	21 (0.82)	32 (90)	Uniform	6D-1.88 (74)	845 (1554)	1052 (1926)	207 (372)	137	310	507	4G, 5G, 11IJK, 12IJK, 13JK
11	34711[a]	0.13 (19)	888 (1630)	1.4 (0.42)	17 (0.67)	33 (91)	Uniform	9E-1.93 (76)	855 (1571)	1119 (2045)	264 (474)	135	361	600	4G, 5G, 11IJK, 12IJK, 13JK
12	35212[a,c]	0.14 (20)	879 (1613)	1.4 (0.42)	11 (0.43) 178 sec 79 (3.1)	32 (89)	Uniform	9E-1.83 (72)	830 (1526)	1231 (2247)	401 (721)	173	236	294	4G, 5G, 11IJK, 12IJK, 13JK
	35912[a]	0.14 (20)	889 (1632)	0.89 (0.27)	11 (0.42)	34 (93)	Uniform	9G-2.29 (90)	802 (1476)	1128 (2062)	326 (586)	289	558	789	4G, 5G, 11IJK, 12IJK, 13JK
13	32013	0.41 (60)	887 (1629)	2.3 (0.70)	26.4 (1.04)	66 (150)	Uniform	6L-1.93 (76)	846 (1555)	1171 (2139)	325 (584)	115	269	461	4G, 5G
SUBCOOLING															
14	32114	0.28 (40)	893 (1639)	2.3 (0.70)	25–31 (1.0–1.22)	125 (257)	Uniform	6L-1.88 (74)	840 (1544)	1189 (2172)	349 (628)	114	405	633	4G, 5G
	35114	0.28 (40)	892 (1638)	2.4 (0.74)	25 (0.98)	123 (253)	Uniform	9O-1.83 (72)	886 (1628)	1192 (2178)	306 (550)	123	394	651	4G, 5G, 11IJK, 12IJK, 13JK
15	31615	0.14 (20)	876 (1609)	2.3 (0.70)	0 (0)	-	Uniform	11H-1.70 (67)	881 (1617)	1220 (2228)	339 (611)	57	-	-	4G, 5G
	34815[a]	0.14 (20)	895 (1643)	2.4 (0.74)	25 (0.98)	94 (221)	Uniform	7J-1.83 (72)	870 (1597)	1178 (2152)	308 (555)	132	562	919	4G, 5G, 11IJK, 12IJK, 13JK
16	34316	0.28 (40)	889 (1631)	2.4 (0.74)	25 (0.97)	51–119 (124–246)	Uniform	6D-1.88 (74)	849 (1560)	1207 (2206)	358 (646)	107	349	592	4G, 5G, 11IJK, 12IJK, 13JK
INITIAL CLAD TEMPERATURE															
17	30817	0.27 (39)	531 (987)	2.3 (0.70)	38.6 (1.52)	53 (128)	Uniform	10J-1.98 (78)	519 (965)	832 (1530)	313 (565)	84	219	395	4G, 5G
18	30518	0.28 (40)	256 (494)	2.3 (0.70)	38.9 (1.53)	52 (126)	Uniform	8H-1.98 (78)	246 (475)	653 (1208)	407 (732)	96	187	344	4G, 5G
19	30619	0.134 (19.5)	256 (494)	2.3 (0.70)	38.9 (1.53)	36 (96)	Uniform	2H-1.98 (78)	243 (469)	727 (1340)	484 (871)	142	292	572	4G, 5G

c. Scrammed at 178 seconds because of high rod temperature

Table A4-1 (cont.)

FLECHT SEASET UNBLOCKED BUNDLE REFLOOD TEST DATA SUMMARY

Test No.	Run No.	As-Run Test Conditions: Upper Plenum Pressure [MPa (psia)]	Rod Initial T_{clad} at 1.83m (72 in.) [°C(°F)]	Rod Peak Power [kw/m (kw/ft)]	Flooding Rate [mm/sec (in./sec)]	Coolant Temperature [°C(°F)]	Radial Power Distribution	Results: Hottest Rod T/C and Elevation [m(in.)]	Initial Temperature [°C(°F)]	Maximum Temperature [°C(°F)]	Temperature Rise [°C(°F)]	Turnaround Time (sec)	Quench Time (sec)	Bundle Quench Time (sec)	Disconnected Rod Location
20	34420	0.27 (39)	1119 (2045)	2.4 (0.74)	38.9 (1.53)	51 (124)	Uniform	7J-1.83 (72)	1102 (2016)	1207 (2205)	105 (189)	34	222	376	4G, 5G, 11IJK, 12IJK, 13JK
ROD PEAK POWER															
21	30921(d)	0.27 (39)	879 (1614)	1.3 (0.40)	38.9 (1.53)	52 (126)	Uniform	9I-1.78 (70)	887 (1629)	949 (1740)	62 (111)	17	152	158	4G, 5G
	31021	0.28 (40)	880 (1615)	1.3 (0.40)	38.6 (1.52)	52 (126)	Uniform	9H-1.78 (70)	891 (1635)	941 (1726)	50 (91)	14	158	271	4G, 5G
22	31922	0.14 (20)	883 (1621)	1.3 (0.40)	27.2 (1.07)	35 (95)	Uniform	6F-1.83 (72)	883 (1621)	975 (1787)	92 (166)	70	229	435	4G, 5G
23	30223	0.27 (39)	258 (497)	1.3 (0.40)	37.8 (1.49)	54 (129)	Uniform	6F-1.93 (76)	261 (501)	455 (852)	194 (351)	44	113	181	None
	30323	0.27 (39)	259 (499)	1.3 (0.40)	38.6 (1.52)	52 (126)	Uniform	6F-1.98 (78)	256 (494)	459 (859)	203 (365)	57	115	171	None
24	34524	0.28 (40)	878 (1612)	3.0 (1.0)	39.9 (1.57)	52 (125)	Uniform	7J-1.83 (72)	873 (1604)	1204 (2199)	331 (595)	89	266	520	4G, 5G, 11IJK, 12IJK, 13JK
RADIAL POWER DISTRIBUTION															
25	Not run														
26	35426(a)	0.28 (40)	886 (1627)	2.54 (0.773) 2.42 (0.737) 2.08 (0.633)	25.7 (1.01)	52 (126)	FLECHT	9F-1.93 (76)	814 (1497)	1229 (2243)	415 (746)	113	240	485	4G, 5G, 11IJK, 12IJK, 13JK
	36026(a)	0.28 (40)	900 (1651)	2.42 (0.737) 2.31 (0.703) 2.19 (0.667)	25 (1.0)	51 (124)	FLECHT	11F-1.88 (74)	862 (1583)	1174 (2145)	312 (562)	113	286	475	4G, 5G, 11IJK, 12IJK, 13JK
27	Not run														
28	Not run														
REPEAT TESTS															
29	35304														

d. Scrammed because of high-temperature thermocouple failure at 125 seconds

Table A4-1 (cont.)

FLECHT SEASET UNBLOCKED BUNDLE REFLOOD TEST DATA SUMMARY

As-Run Test Conditions						Results								
Upper Plenum Pressure [MPa (psia)]	Rod Initial T_{clad} at 1.83m (72 in.) [°C(°F)]	Rod Peak Power [kw/m (kw/ft)]	Flooding Rate [mm/sec (in./sec)]	Coolant Temperature [°C(°F)]	Radial Power Distribution	Hottest Rod T/C and Elevation [m(in.)]	Initial Temperature [°C(°F)]	Maximum Temperature [°C(°F)]	Temperature Rise [°C(°F)]	Turn-around Time (sec)	Quench Time (sec)	Bundle Quench Time (sec)	Disconnected Rod Location
NG RATE														
0.28 (40)	889 (1631)	2.3 (0.70)	162 (6.36) 5 sec 21 (0.82) onward	52 (125)	Uniform	6L-1.93 (76)	843 (1550)	1148 (2099)	305 (549)	131	337	639	4G, 5G
0.14 (20)	888 (1630)	2.3 (0.70)	166 (6.53) 5 sec 25 (0.98) 200 sec 16 (0.62) onward	31 (88)	Uniform	6K-1.98 (78)	823 (1514)	1146 (2096)	323 (582)	142	546	964	4G, 5G
			Injection Rate kg/sec (lbm/sec)										
0.27 (39)	878 (1611)	2.3 (0.70)	5.80 (12.8) 15 sec 0.785 (1.73) onward	52 (125)	Uniform	10H-1.78 (70)	891 (1636)	910 (1670)	19 (34)	4	121	174	4G, 5G
0.28 (40)	871 (1600)[e] 591 (1096)[f]	2.3 (0.70)[e] 1.3 (0.40)[f]	5.9 (13) 15 sec 0.807 (1.78) onward	52 (125)	Hot/ cold channels	10H-1.78 (70)	906 (1664)	925 (1697)	19 (33)	6	76	181	4G, 5G

Table A4-1 (cont.)

FLECHT SEASET UNBLOCKED BUNDLE REFLOOD TEST DATA SUMMARY

Test No.	Run No.	As-Run Test Conditions: Upper Plenum Pressure [MPa (psia)]	Rod Initial T_{clad} at 1.83m (72 in.) [°C(°F)]	Rod Peak Power [kw/m (kw/ft)]	Injection Rate [kg/sec (lbm/sec)]	Coolant Temperature [°C(°F)]	Radial Power Distribution	Results: Hottest Rod T/C and Elevation [m(in.)]	Initial Temperature [°C(°F)]	Maximum Temperature [°C(°F)]	Temperature Rise [°C(°F)]	Turn-around Time (sec)	Quench Time (sec)	Bundle Quench Time (sec)	Disconnected Rod Location
39	Not run														
HOT AND COLD CHANNELS															
40	Not run														
41	Not run														
42	Not run														
43	Not run														
AXIAL TEMPERATURE DISTRIBUTION															
44	33544	0.27 (39)	196 (385)(g) (0 to 3) 874 (1605)	2.3 (0.69)	5.85 (12.9) 15 sec 0.780 (1.72) onward	52 (125)	Uniform	11K-1.93 (76)	877 (1610)	908 (1668)	31 (58)	8	121	213	4G, 5G
	33644	0.27 (39)	182 (359)(g) (0 to 3) 877 (1610)	2.3 (0.70)	5.81 (12.8) 15 sec 0.789 (1.76) onward	52 (125)	Uniform	7D-1.93 (76)	884 (1623)	930 (1705)	46 (82)	9	104	250	4G, 5G
STEAM COOLING															
45	32652 through 33056														
46	36160 through 37170														
OVERLAP COSINE TESTS															
47	Not run														
48	Not run														

g. Axial temperature distribution - simulated gravity reflood

Table A4-1 (cont.)

FLECHT SEASET UNBLOCKED BUNDLE REFLOOD TEST DATA SUMMARY

Test No.	Run No.	As-Run Test Conditions						Results							
		Upper Plenum Pressure [MPa (psia)]	Rod Initial T_{clad} at 1.83m (72 in.) [°C(°F)]	Rod Peak Power [kw/m (kw/ft)]	Flooding Rate [mm/sec (in./sec)]	Coolant Temperature [°C(°F)]	Radial Power Distribution	Hottest Rod T/C and Elevation [m(in.)]	Initial Temperature [°C(°F)]	Maximum Temperature [°C(°F)]	Temperature Rise [°C(°F)]	Turn-around Time (sec)	Quench Time (sec)	Bundle Quench Time (sec)	Disconnected Rod Location
COMPARISON WITH WESTINGHOUSE PROPRIETARY REFLOOD DATA															
49	33749	0.27 (39)	745 (1374)	1.9 (0.57)	26.9 (1.06)	61 (142)	Uniform	11K-1.88 (74)	730 (1346)	1017 (1861)	287 (515)	103	250	430	4G, 5G
	33849(h)	0.28 (40)	745 (1374)	1.9 (0.57)	25.9 (1.02)	58 (138)	Uniform	8K-1.98 (78)	705 (1302)	1025 (1878)	320 (576)	105	254	437	4G, 5G
50	35050(a)	0.14 (20)	758 (1397)	1.6 (0.48)	25.9 (1.02)	43 (109)	Uniform	9D-1.83 (72)	758 (1397)	958 (1758)	200 (361)	98	243	433	4G, 5G, 111JK, 121JK, 13JK
POWER DECAY															
51	Not run														

h. Rod 12J failed during test.

Appendix A-5 Literature Review

Test Facility Name: FEBA - Flooding Experiments with Blocked Arrays

Dates When Tests Were Performed: 1977

References:

R9. P. Ihle, K. Rust - FEBA - Flooding Experiments with Blocked Arrays Evaluation Report - KfK 3657 - March 1984

R10. P. Ihle, K. Rust - FEBA - Flooding Experiments with Blocked Arrays Data Report 1, Test Series I through IV - KfK 3658 - March 1984

R11. P. Ihle, K. Rust - FEBA - Flooding Experiments with Blocked Arrays Data Report 2, Test Series V through VIII - KfK 3659 - March 1984

Availability of Data:

Reduced instrument responses are presented in References R9 to R11 in a variable versus time plot format. Tables and figures describing instrument locations are provided. Results are presented in 'almost-SI' units. Listing of computer channel numbers and of data identification are available on tapes or in the USNRC/RSR Data Bank.

Test Facility Description, Types of Tests:

The test facility is designed for a separate effect test program involving a constant flooding rate and a constant back pressure to allow investigation of the influence of coolant channel blockages independently of system effect.

Figure A-5.1 shows a scheme of the test facility. The coolant water is stored in tank and during operation the flow is forced into the bundle with a back pressure control system. A 1x5 as well as 5x5 rod array are placed in a full length stainless steel housing which have a wall thickness of ¼ inches. The heater rods were 0.423-inches (10.75 mm) in diameter and were arranged on a square pitch of 0.563-inches (14.3 mm) and had heated length of 12.8 ft (3900 mm) for the 5x5 rod bundle tests and 9.5-ft (2900 mm) for the 1x5 rod bundle tests. The axial power profile is shown in Figure A-5.2. Top-down quenching was prevented in the experiments by using a particular upper plenum design (Figure A-5.3)

The range of conditions include:

Constant Mass Flow Rate 0.8 - 3.7 in/sec (2.0 - 9.5 cm/s)

Pressure	29.4 - 91.1 psia (2.0 - 6.2 bar)
Initial Clad Temperature	694 - 1461 F (368 - 794 C)
Power Axial Peak Factor	1.19
Initial Average Power	120% ANS: 40s after Reactor Trip
Inlet Temperature	104 - 257 F (40 - 125 C)
Initial Housing Temperature	527 - 1400 F (275 - 760 C)
Flow Blockage ratio	(0%, 62%, 90%, 90%+62%)
Flow Blockage Geometry	Various

The FEBA 5x5 rod bundle program consisted of eight test series with different grid spacer and sleeve blockage arrays within the bundle (Figure A-5.4). Series I are base-line tests with undisturbed bundle geometry. Series II tests investigate the grid spacer effect on the axial temperature profile at bundle mid-plane. Series III and IV consider 90% and 62% blockage at bundle mid-plane respectively. Series V consider both the blockage and the grid spacer effects while Series VI has a double blockage and investigate on the possibility of a hot region between the two blockages. Finally Series VII and VIII investigate on cooling enhancement downstream the blockages.

Instrumentation and Data From Tests:

Thermocouples (Chromel-Alumel) are imbedded in each of the rods as shown in Figure A-5.5 and A-5.6. They are used to measure cladding, sleeve, grid spacers and housing temperatures at different locations (Figure A-5.7). Fluid temperatures were measured with three different thermocouples (Figure A-5.8) and probes in order to provide information about two separate phases. The signals of all three fluid thermocouples indicated roughly same temperature during most part of reflood. Radiation effect for the unshielded thermocouple was not detected however shielding led to earlier quenching of the shielded thermocouples. Pressure and pressure differences were measured with pressure transducers. In addition to inlet and outlet pressure, the pressure differences along the midplane as well as along both the lower and upper portion of the bundle were measured. The floooding rate was measured with a turbine flow meter. The amount of water carry over was measured continuously by a pressure transducer on the water collecting tank. All data were digitally recorded with a scan frequency of 10 Hz.
The water level rising in the lower plenum at the onset of reflood was detected by thermocouples. In some tests high-frequency probes were used to detect the presence of water in the flow channel.

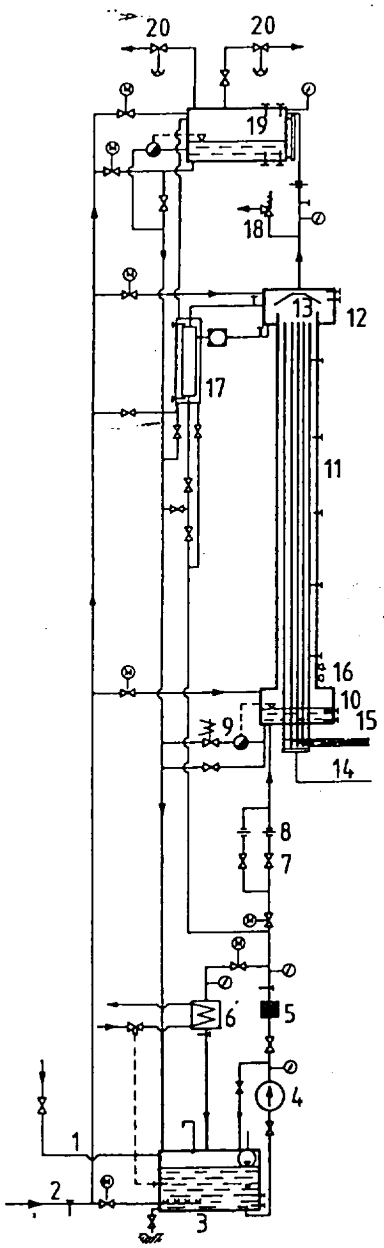

LEGEND

1 Water Supply
2 Steam Supply
3 Storage Tank
4 Water Pump
5 Filter
6 Heat Exchanger
7 Throttle Valve
8 Turbine Meter
9 Water Level Regulation Valve

10 Lower Plenum
11 Test Section
12 Upper Plenum
13 Water Separator

14 Power Supply
15 Rod Instrumentation Exits
16 Water Level Detector
17 Water Collecting Tank
18 Outlet Valve
19 Buffer
20 Pressure Regulator

A5-3

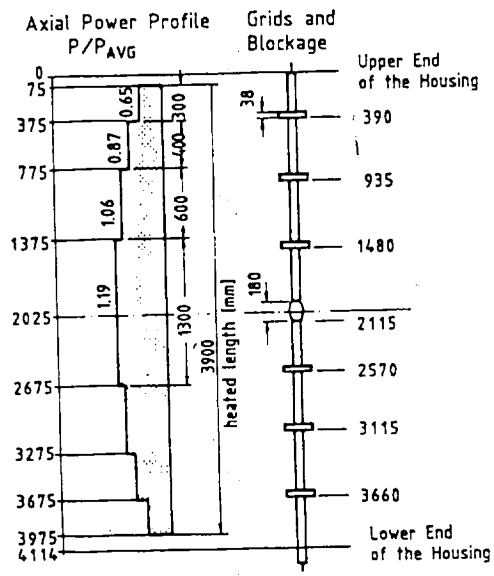

Figure A-5.2: Axial Power Profile

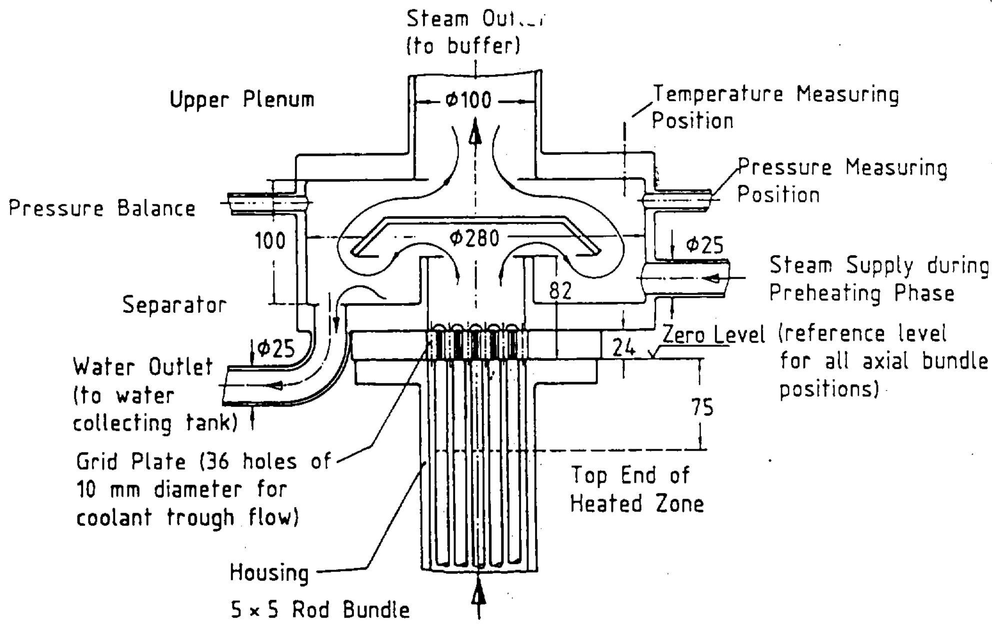

Figure A-5.3: Upper bundle end and Upper plenum

A5-5

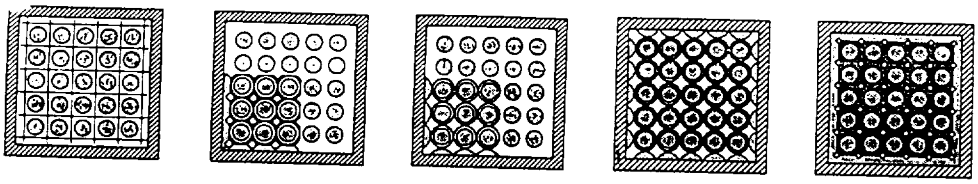

FLOODING PARAMETERS

Test Series		I	II	III	IV	V	VI	VII	VIII
Flooding Velocity (cold bundle) Constant During Each Test	cm/s	3.8, 5.8	3.8, 5.8	3.8, 5.8	3.8, 5.8 (2.2, 10.)	2.2, 3.8 5.8	2.2, 3.8 5.8	3.8, 5.8 (2.2)	3.8, 5.8 (2.2)
System Pressure Constant During Each Test	bar	2, 4, 6	2, 4, 6	2, 4, 6	2, 4, 6 (4)	4	4	2, 4, 6 (4)	2, 4, 6 (2, 4)
Feedwater Temperature Constant During Each Test	°C	40 °C, some few tests with 80 °C							
Max. Cladding Temperature (at start of reflooding)	°C	between 700 and 800 °C, some few tests between 600 and 700°C							
Max. Housing Temperature (at start of reflooding)	°C	between 600 and 700 °C, some few tests between 500 and 600°C							
Bundle Power	kW	at start of reflooding 200 kW, 120% ANS decay heat transient 40 s after shutdown, some few tests with constant bundle power							

Steam Cooling Tests — Test series VII and VIII include steady state and transient tests for which low bundle power and system pressures of 2, 4 and 6 bar were selected.

Figure A-5.4: 5x5 Rod Bundle, Test Matrix for Series I through VIII

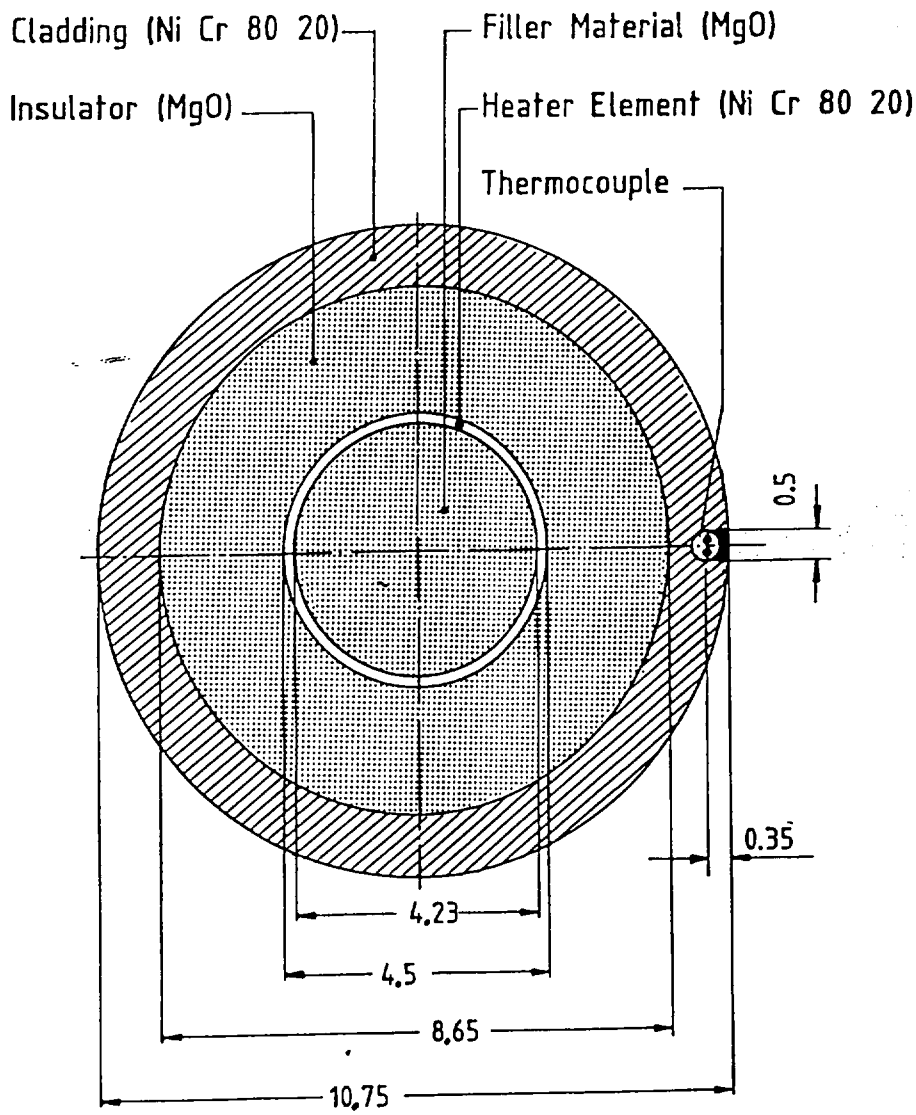

Dimensions are in millimeters

Figure A-5.5: Rod Geometry and location of Thermocouple

Figure A-5.6: Radial and Axial location of cladding, fluid and housing TC's for Test Series 1

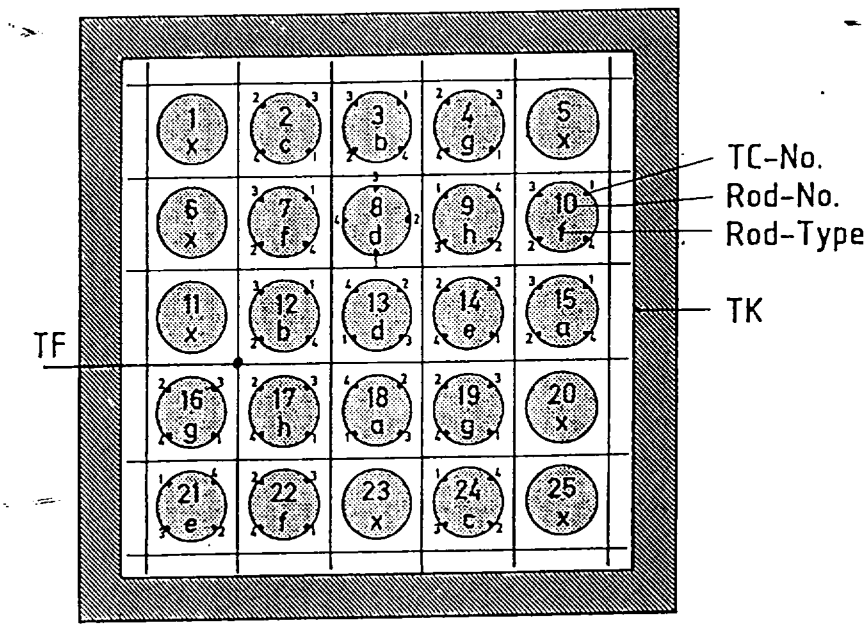

Rod Type	TC No.	Axial Level mm
a	1	2225
	2	2770
	3	3315
	4	3860
b	1	45
	2	590
	3	1135
	4	1680
c	1	3725
	2	3825
	3	3925
	4	4025
d	1	2025
	2	2025
	3	2025
	4	2025

Rod Type	TC No.	Axial Level mm
e	1	2075
	2	2125
	3	2175
	4	2225
f	1	2125
	2	2225
	3	2325
	4	2425
g	1	1625
	2	1725
	3	1825
	4	1925
h	1	1925
	2	2025
	3	2125
	4	2225

Rod Type	TC No.	Axial Level mm
x	without TC's	

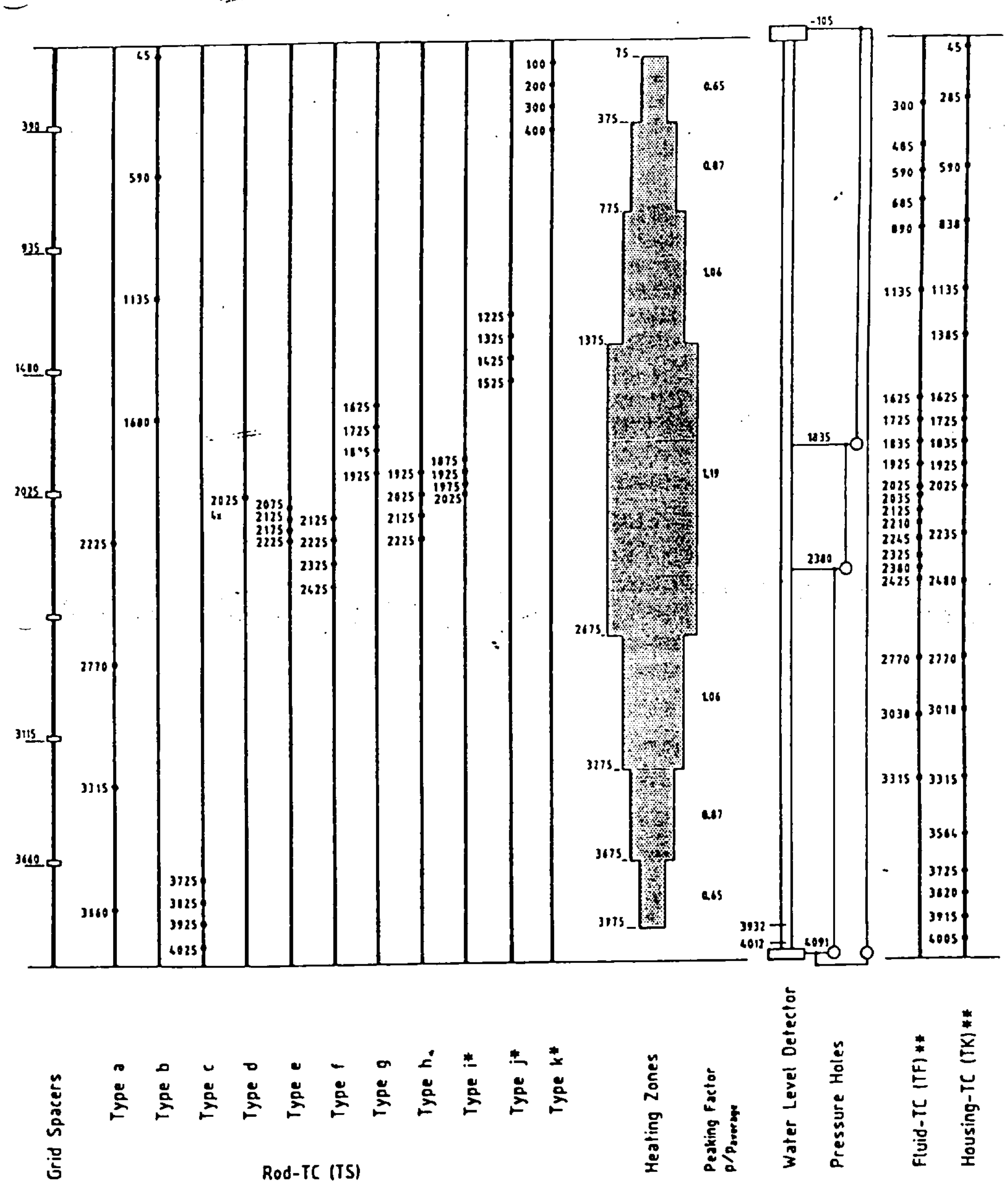

in Test Series V through VIII only

** not all positions set for the individual tests

Figure A-5.7: Axial locations of various thermocouples in 5x5 rod bundle

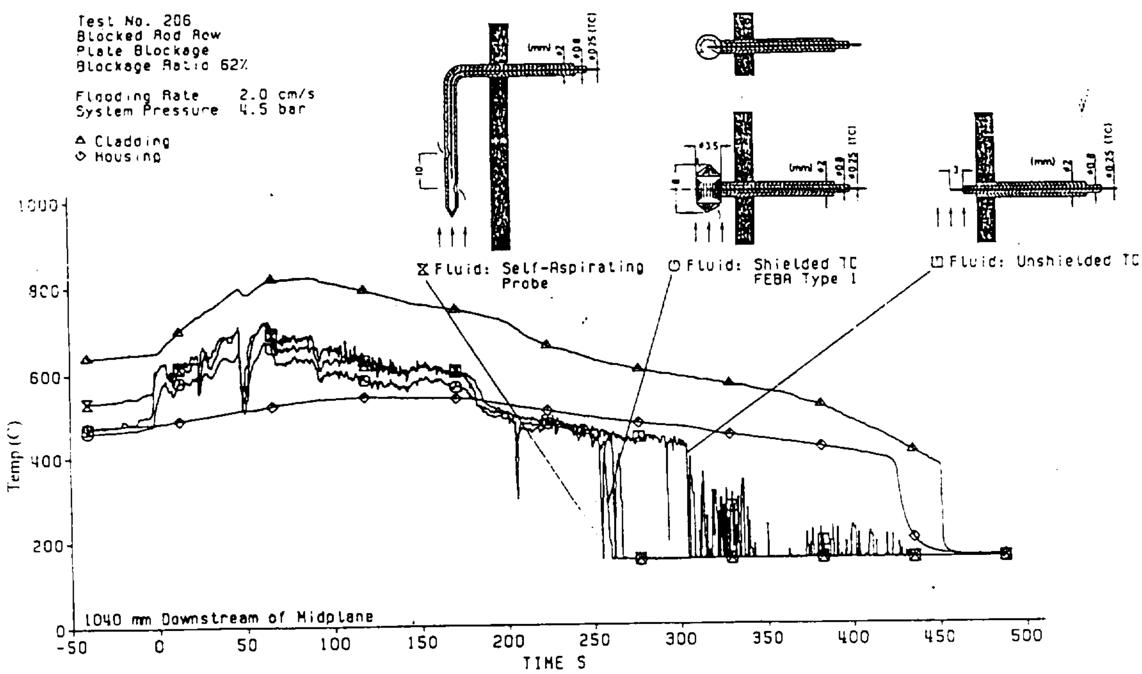

Figure A-5.8: 5 rod row: Comparison of different fluid temperature measuring devices

Table 1
Assessment of FEBA Test to RBHT PIRT:
Single Phase Liquid Convective Heat Transfer in the Core Component During Reflood Below the Quench Front

Process/Phenomena	Ranking	Basis	FEBA
1ϕ Liquid Convective Heat Transfer	L	1ϕ Convective H.T. data has been correlated for rod bundles, uncertainty will not effect PCT.	Can be back calculated.
- Effects of Geometry	L	De has been shown to be acceptable for P/D or 1.3 [5].	P/D = 1.33
- Effects of Spacers	L	Effects of spacers in ϕ convective H.T. is known, see[6]. No impact on PCT uncertainty.	Separate tests with and without grid spacers have been run. The effect can be estimated from clad and fluid temperatures below the quench front.
- Effects of Properties	*L	Property effects are accounted for in analysis for 1ϕ H.T. little uncertainty.	Insufficient data.
1ϕ Liquid Natural Connection H.T.	L	Must test Gr/Re to determine regime.	Not applicable.
Effects of Geometry	L	Limited data exists which can be used as a guide, should have little uncertainty on PCT.	Not applicable.
Effects of Spacers	L	Effect unknown for natural convection, but enhances H.T. No impact on PCT uncertainty.	Not applicable.
Effects of Properties	L	Accounted for in dimensionless parameters, little uncertainty.	Not applicable.
Decay Power	H	Source of energy for rods, boundary convection for test.	Measured.

Table 2
Assessment of FEBA Test to RBHT PIRT:
Subcooled and Saturated Boiling The Core Component Below the Quench Front

Process/Phenomena	Ranking	Basis	FEBA
Subcooled Boiling	L	A significant variation in the subcooled boiling H.T. coefficient will not effect the PCT uncertainty since rod is quenched.	Temperature measurements (fluid and clad) are available but void fraction data are insufficient.
-Effects of Geometry, P/D, De	L	Boiling effects in rod bundles have been correlated for our P/d, De range with acceptable uncertainty[8].	P/D = 1.33 for tests.
-Effects of Spacers	L	Locally enhances H.T.; Correlations/ Models are available,acceptable uncertainty.	Separate tests with and without grid spacer have been run to address the effect.
-Effects of Properties	L	Data exists for our Range of Conditions, little uncertainty.	Insufficient α data.
Saturated Boiling	L	Similar to subcooled boiling, data is available for our P/D, De range. The uncertainty of Saturated Boiling H.T. coefficient will not significantly impact the PCT since rod is quenched.	Heater rod and fluid temperatures are available, but void fraction data are insufficient.
-Effects of Geometry, P/D, De	L	Data exists in the range of P/D, De with acceptable uncertainties[8].	P/D = 1.33
-Effects of Spacers	L	Locally enhances H.T., Correlations/ Models are available[8], with acceptable uncertainty.	Separate tests with and without grid spacer have been run to address the effect.
-Effects of Properties	L	Data exists for our range of conditions, little uncertainty.	Insufficient void fraction data.
Decay Power	H	Source of energy for rods, boundary condition for the test.	Measured.

Table 3
Assessment of FEBA Tests to RBHT PIRT:
Quench Front Behavior in the Core Component

Process/Phenomena	Ranking	Basis	FEBA
Fuel /Heater Rod Quench			
Fuel/heater rod materials, ρ, C_p, k, rod diameter	H	These properties effect the stored energy in the fuel/heater rod and its quench rate, uncertainty directly impacts PCT.	Rod properties are known, as are dimensions, stored energy can be calculated.
Gap heat transfer coefficient	M	Second largest resistance in fuel rod. Can limit heat release rate from fuel pellet. Gap heat transfer coefficient has large uncertainty, but its impact on PCT is smaller since all stored energy will be released, timing may change however.	0.5mm gap is present between rod and sleeve in blocked bundle experiments. Rod and sleeve temperatures are measured.
Cladding materials ρ, C_p, k	L	Both Inconel and Zirc have approximately same conductivity most existing data is on stainless steel. Small uncertainty.	Cladding material properties are known Ni-Cr 80-20 cladding was used.
Cladding surface effects • Oxides • Roughness • Materials • T_{min} • T_{CHF}	H	Since zirc can oxidize, the oxide layer will quench sooner due to its low conductivity, verses Inconel or Zirc. Also roughness from oxide promotes easier quenching. The surface condition effects T_{min} which is the point where quenching is initiated[9],[10]. Quenching is a quasi-steady two-dimensional process, values of T_{min} and T_{CHF} can be estimated. Large uncertainty and impact on PCT.	Surface properties effects were not addressed in the analysis and insufficient information are available.
Transition Boiling Heat Transfer	H	Determines the rate of heat release at Quench Front directly impacts PCT, large uncertainty.	Insufficient data.
Steam generation at quench front	H	It is the rapid amount of steam generation which creates the liquid entrainment, large uncertainty and impact on PCT.	Not given in the data analysis.

Table 3
Assessment of FEBA Tests to RBHT PIRT:
Quench Front Behavior in the Core Component(continued)

Decay Power	H	Source of Energy for Rods, boundary condition for the test.	Measured.
Liquid entrainment at quench front which includes liquid ligaments, initial drop size, and droplet number density	H	Liquid entrainment cools the PCT location downstream, directly impacts PCT, high uncertainty.	Total water carryover is measured but no information is available on droplets size, density, velocity etc.
Void fraction/flow regime	H	Determines the wall heat transfer since large α results in dispersed flow, low α is film boiling. Directly impacts PCT.	Only coarse (ΔP) measurements are available. Insufficient data.
Interfacial area	H	Determines the initial configuration of the liquid as it enters the transition region directly impacts liquid/vapor heat transfer and resulting PCT downstream.	Insufficient instrumentation.

Table 4
Assessment of FEBA Tests to RBHT PIRT: FROTH Region for Core Component

Process/Phenomena	Ranking	Basis	FEBA
Void fraction/flow Regime	H	Void fraction/flow Regime helps determine the amount of vapor-liquid heat transfer which effects the downstream vapor temperature at PCT, large uncertainty.	DP measurements are too coarse to calculate the void fraction.
Liquid ligaments, drop sizes, interfacial area, droplet number density	H	Liquid surface characteristics determine the interfacial heat transfer in the transition region as well as the dispersed flow region, large uncertainty.	Insufficient instrumentation.
Film Boiling H.T. at low void fraction classical film boiling (Bromley)	H	The film boiling heat transfer is the sum of the effects listed below in the adjacent column. Each effect is calculated separately and is added together in a code calculation, large uncertainty.	Only rod heat transfer can be calculated from data.
- droplet contact heat transfer	H	Wall temperature is low enough that some direct wall-to-liquid heat transfer is possible with a high heat transfer rate, large uncertainty.	No data or analysis is available.
- convective vapor H.T.	M	Vapor convective heat transfer is not quite as important since the liquid content in the flow is large and the vapor velocities are low, but large uncertainty.	Estimated using Dittus-Boelter correlation.
interfacial H.T.	M	Interfacial heat transfer effects are also smaller since the steam temperature is low, but large uncertainty.	No data available.
radiation H.T. to liquid/vapor	M	The radiation heat transfer effects are also small since the rod temperatures are low.	No data available.
effects of spacers	M	The velocities and Reynolds numbers are low in this region such that droplet breakup and mixing are not as important. Drop deposition could occur.	Measured. Separate tests with and without grid spacer were run to investigate the effect.
Decay Power	H	Source of power for rods.	Measured.

Table 5
Assessment of FEBA Tests to RBHT PIRT:
A Dispersed Flow Region for Core Component (continued)

- Radiation Heat Transfer to: • surfaces • vapor • droplets	 M/H M/H M/H	This is important at higher bundle elevations (H) where the convective heat transfer is small since the vapor is so highly superheated. Very important for BWR reflood with sprays, and colder surrounding can. Large uncertainty.	Radiation heat transfer was not considered in the data analysis.
Gap heat transfer	L	Controlling thermal resistance is the dispersed flow film boiling heat transfer resistance. The large gap heat transfer uncertainties can be accepted, but fuel center line temperature will be impacted.	A 0.5mm gap is present between rod and sleeve in blocked bundle experiments. Rod and sleeve temperature were measured in this case.
Cladding Material	L	Cladding material in the tests is Inconel which has the same conductivity as zircalloy nearly the same temperature drop will occur.	Used Ni-Cr 80-20 clad.
Reaction Rate	M	Inconel will not react while Zircalloy will react and create a secondary heat source at very high PCTs, Zirc reaction can be significant	Not present.
Fuel Clad Swelling/Ballooning	L	Ballooning can divert flow from the PCT location above the ballooning region. The ballooned cladding usually is not the PCT location. Large uncertainty.	The effect of clad ballooning was extensively investigated since it was the main issue of FEBA experiment campaign. Large amount of data is available.

Table 5
Assessment of FEBA Tests to RBHT PIRT:
A Dispersed Flow Region for Core Component (continued)

- Radiation Heat Transfer to: • surfaces • vapor • droplets	 M/H M/H M/H	This is important at higher bundle elevations (H) where the convective heat transfer is small since the vapor is so highly superheated. Very important for BWR reflood with sprays, and colder surrounding can. Large uncertainty.	Radiation heat transfer was not considered in the data analysis.
Gap heat transfer	L	Controlling thermal resistance is the dispersed flow film boiling heat transfer resistance. The large gap heat transfer uncertainties can be accepted, but fuel center line temperature will be impacted.	A 0.5mm gap is present between rod and sleeve in blocked bundle experiments. Rod and sleeve temperature were measured in this case.
Cladding Material	L	Cladding material in the tests is Inconel which has the same conductivity as zircalloy nearly the same temperature drop will occur.	Used Ni-Cr 80-20 clad.
Reaction Rate	M	Inconel will not react while Zircalloy will react and create a secondary heat source at very high PCTs, Zirc reaction can be significant	Not present.
Fuel Clad Swelling/Ballooning	L	Ballooning can divert flow from the PCT location above the ballooning region. The ballooned cladding usually is not the PCT location. Large uncertainty.	The effect of clad ballooning was extensively investigated since it was the main issue of FEBA experiment campaign. Large amount of data is available.

Table 6
Assessment of FEBA Tests to RBHT PIRT:
Top Down Quench in Core Components

Process/Phenomena	Ranking	Basis	FEBA
De entrainment of film flow	L[1]	The film flow is the heat sink needed to quench the heater rod. This has high uncertainty.	Top down quenching was prevented in these tests by design.
Sputtering droplet size and velocity	L	The droplets are sputtered off at the quench front and are then re-entrained upward. Since the sputtering front is above PCT location, no impact. The entrained sputtered drops do effect the total liquid entrainment into the reactor system, as well as the steam production, in the steam generators.	Not applicable since top down quenching was prevented.
fuel rod/heater rod properties for stored energyρ, C_p, k.	L[1]	These properties are important since they determine the heat release into the coolant. However, since this occurs above PCT level, no impact.	Not applicable since top down quenching was prevented.
Gap heat Transfer	L[1]	Effects therate of energy release from fuel/heater rod.	Not applicable since top down quenching was prevented.

lote: Some of these individual items can be ranked as high (H) within the top down quenching process; however, the entire list is ranked as low for a PWR/BWR since it occurs downstrea ıe PCT location.

Table 7
Assessment of FEBA Tests to RBHT
Preliminary PIRT for Gravity Reflood Systems Effects Tests

Process/Phenomena	Ranking	Basis	FEBA
Upper Plenum - entrainment/de-entrainment	M	The plenum will fill to a given void fracture after which the remaining flow will be entrained into the hot leg, large uncertainty.	Not applicable.
Hot Leg - entrainment, de-entrainment	L	The hot legs have a small volume and any liquid swept with the hot leg will be entrained into the steam generator plenums, medium uncertainty.	Not applicable.
Pressurizer	L	Pressurizer is filled with steam and is not an active component-small uncertainty.	Not applicable.
Steam Generators	H	The generators evaporate entrained droplets and superheat the steam such that the volume flow releases (particularly at low pressure). The result is a higher steam flow downstream of the generators-high uncertainty since a good model is needed. FLECHT-SEASET data exists for reflood.	Not applicable.
Reactor Coolant Pumps	H	This is the largest resistance in the reactor coolant system which directly effects the core flooding rate-low uncertainty.	Not applicable.
Cold Leg Accumulator Injection	H	Initial ECC flow into the bundle.	Not applicable.
Cold Leg Pumped Injection	H	Pumped injection maintains core cooling for the majority of the reflood transient.	Not applicable.
Pressure	H	Low pressure (20psia) significantly impacts the increased vapor volume flow rate, which decreases the bundle flooding rate.	Low pressure (30 psia) simulated.
Injection Subcooling	M/H	Lower subcooling will result in boiling below the quench front such that there is additional vapor to vent.	Low subcooling simulated.
Downcomer wall heat transfer	H	The heat transfer from the downcomer walls can raise the ECC fluid temperature as it enters the core, resulting in more steam generation.	Not applicable.
Lower Plenum Wall Heat Transfer	M	Source effect as downcomer but less severe.	Not applicable.
Break	L	Excess ECC injection spills, but break ΔP helps pressurize reactor system.	Not applicable.

Table 8
Assessment of FEBA Tests to RBHT PIRT for High Ranked BWR Core Phenomena

Process/Phenomena	Basis	FEBA
Core		
• Film Boiling	PCT is determined in film boiling period.	Total heat transfer is measured.
• Upper Tie Plate CCFL	Hot Assembly is in co-current up flow above CCFL limit.	Not applicable.
• Channel-bypass Leakage	Flow bypass will help quench the BWR fuel assembly core.	Not applicable.
• Steam Cooling	A portion of the Dispersed Flow Film Boiling Heat Transfer.	Steam cooling heat transfer is estimated from data.
• Dryout	Transition from nucleate boiling and film boiling.	Quench front is measured.
• Natural Circulation Flow	Flow into the core and system pressure drops.	Not applicable.
• Flow Regime	Determines the nature and details of the heat transfer in the core.	Movies exist to determine flow regime.
• Fluid Mixing	Determines the liquid temperature in the upper plenum for CCFL break down.	Not applicable.
• Fuel Rod Quench Front	Heat release from the quench front will determine entrainment to the upper region of the bundle.	Quench front data exists.
• Decay Heat	Energy source for heat transfer.	Measured as initial/boundary conditions.
• Interfacial Shear	Effects the void fraction and resulting droplet and liquid velocity in the entrained flow.	Not measured.
• Rewet: Bottom Reflood	BWR hot assembly refloods like PWR.	Total reflood heat transfer measured.
• Rewet Temperature	Determines the quench front point on the fuel rod.	Quench temperature is measured.
Top Down Rewet	Top of the hot assembly fuel will rewet in a similar manner as PWR.	Top down rewet quench front measured.
Void Distribution	Gives the liquid distribution in the bundle.	Not measured.
Two-Phase Level	Similar to quench front location, indicates location of nucleate and film boiling.	Measured by rod T/Cs, collapsed level measured, 2ϕ level estimated from DP cells.

Conclusions

The FEBA experiments provide very good information concerning the separate effect of grids and blocked bundle regions on the heat transfer during reflood. Separate tests were run with the same boundary conditions with and without grids, with and without blockage to address this effect. On the other hand a very little effort has been dedicated to investigate the single thermal-hydraulic process involved in the heat transfer during reflood (droplets behavior, entrainment etc.) which does not provide sufficient data to develop and validate mechanistic models to be used in best-estimate code.

Appendix A-6 Literature Review

Test Facility Name: Oak Ridge National Laboratory Thermal-Hydraulic Test Facility (THTF)

Dates when tests were performed: 1980 - 1982

References:

R12. Mullins, C. B., et al., "ORNL Rod Bundle Heat Transfer Test Data," NUREG/CR - 2525, Vol. I to Vol. 5, 1982.

R13. Yoder, G. L., et al., "Dispersed Flow Film Boiling in Rod Bundle Geometry - Steady State Heat Transfer Data and Correlations Comparisons," NUREG/CR - 24351, 1982.

Availability of Data:

Reduced instrument responses are presented in Reference R12 for transient film boiling in upflow. Microfiche of the reduced data in graphical form exist along with three types of tables to assist the reader in using the data. The first table lists instrumentation in terms of instrument function, type and location. The second table lists instruments in the order they appear graphically in the microfiche. The third table lists instruments alphabetically in terms of the instrument application number (IAN). In addition to the transient data, steady state data exist in ReferenceRl3fordispersedflowfdmboiEng. The data are presented in two separate sets of tables, one in SI units and the other in English units, listing fluid conditions, surface conditions and correlation - predicted versus experimentally determined heat transfer coefficients.

Test Facility Description, Types of Tests

Both the transient and steady state experiments were performed in the Thermal-Hydraulic Test Facility (THTF), as shown in Figure A-6. 1. The THTF was a heavily instrumented nonnuclear pressurized-water loop containing 64 full-length rods arranged in an 8x8 bundle; 60 of the rods were electrically heated (see Figure A-6.2). The rod diameter was 0.374" (0.0095 m) and the rod pitch was 0.501" (0.0127 m) on a square lattice, typical of PWRs with 17xl7 fuel rod assemblies. Figure A-6.3 shows a simplified cross section of a typical fuel rod simulator. The axial and radial power profile was flat. The heated length of the bundle was 12 ft (3.66 m) and there were eight spacer grids in the heated length, as shown in Figure A-6.4. The spacer grids were of the egg-crate type installed 2 ft (0.61 m) apart.

Two types of tests were performed, one transient and the other steady state. The transient tests were initiated by breaking the outlet rupture disk assembly. Although the THTF had a rupture disk assembly at the inlet, it was not employed to assure a unidirectional flow up through the test section. At the same time the outlet rupture disk was broker4 the pump was tripped and bundle power was ramped up to about 6-8 MW. After the initial power ramped up, the bundle power remained at this high level until most of the sheath temperatures at level G in the bundle

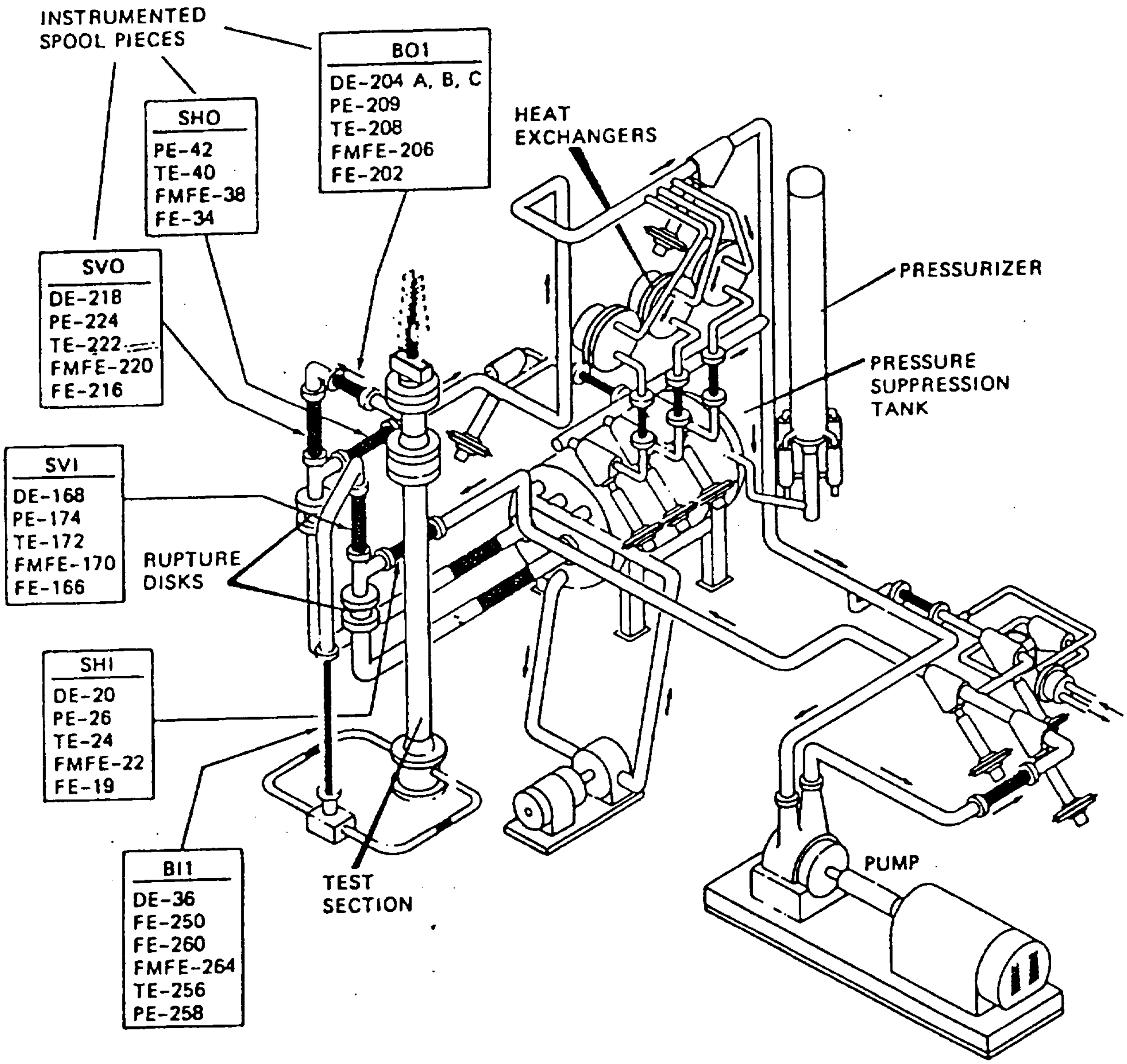

Figure A6.1. THTF system with instrumented spool pieces labeled.

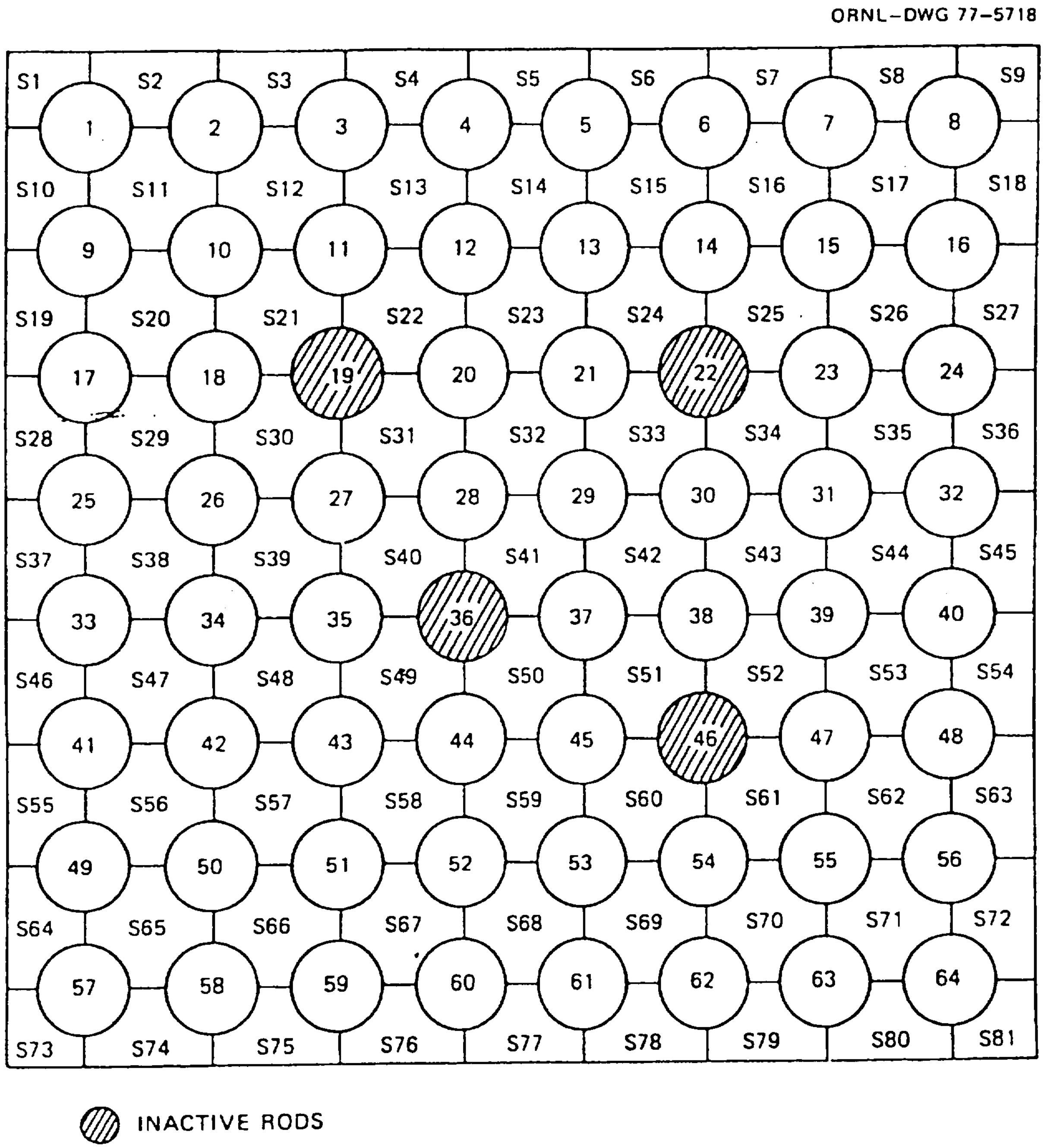

Figure A6.2. Identification of THTF heater rods, subchannel location, and inactive rods in THTF heater bundle.

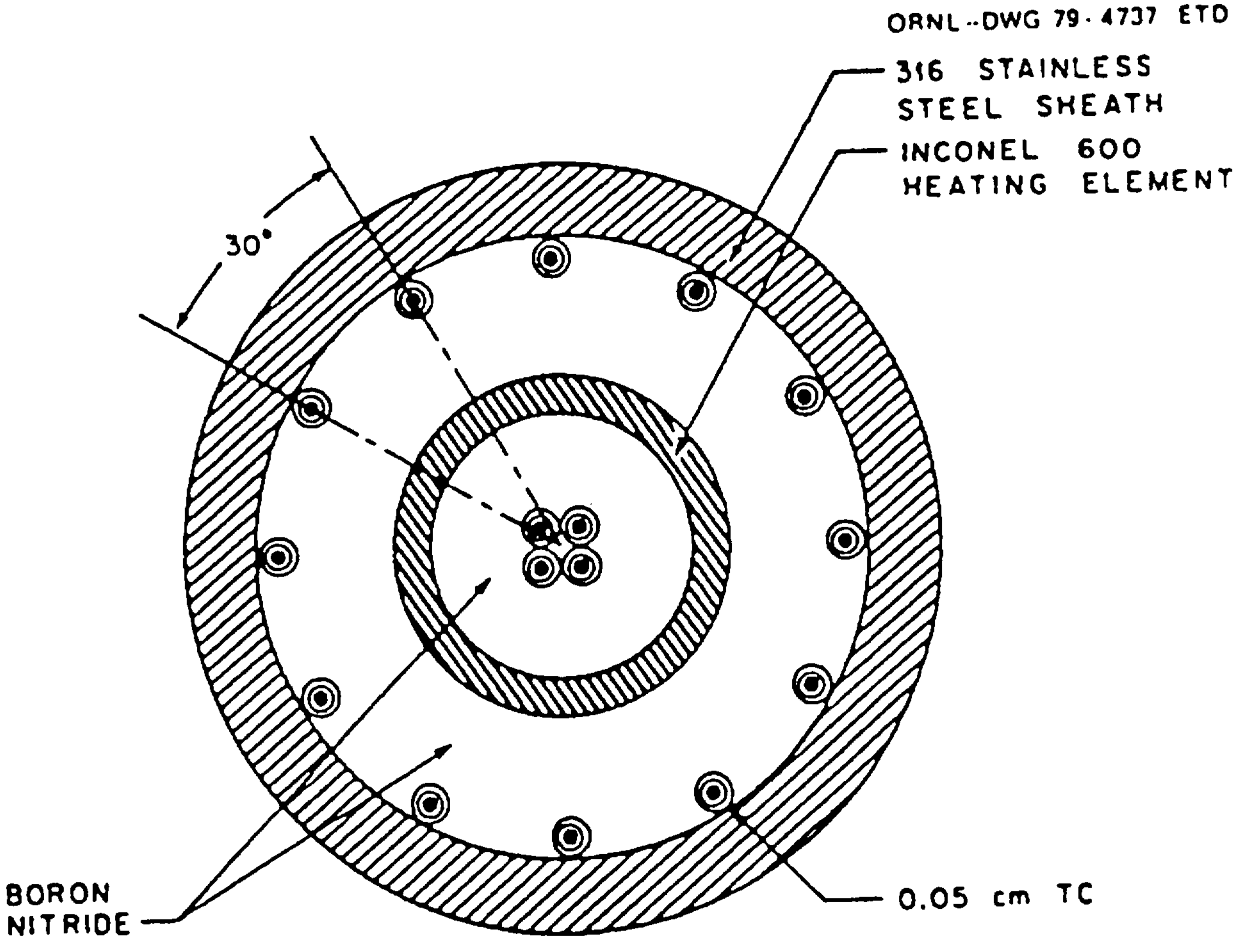

Figure A6.3. Cross-section of a typical FRS.

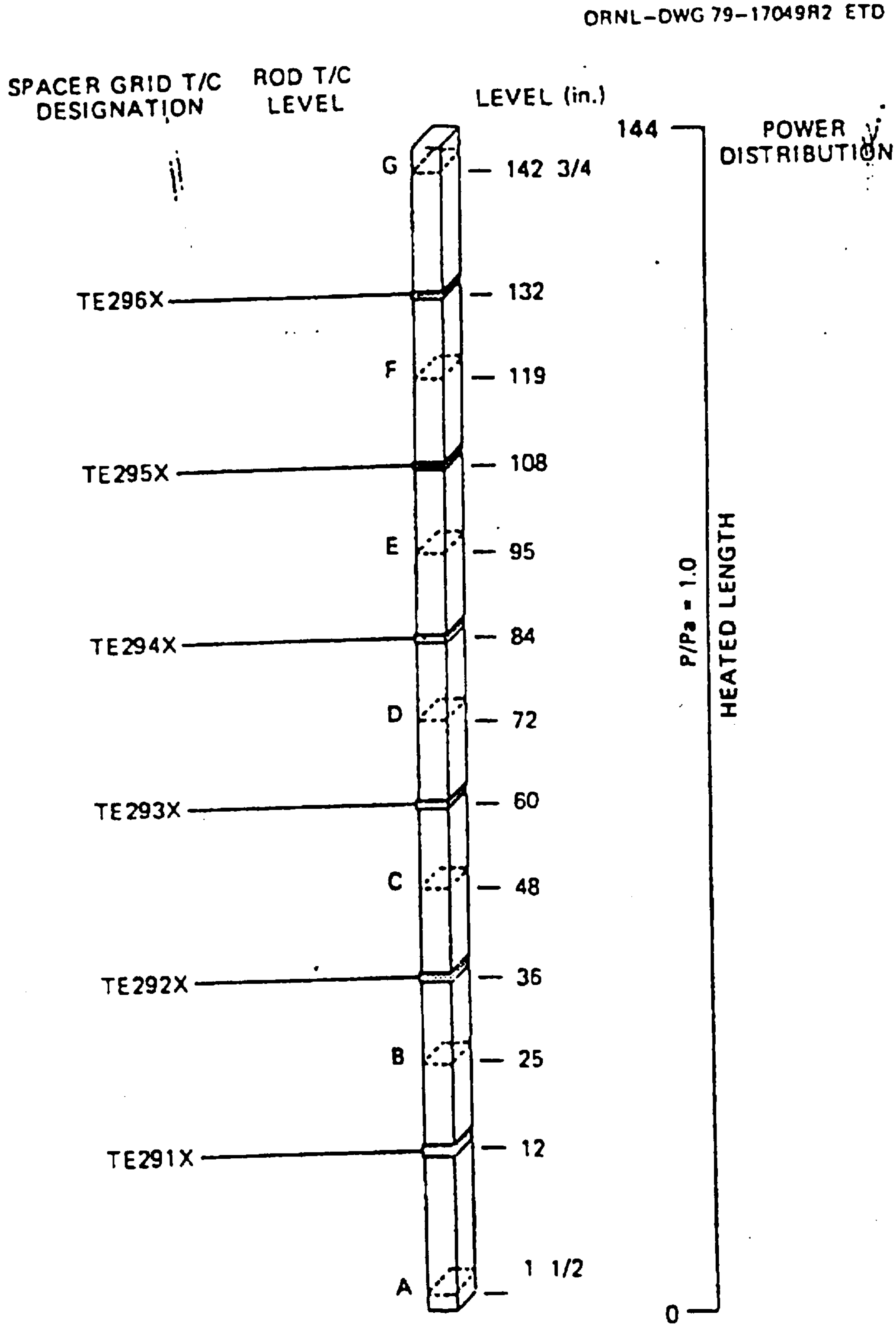

Figure A6.4. Axial location of spacer grid and FRS thermocouples.

reached 1000°F (811 K). The bundle power was then ramped down to maintain high rod sheath temperatures in the upper bundle without reaching the safety limit of 1550°F (1116 K). All test series including test 3.03.6AR, test 3.06.6B and test 3.08.6C were conducted under reactor accident-type conditions to obtain transient film boiling data. The ranges of conditions are given are given below.

Test 3.03.6AR:

Mass Velocity	136 – 502 kg/m^{2}s (1x10^5 to 3.7x10^5 lb$_m$/h.ft^2)
Quality	23 – 100%
Pressure	5 – 10 MPa (700 – 1500 psi)
Heat Flux	158 – 1000 kW/m^2 (5x10^4 to 3.2x10^5 Btu/h.ft^2)

Test 3.06.6B:

Mass Velocity	136 – 610 kg/m^{2}s (1x10^5 to 4.5x10^5 lb$_m$/h.ft^2)
Quality	5 – 100%
Pressure	6 – 13 MPa (875 – 1900 psi)
Heat Flux	158 – 630 kW/m^2 (5x10^4 to 2x10^5 Btu/h.ft^2)

Test 3.08.6C:

Mass Velocity	330 – 1090 kg/m^{2}s (2.4x10^5 to 8x10^5 lb$_m$/h.ft^2)
Quality	35 – 100%
Pressure	6.6 – 11.7 MPa (950 – 1700 psi)
Heat Flux	160 – 1100 kW/m^2 (5x10^4 to 3.5x10^5 Btu/h.ft^2)

In the steady state tests, the working fluid flowed from the pump through two control values, past the inlet rupture disk assembly and through a vertical spool piece before it entered the external downcover. The working fluid then flowed through two spool pieced in the downcover and entered the test section. The fluid was heated as it flowed along the rods within the test section. It then left the test section from the upper plenum, past through the three outlet spool pieces and the heat exchangers, and returned to the pump. During the run, the loop was adjusted to provide the desired inlet fluid temperature and inlet pressure. The bundle power was then increased until the dryout point was at the desired position in the bundle. The steady state operating conditions were assumed to have been reached when the operating pressure and rod surface temperatures stabilized. A total of twenty-two (22) steady-state tests were performed. The ranges of conditions were:

Mass Velocity	226 – 806 kg/m^{2}s (1.66x10^5 to 5.94x10^5 lb$_m$/h.ft^2)
Quality	0 – 100%
Pressure	4.4 – 13.4 MPa (635 – 1938 psi)
Heat Flux	320 – 940 kW/m^2 (1x10^5 to 3x10^5 Btu/h.ft^2)

Instrumentation and Data from Tests

The bundle was fully instrumented with thermocouples at various axial locations (i.e., at A, B, C, D, E, F, G levels) to measure the rod temperatures and in-bundle fluid temperatures. At each axial location where a rod had thermocouples, there were three individual thermocouples spaced azimuthally around the rod. In-bundle fluid temperatures were measured using thermocouples extending a short distance from the rod surface into the fluid as well as thermocouples mounted on the spacer grids. Rods 36 and 46 also contained gamma densitometer instrumentation for measuring in-bundle fluid density. Two flow measurement sites were positioned at each end of the test section containing the rod bundle. Differential pressure and pressure instrumentation was made at various locations along the heated bundle. In addition, there was instrumentation located in the entire piping system including the outlet nozzle, vertical outlet and external downcover spool pieces.

In the transient tests, local bundle fluid conditions were calculated with the homogeneous two-phase flow and thermodynamic equilibrium thermal-hydraulics code RLPSFLUX. The transient data were compared to six existing film boiling correlations. Results of the comparisons were presented in Reference R12. In the steady state tests, mass and energy conservation relationship were used to calculate equilibrium fluid conditions within the rod bundle. These fluid conditions, along with calculated rod surface temperatures, were used to evaluate the six film boiling correlations as well as single-phase vapor correlation. Results of the comparisons were presented in Reference RI 3. In addition to the dispersed flow film boiling data, results were also obtained for the spacer grid effects, which had beneficial influence on the heat transfer due to a boundary layer breakup-rebuild process at the grids.

Table 5
Assessment of ORNL/THTF Data to RBHT PIRT: Dispersed Flow Region for Core Component

Process/Phenomena	Ranking	Basis	ORNL/THTF Data
Decay power	H	Energy source which determines the temperature of the heater rods, and energy to be removed by the coolant.	Known, measured as initial/boundary conditions.
Fuel Rod/Heater Rod properties, ρ, c_p, k	L	The exact properties can be modeled and stored energy release is not important at this time, environmentally.	Heater rod properties are known and approximate those of nuclear rod.
Dispersed Flow Film Boiling	H	Dispersed flow film boiling modeling has a high uncertainty which directly effects the PCT.	Total head transfer coefficients for DFFB have been obtained from the transient and steady state data covering a wide range of mass velocities, qualities and pressures. The coefficients have been compared to existing correlations.
Convection to superheated vapor	H	Principle mode of heat transfer as indicated in FLECHT-SEASET experiments[4].	Total convection heat transfer has been determined.
Dispersed phase enhancement of convective flow	H	Preliminary models indicted that the enhancement can be over 50% in source cases[13].	This component was not isolated.
Direct wall contact H. T.	L	Wall temperatures are significantly above Tmin such that no contact is expected.	This component was not isolated.
Dry wall contact[12]	M	Iloeje[12] indicates this H. T. Mechanism is less important than vapor convection.	This component was not determined.
Droplet to vapor interfacial heat transfer	H	The interfacial heat transfer reduces the vapor temperature which is the heat sink for the wall heat flux.	The quality is known but the interfacial surface area is not.
Radiation Heat Transfer to: • surfaces • vapor • droplets	 M/H M/H M/H	This is important at higher bundle elevations (H) where the convective heat transfer is small since the vapor is so highly superheated. Very important for BWR reflood with sprays, and colder surrounding can. Large uncertainty.	Can be estimated from the data on surface temperatures and fluid conditions.

Table 5
Assessment of ORNL/THTF Data to RBHT PIRT:
Dispersed Flow Region for Core Component (continued)

Gap heat transfer	L	Controlling thermal resistance is the dispersed flow film boiling heat transfer resistance. The large gap heat transfer uncertainties can be accepted, but fuel center line temperature will be impacted.	Not present. Heater rods have no gap.
Cladding Material	L	Cladding material in the tests is Inconel which has the same conductivity as zircalloy nearly the same temperature drop will occur.	Used stainless steel clad.
Reaction Rate	M	Inconel will not react while Zircalloy will react and create a secondary heat source at very high PCTs, Zirc reaction can be significant.	Not present.
Fuel Clad Swelling/Ballooning	L	Ballooning can divert flow from the PCT location above the ballooning region. The ballooned cladding usually is not the PCT location. Large uncertainty.	Not present.

Conclusions

The ONRL/THTF tests provide both transient and steady state film boiling heat transfer data in rod bundle geometry. In general, the steady state results support the conclusions reached in the analysis of the transient results. The experimentally determined heat transfer coefficients may be useful as they have been compared to various existing heat transfer correlations. It is found that the Dougall-Rohsenow correlation often overpredicts the heat transfer coefficient whereas the Groeneveld-Delorme correlation tends to underpredict the heat fluxes near dryout but improves as distance from dryout increases. On the other hand, the Groeneveld 5.7, Groeneveld 5.9 and Condie-Bengston IV correlations give better agreement with the experimental data.

It should be noted that although the steady state and the transient data appear to be consistent with each other, the bundle fluid conditions in both cases are determined from mass and energy conservation consideration based on the assumption of thermodynamic equilibrium. However, non-equilibrium conditions probably exist within the bundle. Thus, a more sophisticated calculational method accounting for the effect of non-equilibrium is needed to determine the actual bundle fluid conditions. Non-equilibrium also implies that liquid droplets can be present in the flow when equilibrium qualities are calculated to be larger than unity.

The ORNL/THTF tests have been focused on the case of dispersed flow film boiling in upflow under high-pressure high-temperature conditions. The data may provide some relevant information in the dispersed flow region for core component in the RBHT PIRT Table 5. However, the results are not applicable to single phase liquid corrective heat transfer in the core component during reflood below the quench front (RBHT PIRT Table 1), subcooled and saturated boiling in the core component below the quench front (RBI-IT PIRT Table 2), quench front behavior in the core component (RBHT PIRT Table 3), froth region for the core component (RBHT PIRT Table 4), top down quench in core component (RBHT PIRT Table 6), and gravity reflood system effects (RBHT PIRT Table 7).

Even in the dispersed flow region, the ORNL/THFT data must be used with caution. This is because the pressure range (4.4 - 13.4 MPa or 635 - 1938 psi) explored in the THTF tests is very high, more characteristic of a PWR or BWR blowdown situation. Thus the results may not be directly applicable to transient stage of reflood heat transfer in rod bundles.

Appendix A-7 Literature Review

Test Facility Name: FRIGG-2 36-Rod Loop (Sweden)

Dates When Tests Were Performed: 1965-1968

References:

R14. Becker, K. M., Flinta, J., and Nylund, O., "Dynamic and Static Burnout Studies for the Full Scale 36-Rod Marviken Fuel Element in the 8 MW Loop FRIGG," Paper presented at the Symposium on Two-Phase Flow Dynamics, Eindhoven, September 1967.

R15. Nylund, 0. *et al.*, "Measurements of Hydrodynamic Characteristics, Instability Thresholds, and Burnout Limits for 6-Rod Clusters in Natural and Forced Circulation," ASEA and AB Atomenergi Report FRIGG-1, 1967.

R16. Nylund, O., Becker, K. M., Eklund, R., Gelius, O., Haga, I., Herngorg, G., Rouhani, Z., and Akerhielm, F., "Hydrodynamic and Heat Transfer Measurements on a Full Scale Simulated 36-Rod Marviken Fuel Element with Uniform Heat Flux Distribution," ASEA and AB Atomenergi Report FRIGG-2, 1968.

Availability of Data:

The experimental investigation simulates the fuel element of a Swedish heavy water cooled Marviken BVRR with 35 uniformly heated heater rods and a unheated (but larger in diameter) center rod simulating the control rod. Experimental data available from the FRIGG-2 tests, all under pressures up to 5 0 bars (71 1 psi), are single- and two-phase pressure drops; burnout (or critical heat flux) in natural and forced circulation; natural circulation mass velocity as a function of total power and inlet subcooling; the stability limit; as well as the details about the system during transient conditions. Additionally, a unique output of the FRIGG-2 tests is the axial and radial void distributions measured by the Cobalt-60 gamma-ray densitometer system. The results have been compared to data obtained from in the previous 6-rod tests (RI 5., FRIGG-1) and to predictions with existing correlations and models. All pressure drop data are consistently agreeable between FRIGG-2, FRIGG-1, and actual Marviken conditions. The natural circulation burnout value is very close to that of forced circulation, but both are about 20% low compared to predictions by the Becker correlation. This is believed to be due to the unfavorable conditions in the inner subchannels of the uniformly heated bundle. The results of natural circulation mass velocity, stability limit, and transient behavior at different power levels agree well with the calculation. Calculations indicate that the conditions in a real Marviken boiling channel are somewhat more favorable than in the FRIGG-2 experiment. That suggests that sufficient margins against burnout and hydrodynamic instability are present in the Marviken reactor.

Test Facility Description, Types of Tests:

The primary purpose of FRIGG-2 tests was to obtain the burnout values of the 36-rod bundle at different mass fluxes and inlet subcoolings to simulate the core conditions of a Marviken BWR. The geometric features of the test section are:

Number of heated rods	35	Rod diameter	13.8 mm (0.5433")
Number of unheated rods	1	Unheated rod dia.	20 mm (0.7874")
Circular housing diameter	160 mm (6.30")	Number of spacers	8
Average hydraulic dia.	26.9 mm (1.06")	Heated hydraulic dia.	36.6 mm (1.44")
Heated length (uniform)	4375 mm (172")	Number of burnout T/C's	4

Tests were run with 35 rods electrically heated and I center rod unheated. Both the axial and radial power profiles are uniform. A cross-sectional view of the test section is shown in Fig. A-7. 1, indicating the placement pattern of the unheated center rod and 3 5 heated rods in three orbital rows. The flow diagram of the FRIGG-2 loop is shown in Fig. A-7.2. For burnout tests FRIGG-2 requires a significant DC electrical power: 80 MW, 80 kA, and DC voltage regulation from 0 to- 200 V. The heater rods were of a type with coaxial feeder rod eliminating the electromagnetic forces between the rods. Most of the heat is produced in the 0.8 mm stainless steel canning of the rod, which is isolated from the center copper conductor. This means that the reactor fuel time constant (or heat capacity) is <u>not</u> correctly simulated. There are 4 electrically isolated burnout detectors (or thermocouples) measuring temperatures at different elevations and there wires running axially along the inside surface of the stainless steel canning. If a burnout event is detected by any of the burnout detectors in the bundle, the DC power applied to the bundled would be immediately reduced by 20% within 0. I second and the histories of all important fluid and thermal parameters are recorded. These burnout conditions are the primary objective of the FRIGG-2 tests.

A secondary but important test of FRIGG-2 is the void fraction measurement in both the axial and radial directions of the bundle. The measurement system comprises one gamma source, Co-60, and four scintillation detectors with adjustable collimators. The pulses from the detectors are amplified, analyzed and counted in separate scalars built into the data collection system. The penetration paths of the four gamma beams can be changed between three prefixed radial positions within the bundle. The void at a certain level is thus evaluated from the twelve measurements covering different parts of the bundle. This gives a rather good cross sectional mean value of the void and also information about the radial void distribution. The void measurement system is moved up and down the test section by means of an electric elevator that allows for axial void distribution measurement.

Other instrumentation includes Chromel-alumel thermocouples for fluid temperature distribution measurement; fast response DP cells with venturi units and turbine flow meters for mass velocity measurement; and impedance void gauge to measure the outlet quality. Standard single- and two-phase pressure drops at all test conditions are also measured using differential and absolute pressure sensors.

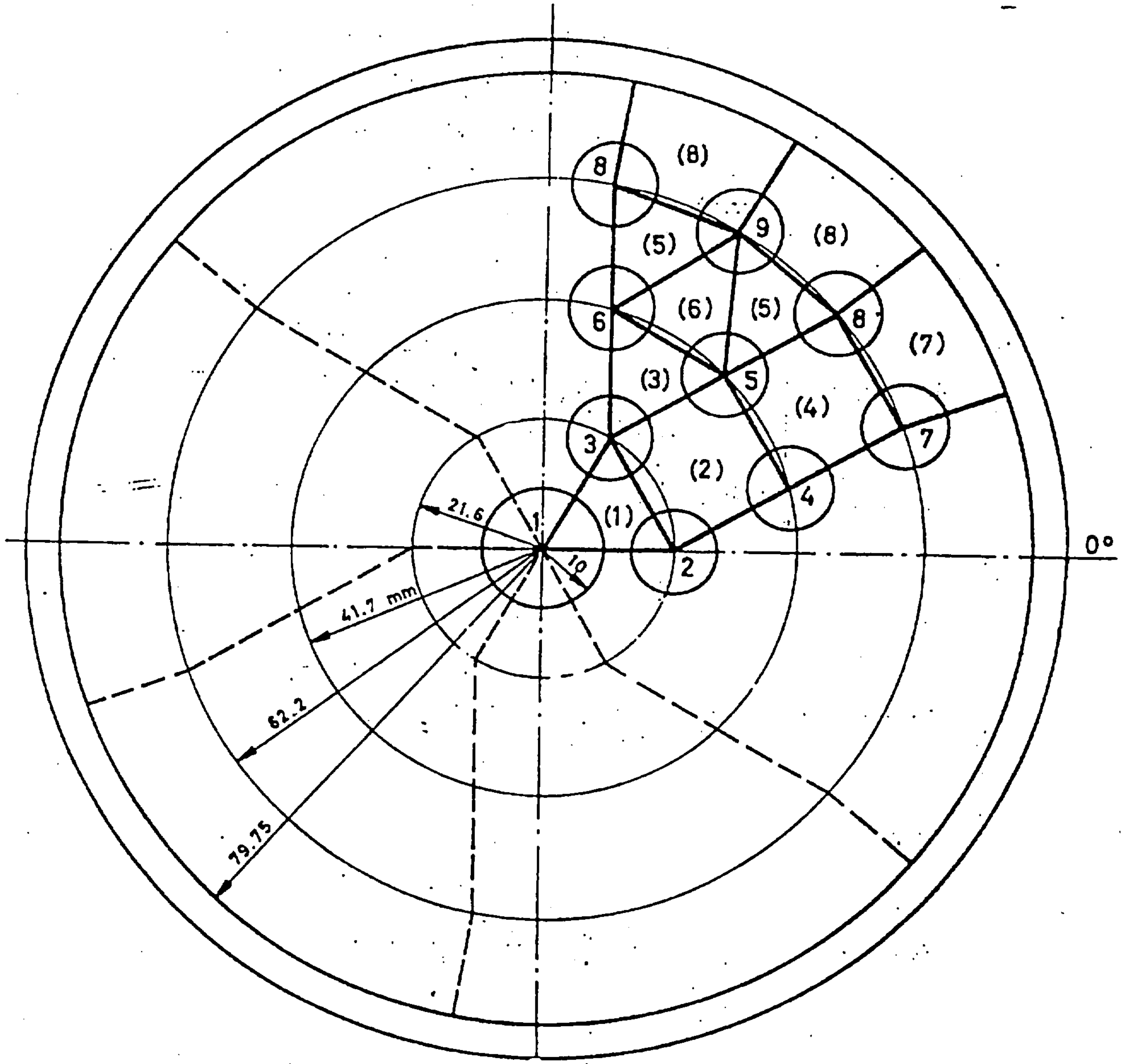

Figure A-7.1 36-Rod Bundle of the FRIGG-2

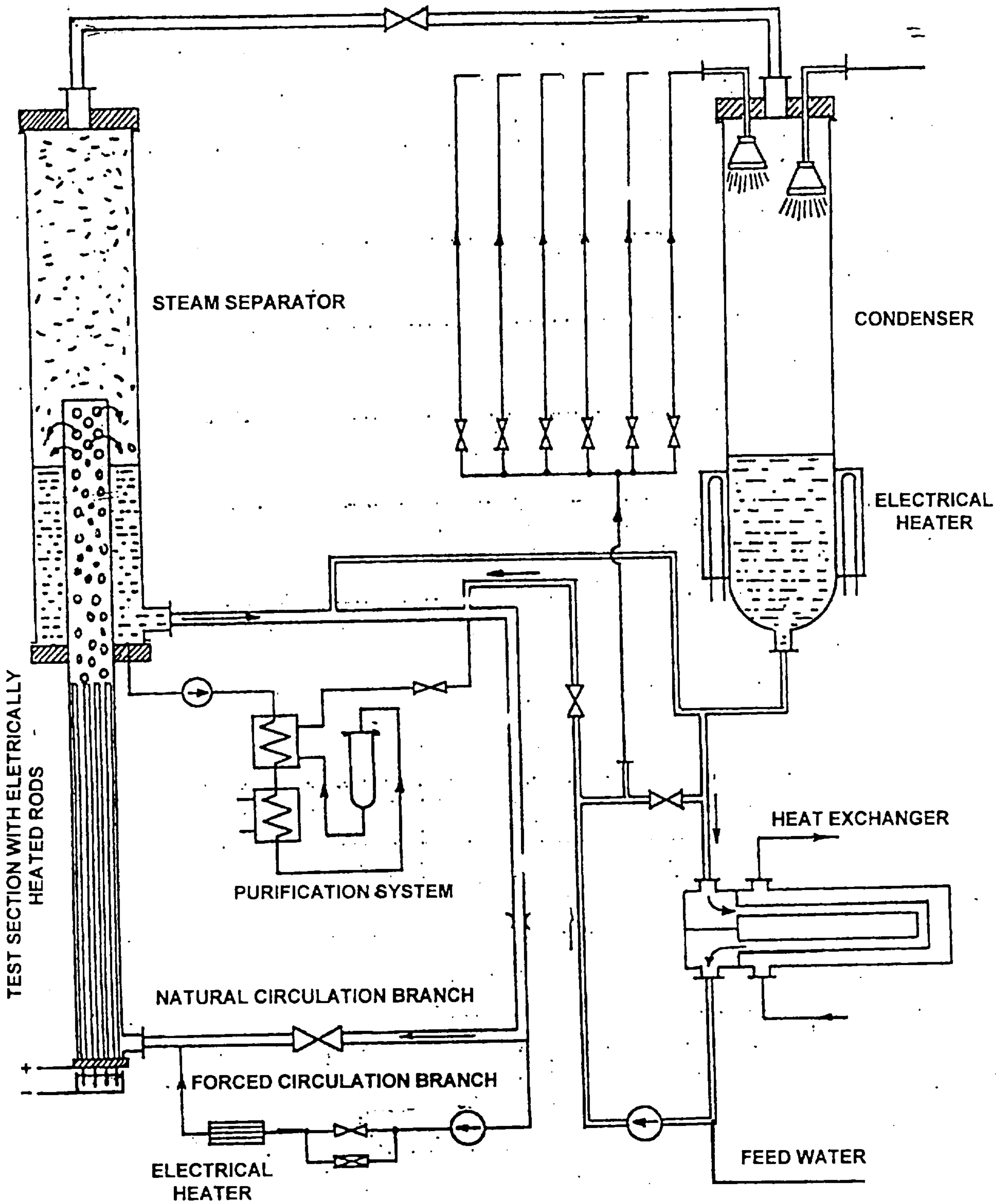

CONSTRUCTION MATERIAL: CARBON STEEL
COOLING CAPACITY: 8MW
MAX. PRESSURE: 100 Bars

Figure A-7.2 Flow Diagram of the FRIGG-2 Loop

The ranges of test conditions include,

Single-phase (cold) mass flux	840 - 3195 kg/m^2s (0.618 – 2.35x10^6 lbm/ft^2hr)
Two-phase mass flux	366 - 1492 kg/m^2s (0.269 – 1.098x10^6 lbm/ft^2hr)
Pressure	50 bars (711 psi)
Rod Temperature	measured with thermocouples serving as burnout detectors
Average heat flux	8.1 - 103 W/cm^2 (0.0257 – 0.326x10^6 Btu/ft^2hr)
Exit quality	2.2% - 51.5%
ΔT_{sub}	2.4 - 29.4 °C
Flow regimes	Liquid 1-ϕ, bubbly, transition, annular (typical of BWR)
Void Fraction	0% -100%

Instrumentation and Data from Tests

Each of the heater rods was instrumented with four (4) thermocouples. These thermocouples are primarily for burnout detectors and thus calibration is not necessary. Neither was any visualization view port provided, such that the identification of flow regimes was based on empirical correlations from the state of local quality. Heat transfer information were mainly derived from the voltage and current parameters of the DC power system, thus only global heat flux (rather than local heat flux) were obtained. Although the heater rods were pushed to the burnout limits in order to obtain the critical heat flux (CHF), the normal BWR operating mass flux range was maintained. Therefore the post-LOCA reflood (or blowdown) scenarios were not addressed, neither were the radiation heat transfer and dispersed flow film boiling phenomena as normally encountered in a uncovered core during reflood. However, the FRIGG-2 gamma-ray densitometer experiments provided valuable information on the axial and radial distribution of void faction. It could facilitate the physical correlation between void fraction, local quality, and interfacial slip.

Extensive single- and two-phase flow pressure drop data were obtained in the FRIGG-2 tests. These pressure drop data are specific to the Marviken reactor core condition, but have compared favorably with the Martinelli-Nelson and Becker correlations.

The only complete natural circulation curve was also obtained at conditions close to the Marviken reactor's. However, by far, the most important data obtained from the FRIGG-2 tests are the CHF data for the particular fuel type and grid spacer pattern, as well as the void fraction distribution of the 36-rod bundle.

Conclusion

For the burnout experiments in FRIGG-2, all independent parameters (mass flux, inlet subcooling, pressure, and power to the bundle) have been carefully and independently controlled Due to the uniform axial and radial power profiles of FRIGG-2, which resulted in a less favorable heat transfer condition in FRIGG-2 as compared to the actual Marviken core, the measured burnout data were approximately 20% lower than those predicted. This points out the major deficiency of the uniform power profiles of FRIGG-2. Follow-up tests using the actual Marviken reactor's power profiles have been suggested and recognized.

The natural circulation mass flow rate in Marviken is 10-15% above the experimental values of FRIGG-2 in the power range of interest, while there is a close agreement between the calculated and measured FRIGG-2 flows. The differences are attributed to the Marviken's coolant (heavy water); larger radial heat loss of Marviken channel; and distributed power profiles of Marviken fuel assembly.

Although the FRIGG-2 facility has improved our understanding of the burnout limits and natural circulation flows of a simulated Marviken core, it did not address the heat transfer phenomena associated with post-LOCA reflood conditions, in which the quench front progression, froth region propagation, and dispersed flow film boiling are of major interest. However, the following relevant heat transfer information of FRIGG-2 may be assessed against the RBHT PIRT:

Table 1
Assessment of FRIGG-2 36-Rod Bundle Test to RBHT PIRT:
Single Phase Liquid Convective Heat Transfer in the Core Component During Reflood Below the Quench Front

Process/Phenomena	Ranking	Basis	FRIGG-2 36-Rod Bundle Test
1ϕLiquid Convective Heat Transfer	L	1ϕConvective H.T. data ha been correlated for rod bundles, uncertainty will not effect PCT.	Flows are substantially higher than proposed RBHT reflood flows.
• Effects of Geometry	L	De varies radially	P/D varies radially
• Effects of Spacers	L	Effects of spacers in 1ϕ convective H.T. is known. No impact on PCT uncertainty.	Rod T/C's are used for burnout detectors only.
• Effects of Properties	L	Property effects are accounted for in analysis for 1ϕH.T. little uncertainty.	Insufficient instrumentation for T_b.
1ϕLiquid Natural Convection H.T.	M	Must test Gr/Re^2 to determine regime.	Natural circulation flow measured, but at powers substantially higher than the decay power.
• Effects of Geometry	L	Limited data exists which can be used as a guide, should have little uncertainty on PCT.	Insufficient instrumentation for T_b.
• Effects of Spacers	L	Effect unknown for natual convection, but enhances H.T. No impact on PCT uncertainty.	Insufficient rod T/C instrumentation.
• Effects of Properties	L	Accounted for in dimensionless parameters, little uncertainty.	Insufficient instrumentation for T_b.
Decay Power	H	Source of energy for rods, boundary convection for test.	Decay power not simulated

Table 2
Assessment of FRIGG-2 36-Rod Bundle Tests to RBHT PIRT:
Subcooled and Saturated Boiling in The Core Component Below the Quench Front

Process/Phenomena	Ranking	Basis	FRIGG-2 36-Rod Bundle Tests
<u>Subcooled Boiling</u>	L	A significant variation in the subcooled boiling H. T. coefficient will not effect the PCT uncertainty since rod is quenched.	Heater rod temperatures are measured, but only used as burnout detectors.
• Effects of Geometry, P/D, De	L	Boiling effects in rod bundles have been correlated for our P/d, De range with acceptable uncertainty.	P/D varies radially
• Effects of Spacers	L	Locally enhanced H. T.	Not quantified by the experiments
• Effects of Properties	L	Data exists for our Range of Conditions, little uncertainty.	Heater rods do not simulate nuclear rods
<u>Saturated Boiling</u>	L	Similar to subcooled boiling, data is available for our P/D, De range. The uncertainty of Saturated Boiling H. T. coefficient will not significantly impact the PCT since rod is quenched.	Heater rod temperatures are available, but only used as burnout detectors.
• Effects of Geometry, P/D, De	L	Data exists in the range of P/D, De with acceptable uncertainties.	P/D varies radially
• Effects of Spacers	L	Locally enhanced H. T., Correlations/ Models are available, with acceptable uncertainty.	Not quantified by the experiments.
• Effects of Properties	L	Data exists for our range of conditions, little uncertainty.	Heater rods do not simulate nuclear rods
<u>Decay Power</u>	H	Source of energy for rods, boundary condition for the test.	Tests were conducted at Marviken operating power, not at decay power.

Table 3
Assessment of FRIGG-2 36-Rod Bundle Tests to RBHT PIRT for High Ranked BWR Core Phenomena

Process/Phenomena	Basis	FRIGG-2 36-Rod Bundle Tests
Core		
• Film Boiling	PCT is at the end of the heated length, but not measured.	Only occurs in dryout DNB tests
• Upper Tie Plate CCFL	Hot Assembly is in co-current up flow above CCFL limit.	Not applicable
• Channel-bypass Leakage	Flow bypass will help quench the BWR fuel assembly core.	Not applicable
• Steam Cooling	A portion of the Dispersed Flow Film Boiling Heat Transfer.	Pot-dryout condition, not enough H.T. measurement
• Dryout	Transition from nucleate boiling and film boiling.	Indicated from the burnout detectors
• Natural Circulation Flow	Flow into the core and system pressure drops.	At Marviken's normal power
• Flow Regime	Determines the nature and details of the heat transfer in the core.	Bubbly, transitional, and annular flows identified from flow-regime map, typical of BWR.
• Fluid Mixing	Determines the liquid temperature in the upper plenum for CCFL break down.	Not applicable
• Fuel Rod Quench Front	Heat release from the quench front will determine entrainment to the upper region of the bundle.	Not applicable
• Decay Heat	Energy source for heat transfer	Not applicable
• Interfacial Shear	Effects the void fraction and resulting droplet and liquid velocity in the entrained flow.	Insufficient measurement
• Rewet: Bottom Reflood	BWR hot assembly refloods like PWR.	Not applicable
• Rewet Temepratures	Determines the quench front point on the fuel rod.	Not applicable
• Top Down Rewet	Top of the hot assembly fuel will rewet in a similar manner as PWR.	Not applicable
• Void Distribution	Gives the liquid distribution in the bundle.	Measured by the gamma-ray densitometer
• Two-Phase Level	Similar to quench front locations, indicates location of nucleate and film boiling.	Not applicable

Appendix A-8 Literature Review

Test Facility Name: General Electric Nine-rod Bundle Facility

Dates When Tests Were Performed: 1968-1970

References:

R17. Lahey, R. T., and Schraub, F. A., "Mixing, Flow Regimes, and Void Fraction for Two-Phase Flow in Rod Bundles," *Two-Phase Flow and Heat Transfer in Rod Bundles*, ASME, Nov. 1969.

R18. Lahey, R. T., Shiralkar, B. S., and Radcliff, D. W., "Two-Phase Flow and Heat Transfer in Multirod Geometries: Subchannel and Pressure Drop Measurements in a Nine-rod Bundle for Diabatic and Adiabatic Conditions," GEAP-13049, AEC, 1968.

Availability of Data:

In the 3x3 9-rod bundle configuration for typical BWR operating conditions, there are three (3) types of geometrical subchannels: comer, side, and center subchannels. Subchannels are also classified into hot (locally heated), cold (unheated), and uniform (uniformly heated) subchannels. Data for all test points are available in tabulated form for all types of subchannel. Bundle average mass flux, bundle average exit quality, measured subchannel mass flux, and subchannel quality are tabulated against the test points in Refs. R17 and R18. Substantial differential pressure drop data for both single- and two-phase flows are available in the same references. Other reduced or analyzed data are also available in graphic forinat that include: subchannel quality-vs-average quality; subchannel energy flux-vs-subchannel mass flux; subchannel quality-vs-subchannel type; subchannel mass flux-vs-subchannel type; etc. Single-phase friction factors are graphed against the Reynolds number, while two-phase friction multipliers are graphed against flow quality and favorably compared with the Martinelli-Nelson correlation.

Test Facility Description, Types of Tests:

The primary purpose of this investigation was to obtain the mass flux and enthalpy distribution in a simulated rod bundle for a BWR. The geometric features of the test section are

Number of rods	9	Rod diameter	0.570"
Radius of channel comer	0.400"	Rod-rod clearance	0.168"
Rod-wall clearance	0.135"	Hydraulic diameter	0.474"
Heated length	72"		

Tests were run with all 9 rods electrically heated. The radial local peaking was either uniform or a peaking pattern typical of BWR conditions. A cross-sectional view of the test section is shown in Fig.A-8.1, indicating the corner, side, and center subchannels. One of the unique features of the facility is that provisions are made for bringing static and differential pressure lines at the same axial location but for different subchannels. To measure the flow in any given subchannel, that subchannel is isolated at some point from the rest of the channel. The subchannel flow, also referred as sample flow as shown in Fig. A-8.2, can then be taken through special ducting to another point outside the test section, where both the flow rate and enthalpy can be measured. Flow splinters made of thin metal sheets are used to separate and isolate flow of a subchannel at the end of the heated length. Such an isolated flow is guided through a tube before passing out the test section flange and entering a heat exchanger (calorimeter), Fig. A-8.2. The condensed flow is monitored by a turbine flow meter for subchannel flow measurement.

The sample enthalpy was determined by a heat balance on the calorimeter. For this purpose, the cooling water flow and temperature rise are carefully measured to provide as accurate energy information as possible. The outlet thermocouples are inserted beyond a right-angle bend in the piping to ensure good mixing in the water. Pressure drop measurements were also made during both single- and two-phase tests. All pressure drop measurements were corrected-for the hydrostatic head in the pressure tap lines based on the average density of water between the relevant pressure taps.

The ranges of test conditions include,

Single-phase (cold) mass flux	0.311 - 2.273×10^6 lbm/ft^{2}hr
Two-phase mass flux	0.372 - 1.180×10^6 lbm/ft^{2}hr
Pressure	1100 - 1200 psi
Rod Temperature	not measured
Average heat flux	0.219 - 0.797×10^6 Btu/ft^{2}hr
Exit quality	3.1% - 44.4%
Δh_{sub}	290 - 533 Btu/lbm
Flow regimes	Liquid 1-ϕ, bubbly, transition, annular

Instrumentation and Data from Tests

The heater rods were not instrumented with thermocouples. Thus, little local heat transfer information could be obtained. Neither was any visualization view port provided, such that the identification of flow regimes was based on empirical correlations from the state of local quality. Since the heater rods were sufficiently cooled under the normal BWR operating conditions and the issues of DNB and LOCA/reflood were not addressed, radiation heat transfer was not a important factor. However, flow and enthalpy distributions among the subchannels that are unique to BWR conditions were carefully measured and addressed. The tests were able to measure flow, enthalpy, and derive local quality in each individual subchannel. Thus the facility can yield some significant information on the heterogeneous flow core, of which the cross flow phenomenon is of importance.

While the heater rods were uniformly heated in the axial direction, the radial power distribution was controlled by peaking the individual transformers. Thus the flow, enthalpy, and

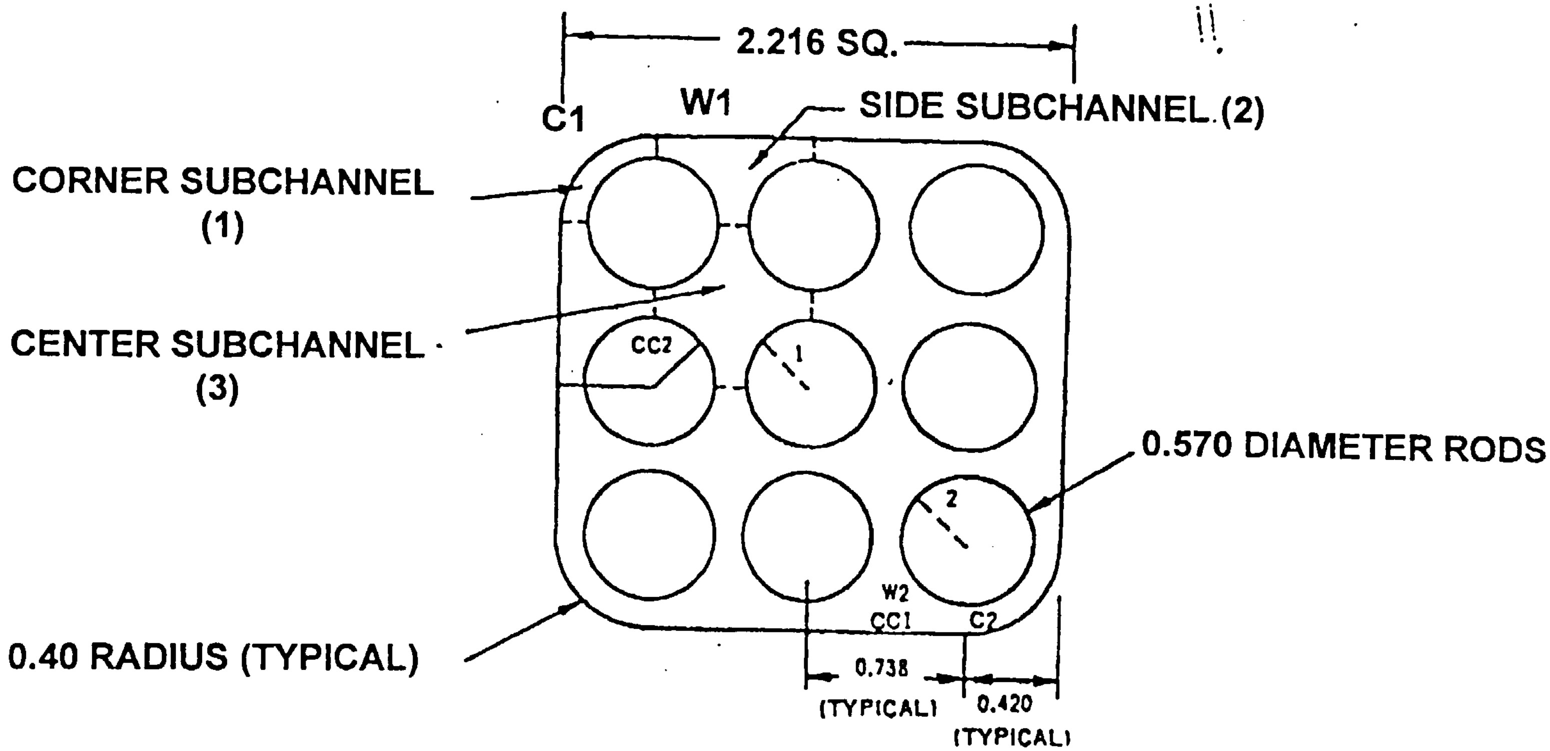

SECTION "A-A
(NOTE SPLITTER POSITIONS FOR THE VARIOUS SUBCHANNELS)

Figure A-8.1 Positions of Pressure Taps for Setting Isokinetic Conditions

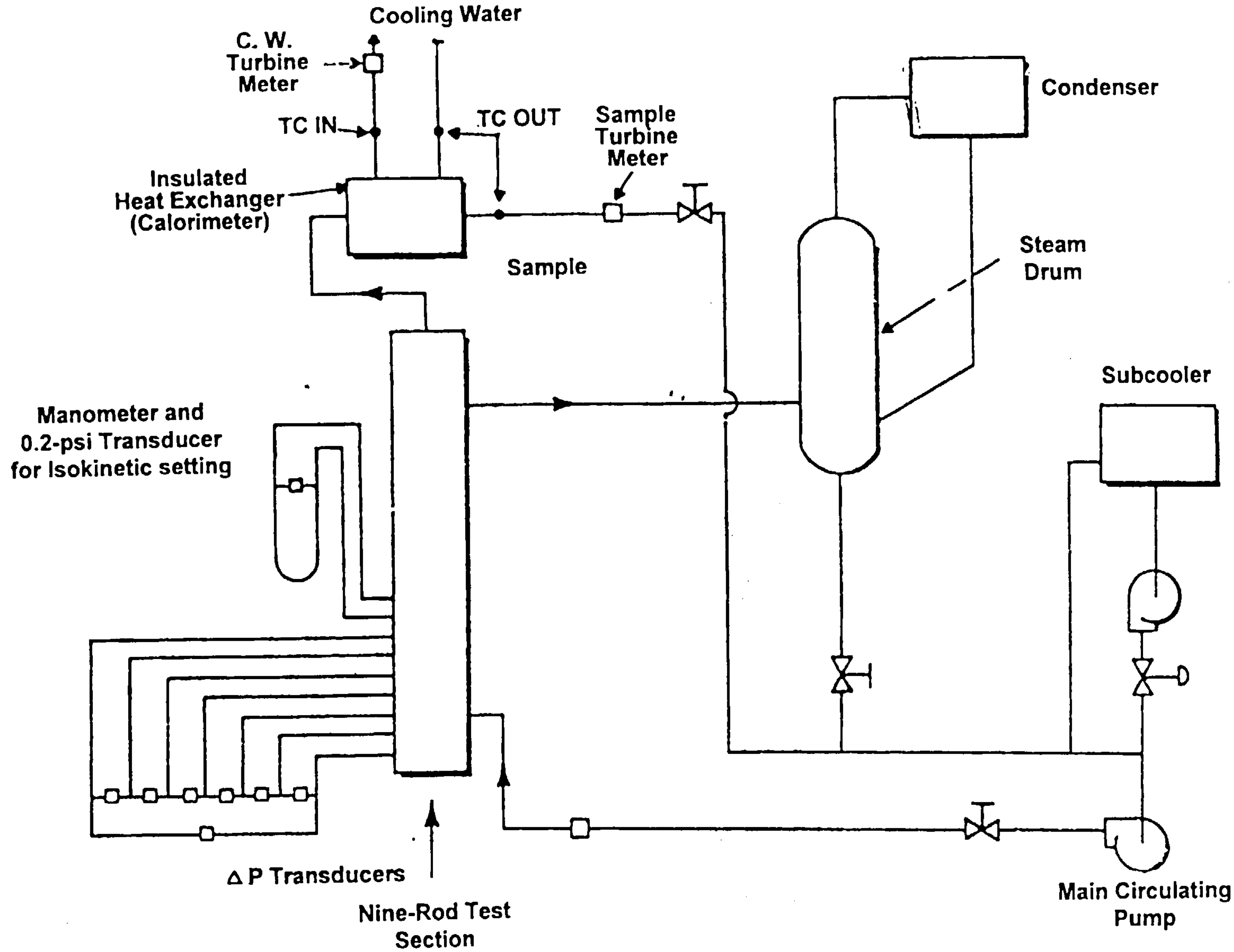

Figure A-8.2 Schematic of Loop Showing Sampling Circuit quality distributions across the subchannels due to radial power peaking were also unique output of the facility.

Pressure drop data for single- (cold) and two-phase flow tests were obtained for frictional loss correlation. At the same axial locations, cross-flow phenomenon (between subchannels) was interpreted from the pressure differential between subchannels (non-isokinetic cases).

Conclusion

Subchannel test data were taken for a 9-rod bundle in typical BWR operating conditions. In general the following observations are valid:

1. The comer subchannel runs a mass flux and quality below the bundle average values.
2. The side subchannel has mass flux and quality approximately equal to or slightly less than the bundle average.
3. The center subchannel has both mass flux and quality above the bundle average values.
4. There is an observable, though somewhat inconsistent, tendency for the subchannels to approach bundle average condition in the regions of slug-annular flow-regime transition.
5. The effect of heat flux on subchannel enthalpy distribution was small for low flows, but showed a strong effect at the high flows.
6. The effect of the bundle average mass flux on subchannel mass flux distribution was to increase the mass flux in the comer and center subchannels, and decrease the mass flux in the side subchannels, as the bundle average mass flux was increased.
7. The effect of heat flux on subchannel mass flux distribution was to decrease the mass flux in the comer subchannel but leave the mass flux in other subchannels relatively unchanged.
8. The adiabatic single-phase friction factor for the clean 9-rod bundle under consideration was slightly higher than the smooth-tube friction factor, for all Reynolds numbers.
9. The two-phase friction drop multiplier showed only a very minor flow effect, and the data was well correlated by the classical Martinelli-Nelson curve.

Although this facility and work improved our understanding of subchannel flow and energy diversions in typical BWR conditions, it did not address the heat transfer phenomena associated with post-LOCA reflood conditions, in which the quench front progression, froth region propagation, and dispersed flow film boiling are of major interest. However, the following relevant heat transfer information may be assessed against the RBHT PIRT:

Table 1
Assessment of General Electric 9-Rod Bundle Tests to RBHT PIRT:
Subcooled and Saturated Boiling in The Core Component Below the Quench Front

Process/Phenomena	Ranking	Basis	GE 9-Rod Bundle Tests
<u>Subcooled Boiling</u>	L	A significant variation in the subcooled boiling H. T. coefficient will not effect the PCT uncertainty since rod is quenched.	Heater rod temperatures are not measured, but subchannel flow, temperature, quality are measured.
• Effects of Geometry, P/D, De	L	Boiling effects in rod bundles have been correlated for our P/d, De range with acceptable uncertainty.	P/D = 1.295 for tests.
• Effects of Spacers	L	Locally enhanced H. T.; Correlations/Models are available, acceptable uncertainty.	Subchannel flow and enthalpy should be redistributed by the spacers, but was not investigated.
• Effects of Properties	L	Data exists for our Range of Conditions, little uncertainty.	No heater rod temperature measurement
<u>Saturated Boiling</u>	L	Similar to subcooled boiling, data is available for our P/D, De range. The uncertainty of Saturated Boiling H. T. coefficient will not significantly impact the PCT since rod is quenched.	Heater rod temperatures are not available, but subchannel flow, temperature, and quality are measured.
• Effects of Geometry, P/D, De	L	Data exists in the range of P/D, De with acceptable uncertainties.	P/D = 1.295.
• Effects of Spacers	L	Locally enhanced H. T., Correlations/ Models are available, with acceptable uncertainty.	Subchannel flow and enthalpy should be redistributed by the spacers, but was not investigated.
• Effects of Properties	L	Data exists for our range of conditions, little uncertainty.	No heater rod temperature measurement.
<u>Decay Power</u>	H	Source of energy for rods, boundary condition for the test.	Test were conducted at BWR operating power, not at decay power.

Table 2
Assessment of General Electric 9-Rod Bundle Tests to RBHT PIRT for High Ranked BWR Core Phenomena

Process/Phenomena	Basis	General Electric 9-Rod Bundle Tests
Core		
• Film Boiling	PCT is at the end of the heated length, but not measured.	Not applicable
• Upper Tie Plate CCFL	Hot Assembly is in co-current up flow above CCFL limit.	Not applicable
• Channel-bypass Leakage	Flow bypass will help quench the BWR fuel assembly core.	Subchannel cross flow observed
• Steam Cooling	A portion of the Dispersed Flow Film Boiling Heat Transfer.	Not applicable
• Dryout	Transition from nucleate boiling and film boiling.	Not applicable
• Natural Circulation Flow	Flow into the core and system pressure drops.	Not applicable
• Flow Regime	Determines the nature and details of the heat transfer in the core.	Bubbly, transitional, and annular flows identified from flow-regime map.
• Fluid Mixing	Determines the liquid temperature in the upper plenum for CCFL break down.	Not applicable
• Fuel Rod Quench Front	Heat release from the quench front will determine entrainment to the upper region of the bundle.	Not applicable
• Decay Heat	Energy source for heat transfer	Not applicable
• Interfacial Shear	Effects the void fraction and resulting droplet and liquid velocity in the entrained flow.	Not applicable
• Rewet: Bottom Reflood	BWR hot assembly refloods like PWR.	Not applicable
• Rewet Temepratures	Determines the quench front point on the fuel rod.	Not applicable
• Top Down Rewet	Top of the hot assembly fuel will rewet in a similar manner as PWR.	Not applicable
• Void Distribution	Gives the liquid distribution in the bundle.	Not directly measured, however, the enthalpy distribution of the 9-rod bundle was measured.
• Two-Phase Level	Similar to quench front locations, indicates location of nucleate and film boiling.	Identified from the flow-regime map.

Appendix A-9, Literature Review

Test Facility Name: PNL LOCA Simulation Program at NRU Reactor, Chalk River, Canada

Dates When Tests Were Performed: October 1980 - November 1981

References:

R19. C.L.Mohr et al, "Data Report for thermal-Hydraulic Experiment 2 (TH-2)", NUREG/CR-2526, PNL-4164, November 1982

R20. C.L.Mohr et al, "Data Report for thermal-Hydraulic Experiment 3 (TH-3)", NUREG/CR-2527, PNL-4165, March 1983

Availability of Data:

Graphical data demonstrating fuel cladding temperature control using the preset reflood flow and temperature feedback. Photographs of guard and test fuel used are shown. Data in graphical form on the test assembly temperatures, cooling flow and the neutronic environment are also presented. Data is available in both SI and British units. Microfiche of the entire report is available with NTIS.

Test Facility Description, Types of Tests:

The TH-2 included 14 tests. A schematic of the test train used is depicted in figure A-9.1. The fuel assembly consists of 6 by 6 segment of a 17 by 17 PWR fuel assembly with four corner rods removed providing a basic fuel array of 32 rods. The 20 guard rods in the outer row reduced the heat net heat transfer from the inner test rods during the test. All the inner 12 test fuel rods were arranged in cruciform pattern. All the 32 unpressurized fuel rods were filled with helium. The core configuration is shown in figure A-9.2.

The following table gives the test fuel rod design variables.

Cladding Material	Zircaloy-4
Cladding Outside Diameter (OD)	0.963 cm (0.379 in)
Cladding Inside Diameter (ID)	0.841 cm (0.331 in)
Pitch (rod to rod)	1.275 cm (0.502 in)
Fuel pellet OD	0.826 cm (0.325 in)
Fuel pellet length	0.953 cm (0.375 in)
Active fuel length	3.66 m (12 ft)

The TH-2 experiment included a preconditioning phase and 14 successive tests, each having a pretransient and a transient phase. The average test assembly fuel rod power during preconditioning was ~18.7 kW/m (5.7 kW/ft) with the U-2 loop providing water cooling, this was used for the TH-3 experiment too. System loop pressure was held at 8.62 MPa (1250 psia).

The pretransient stage for the TH-3 tests was conducted with the steam cooling provided by the U-1 loop at a mass flow rate of ~0.379 kg/s (~3000 lbm/hr) and a reactor power of ~7.4 MW. This enabled the total assembly power to remain constant, even though the peak cladding temperature varied from test to test. The transient phase of TH-3 commenced when the steam coolant flow was reduced from ~3000 lbm/hr to 0, with the reactor power being maintained at ~7.4 MW. No preconditioning operation was conducted for the TH-3 experiment.

The test conditions measured during experiment are described in the tables below. Table A-9.1 and A-9.2 represent conditions for TH-2 experiment and TH-3 experiment respectively.

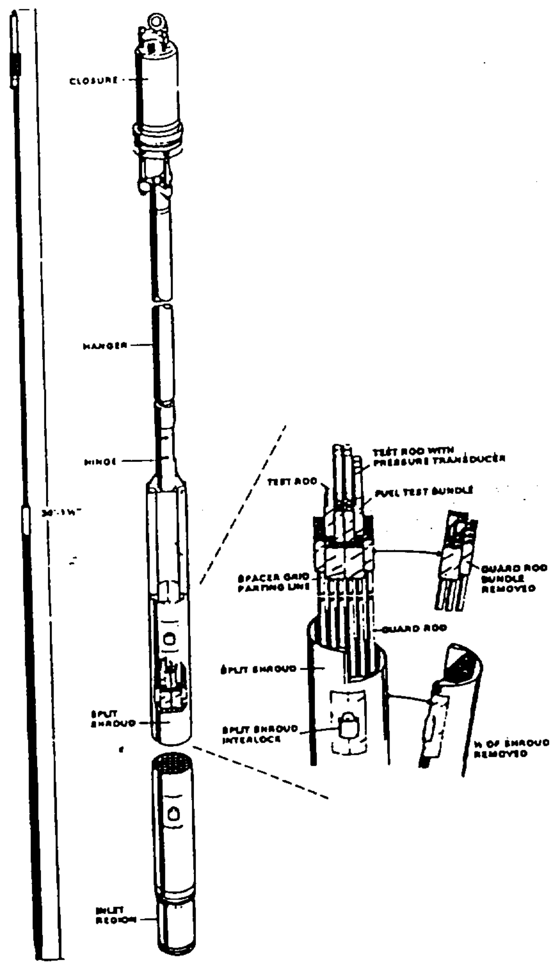

Figure A-9.1 Schematic of NRU Loss-of-Coolant Accident Test Train

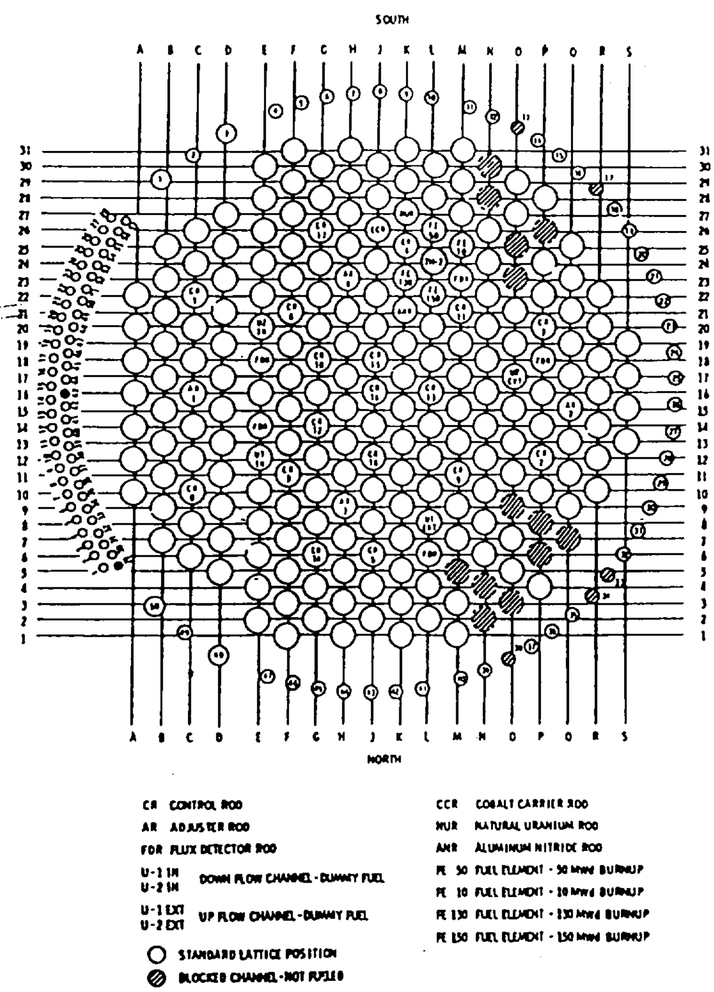

Figure A-9.2 NRU Reactor Core Configuration

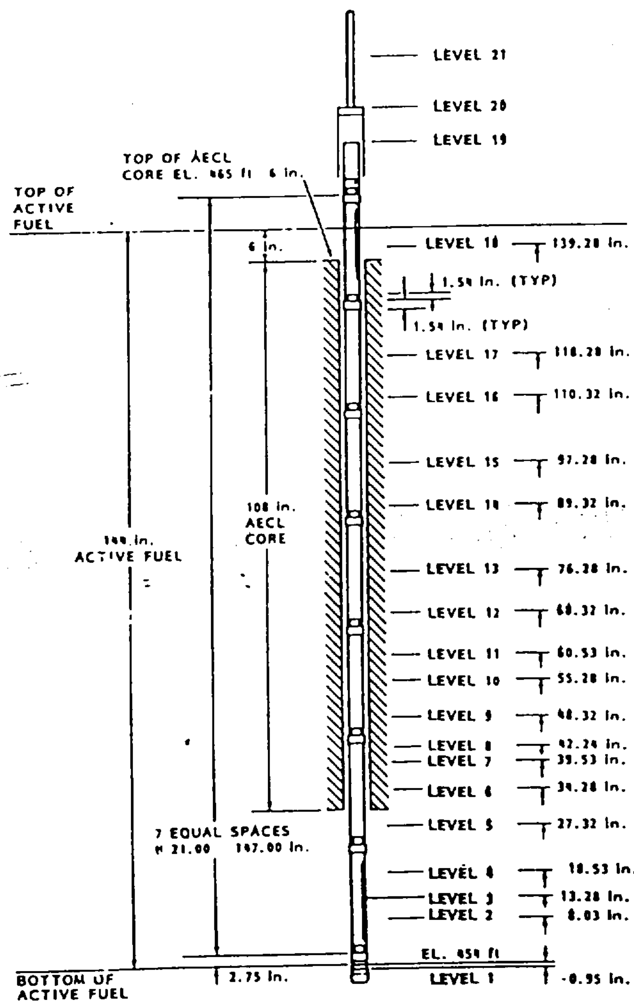

Figure A-9.3 Instrumentation Levels in the TH-2 Test Assembly

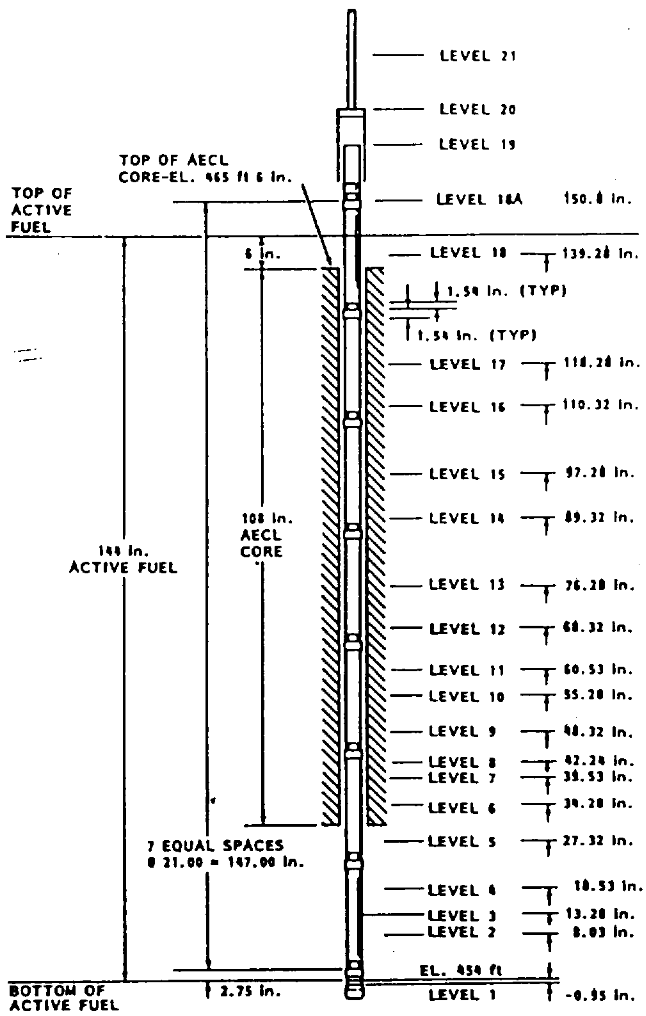

Figure A-9.4 Instrumentation Levels in the TH-3 Test Assembly

Table A-9.1: Measured Conditions for the TH-2 Experiment (1)

Parameter	Preconditioning	Reflood Calibration	Transient TH-2.01	Transient TH-2.02	Transient TH-2.03	Transient TH-2.04	Transient TH-2.05	Transient TH-2.06
Reactor power, MW	127	0	-7.4	-7.4	-7.4	-7.4	-7.4	-7.4
Test assembly power, kW		0						
Coolant	U-2 water	U-1 steam/ reflooding	U-1 steam/re-flooding	U-1 steam/re-flooding	U-1 steam/re-flooding	U-1 steam/re-flooding	U-1 steam/re-flooding	U-1 steam/re-flooding
Coolant flow, kg/s (lbm/h)	0 to 16.30 (0 to 129,400)	0.378 (3000)	0.380 (3010)	0.383 (3040)	0.382 (3030)	0.382 (3030)	0.382 (3030)	0.381 (3020)
Reflood delay, s	NA	0	NA					
Reflood rates, m/s (in/s)	NA	0.0508 (2.0), 0.0254 (1.0), 0.0508 (2.0)						
Pretransient cladding temperatures, K (° F)	NA	NA	707 (813)					
Peak cladding temperature (PCT), K(° F)	700 (800)	433 (320)	1005 (1350)					
Reactor conditional trip criteria (PCT), K(° F)	NA	NA	978 (1300)	1103 (1525)	1103 (1525)	1144 (1600)	1144 (1600)	1144 (1600)
Bundle quench time, (a) s								
Type of test	NA	Reflood	Adiabatic	Transient	Transient	Transient	Transient	Transient
Type of reflood control			NA	LCS (b)	DACS(c) after 85 s	DACS after 85 s	DACS after 85 s	DACS after 85 s

Table A-9.1: Measured Conditions for TH-2 Experiment (continued)

Parameter	Transient TH-2.07	Transient TH-2.08	Transient TH-2.09	Transient TH-2.10	Transient TH-2.11	Transient TH-2.12	Transient TH-2.13	Transient TH-2.14
Reactor power, MW	-7.4	-7.4	-7.4	-7.4	-7.4	-7.4	-7.4	-7.4
Test assembly power, kW						138.7	143.8	142.8
Coolant	U-1 steam/ reflooding	U-1 steam/ reflooding	U-1 steam/ reflooding	U-1 steam/ reflooding	U-1 steam/ reflooding	U-1 steam/ reflooding	U-1 steam/ reflooding	U-1 steam/ reflooding
Coolant flow, kg/s (lbm/h)	0.383 (3040)	0.378 (3000)	0.379 (3010)	0.378 (3000)	0.378 (3000)	0.378 (3000)	0.378 (3000)	0.378 (3000)
Reflood delay, s							NA	
Reflood rates, m/s (in/s)						unable to read from paper	0	unable to read from paper
Pretransient cladding temperatures, K (F)						743 (877)	783 (869)	737 (867)
Peak cladding temperature (PCT), K(F)						1174 (1653)	1013 (1364)	1274 (1834)
Reactor condi tional trip crite ria (PCT), K(F)	1144 (1600)	1144 (1600)	1144 (1600)	1144 (1600)	1144 (1600)	1144 (1600)	1144 (1600)	1144 (1600)
PCT turnaround time, (a) s						273	33	244
Bundle quench time, (a) s						306	NA	338
Type of test	Transient	Transient	Transient	Transient	Transient	Transient	Adiabatic	Transient
Type of reflood control	DACS after 95 s	DACS after 95 s	DACS after 95 s	DACS after 95 s	DACS after 95 s	DACS after 95 s	NA	DACS after 95 s

(1) TH-2.12 and TH-2.14 were the principal

(a) Time after initiation of transient.

(b) LCS-Loop Control System,

(c) DACS - Data Acquisition and Control System

Table A-9.2: Measured Conditions for the TH-3 Experiment

Parameter	Preconditioning	Reflood Calibration	Test TH-3.01	Test TH-3.02	Test TH-3.03
Reactor power, MW	127	0	7.4	7.4	7.4
Test assembly power, kW		0	141.5	134.6	133.5
Coolant	U-2 water	U-1 steam/ reflooding	U-1 steam/ reflooding	U-1 steam/ reflooding	
Coolant flow, kg/s (lbm/h)	0 to 16.30 (0 to 129,400)	0.0254, 0.508 (1.0, 2.0)	0.379 (3010)	0.379 (3004)	0.379 (3009)
Reflood delay, s	NA	NA	NA	9	3
Reflood rates, m/s (in/s)	NA	NA	NA	0.0823(3.24) for 8 s 0.0549(2.16) for 40 s 0.0366(1.44) for 16 s 0.0244(0.96) for 28 s 0.127 (0.5) for 162 s	0.0828(3.26) for 8 s 0.0574(2.26) for 40 s 0.0371(1.46) for 16 s 0.0224(0.88) for 28 s 0.0124(0.49) for 18 s 0.0191(0.75) for 40 s 0.0097(0.38) for 96 s 0.0147(0.58) for 28 s 0.0102(0.4) for 130s
Pretransient cladding temperatures, K (° F)	NA	NA	723 (842)	723 (842)	717 (830)
Peak cladding temperature (PCT), K(° F)	700 (800)		1008 (1354.4)	1318 (1912)	1283 (1850)
Reactor conditional trip criteria (PCT), K(° F)	NA	NA	978 (1300)	1172 (1650)	1200 (1700)
PCT turnaround time, [a] s	NA	NA	35	193	257
Bundle quench time, [a] s	NA	NA	NA	277	407
Type of test	NA	Reflood	Adiabatic	Transient	Transient
Type of reflood control	NA	LCS [b]	NA	DACS [d] after 90 s	DACS after 90 s

(a) Time after initiation of transient,

(b) LCS-Loop Control System,

(c) DACS - Data Acquisition and Control System

Table 5

Assessment of NRU Inpile Reflood Data to RBHT PIRT: Dispersed Flow Region for Core Component

Process/Phenomena	Ranking	Basis	NRU Inpile Reflood Data
Decay Power	H	Energy source which determines the temperature of the heater rods, and the energy removed by the coolant.	Known
Fuel Rod/Heater Rod properties, ρ, C_p, k	L	The exact properties can be modeled and stored energy release is not important at this time, environmentally.	Known properties and dimensions.
Dispersed Flow Film Boiling	H	Dispersed flow film boiling modeling has a high uncertainty which directly effects the PCT.	PCTs known for the tests.
Convection to superheated vapor	H	Principal mode of heat transfer as indicated in FLECHT-SEASET experiments[4]	Not determined
Dispersed phase enhancement of convective flow	H	Preliminary models indicated that the enhancement can be over 50% in source cases[13].	Not determined
Direct wall contact H.T.	L	Wall temperatures are significantly above T_{min} such that no contact is expected.	Not determined
Dry wall contact[12]	M	Iloje indicates that H.T. Mechanism is less important than vapor convection.	Not determined
Droplet to vapor interfacial heat transfer.	H	The interfacial heat transfer reduces the vapor temperature which is the heat sink for the wall heat flux.	Not determined
Radiation Heat Transfer to: • Surfaces • Vapor • Droplets	 M/H M/H M/H	This is important at higher bundle elevations (H) where the convective heat transfer is small since the vapor is so highly superheated. Very important for BWR reflood with sprays, and colder surrounding can. Large uncertainty.	May be estimated from the values of test rod temperatures and the flow conditions

Table 5

Assessment of NRU Inpile Reflood Data to RBHT PIRT:
Dispersed Flow Region for Core Component (continued)

Process/Phenomena	Ranking	Basis	NRU Inpile Reflood Data
Gap heat transfer	L	Controlling thermal resistance is the dispersed flow film boiling heat transfer resistance. The large gap heat transfer uncertainties can be accepted, but the fuel center line temperature will be impacted.	Gap existed and gap conductance can be estimated.
Cladding Material	L	Cladding material in the tests is Inconel which has the same conductivity as Zircaloy, nearly same temperature drop will occur.	Used Zircaloy-4.
Reaction Rate	M	Inconel will not react while Zircaloy will react and create a secondary heat source at very high PCTs, zirc reaction can be significant.	Should exist because zircaloy is used.
Fuel Clad Swelling/Ballooning	L	Ballooning can divert flow from the PCT location above the ballooning region. The ballooned cladding usually is not the PCT location. Large uncertainty.	This effect was modeled in the tests.

Table 8

Assessment of NRU Inpile Reflood Data to RBHT PIRT for High Ranked BWR Core Phenomena

Process/Phenomena	Basis	NRU Inpile Reflood Data
Film Boiling	PCT is determined in film boiling period.	PCT is determined in the tests.
Upper Tie Plate CCFL	Hot Assembly is in co-current upflow above CCFL limit.	Not simulated
Channel-bypass Leakage	Flow bypass will help quench the BWR fuel assembly core.	Not simulated
Steam Cooling	A portion of the Dispersed Flow Film Boiling Heat Transfer	Simulated but overall heat transfer was measured.,
Dryout	Transition from Nucleate boiling and Film boiling.	Quench front location not known
Natural Circulation Flow	Flow into the core and system pressure drops.	Not applicable
Flow Regime	Determines the nature and details of the test transfer in the core.	Dispersed flow film boiling regime
Fluid Mixing	Determines the liquid temperature in the upper plenum for CCFL breakdown.	Not applicable
Fuel Rod Quench Front	Heat release from the quench front will determine entrainment to the upper region of the bundle.	Simulated with nuclear rods
Decay Heat	Energy source for heat transfer.	Simulated
Interfacial Shear	Effects the void fraction and resulting droplet and liquid velocity in the entrained flow.	Not measured
Rewet: Bottom Reflood	BWR hot assembly refloods like PWR.	Measured
Rewet Temperature	Determines the quench front point on the fuel rod.	Measured
Top Down Rewet	Top of the hot assembly fuel will rewet in a similar manner as PWR.	Not measured
Void Distribution	Gives the liquid distribution in the bundle.	Not measured
Two-Phase Level	Similar to the quench front location, indicates location of nucleate and film boiling.	Measured

Instrumentation and Data from Tests:

The instrumentation for the TH-2 experiment included: 24 self-powered neutron detectors(SPNDs), 115 fuel rod TCs, 18 steam probe TCs and 4 closure head TCs. The instrumentation was located at 21 elevations along the test train assembly. These are shown in the figure A-9.3.

The instrumentation for the TH-3 experiment included: 24 self-powered neutron detectors(SPNDs), 69 fuel rod TCs, 4 hanger TCs and 4 closure head TCs. The instrumentation was located at 22 elevations along the test train assembly. These are shown in the figure A-9.4.

Thermal-hydraulic data was obtained by turbine flowmeters and TCs. Local coolant temperatures were measured with steam probe TCs that protruded into the coolant channel and with TCs attached to the shroud. Azimuthal temperature variations were measured by TCs located at the fuel centerline and attached to the inside of the cladding surface. The cladding temperature was monitored by cladding TCs that were spot welded to the interior cladding surface.

The SPNDs provided neutron flux measurements within the fuel bundle. These measurements were made at opposite corners of the stainless steel shroud at several elevations, ranging from 13.3" to 139.3" above the bottom of the fuel column. The SPNDs provide a measure of the radial neutron flux gradient and neutron flux distribution over the vertical axis of the test assembly. These could also detect the coolant density variations (through flux changes) associated with the quench front that passed each SPND during the reflood phase of the transient. The instrument signals were monitored on a real-time basis with the DACS (Data Acquisition and Control System). The recorded data characterized the coolant flow rates, temperature, neutron flux and operating history.

The reflood flow measurement system included a Fisher-Porter turbine flowmeter in the high flow rate line and a series connected Barton and Fisher-Porter turbine flowmeters in the parallel low flow rate line. Steam probe temperature history provided independent measurements of the reflood coolant level in the test assembly.

Conclusions:

These tests give the average fuel rod cladding temperatures during preconditioning, pretransient and transient phases. Also available are the test coolant and shroud temperatures. However, these tests do not have enough data to make code model changes without the potential for compensating errors. Many of the heat transfer phenomena such as droplet to vapor interfacial heat transfer, dry wall contact are not simulated, though overall wall heat transfer is measured. Therefore, while these tests are useful in simulating the overall reflood heat transfer, they provide limited data which can be used to assess the reflood phenomena which was identified in the PIRT table for the RBHT program.

Appendix A
Literature Review

Appendix A10: ACHILLES Reflood Heat Transfer Tests

Dates when Tests Were Performed: 1989 - 1991

References:

R21 Denham, M. K., Jowitt, D., and K. G. Pearson, "ACHILLES Unballooned Cluster Experiments, Part 1: Description of the ACHILLES Rig, Test Section, and Experimental Procedures", AEEW-R2336, November 1989, Winfrith Technology Centre (Commercial in Confidence).

R22 Denham, M. K., and K. G. Pearson, "ACHILLES Unballooned Cluster Experiments, Part 2: Single Phase Flow Experiments", AEEW-R2337, May 1989, Winfrith Technology Centre (Commercial in Confidence).

R23 K.G. Pearson and M. K. Denham, " ACHILLES Unballooned Cluster Experiments, Part 3: Low Flooding Rate Reflood Experiments", AEEW-R2338, June 1989, Winfrith Technology Centre (Commercial in Confidence).

R24 K.G. Pearson and M.K. Denham, "ACHILLES Unballooned Cluster Experiments, Part 4: Low Pressure Level Swell Experiments", AEEW-R2339, July 1989, Winfrith Technology Centre (Commercial in Confidence).

R25 Dore, P and M.K. Denham, "ACHILLES Unballooned Cluster Experiments, Part 5: Best Estimate Experiments", AEEW-R2412, July 1990, Winfrith Technology Centre, (Commercial in confidence).

R26 Dore, P. and D.S. Dhuga, "ACHILLES Unballooned Cluster Experiments, Part 6: Flow Distribution Experiments", AEA-RS-1064, December 1991, Winfrith Technology Centre (Commercial in Confidence).

Availability of Data

The ACHILLES experiments were performed as part of the safety case for PWR's in the United Kingdom. The ACHILLES tests were funded by the Central Electricity Generating Board (CEGB) and were performed by the United Kingdom Atomic Energy Authority (UKAEA) at the Winfrith Laboratories. The data does have some release restrictions and is not unlimitedly available to the general public. However, more recently, data has been released to interested parties and governments as part of cooperative data exchange. Some of the data was used for an International Standard Problem. Westinghouse has been able to obtain some of the data directly from the CEGB provided that reference was given to the CEGB in the reports prepared by Westinghouse. Therefore, the data should be available to the Nuclear Regulatory Commission.

Test Facility Description, Types of Tests

The ACHILLES tests were specifically conducted to support the PWR (Sizewell) safety case in the United Kingdom in the late 1980's and early 1990's. Since these tests were performed after the FLECHT-SEASET tests, the authors had made some improvements which are of value for the current Rod Bundle Heat Transfer Program. The testing consisted of specific test series which were used to examine specific safety issues and safety analysis issues. Specifically, experiments were performed to examine:

Low reflooding rate behavior similar to FLECHT-SEASET and FLECHT,

Best-Estimate Reflood tests were performed to assess a realistic LOCA transient,

Single-phase flow distribution tests were performed to examine the flow uniformity and single-phase heat transfer within the rod bundle,

Low-pressure level swell experiments were also performed to validate drift flux/void fraction relationships.

There were also gravity feed Reflood tests with loop resistance simulated, and variable injection Reflood tests which simulated evaluation model type system response.

There were also oscillating inlet flow injection tests.

One of the purposes of the ACHILLES test program was to examine the heat transfer performance of a fuel assembly with high blockages caused by the swelling of the zirc cladding (sausage ballooning problem). This issue had been resolved in the US but it still remained as an open item in the United Kingdom safety case for the PWR. The reports given in the review only discuss the unblocked or Unballooned configuration of the test program. There is a continuation of the ACHILLES test program which specifically examines flow blockages of up to 80% to address the clad swelling issues during a LOCA. These tests will not be discussed here.

The ACHILLES bundle is shown in Figure A-10.1 and contains a total of 69 heater rods of 9.5 mm (0.374-inches) in diameter on a square pitch of 12.6 mm (0.496-inches) and have 3.66 m (12-feet) of heated length. ACHILLES used production Inconel mixing vane grids supplied by Westinghouse. All rods were heated in ACHILLES such that there was no simulation of the guide tube thimbles in the bundle such as in the FLECHT-=SEASET experiments. However, experiments were performed in ACHILLES to examine the effects of increased surface-to-surface radiation heat transfer by performing tests with selective unpowered heater rods.

Figure A-10.2 indicates the flow loop schematic for the ACHILLES facility. There was ample flexibility built into the test facility such that both single phase, two-phase, forced Reflood injections could be performed as well as, oscillatory injection and gravity injection tests with little facility modifications. The Test bundle was contained within a circular shroud of wall thickness of 6.5 mm (0.26-inches) and a pressure capability of 6 bars (approximately 90 psia). There were no filler rods in the test bundle design which resulted in excess flow area for the square array of rods within the circular housing. To compensate for the excess flow area and to better simulate an infinite array of fuel rods, the ACHILLES housing was heated with zonal heaters which had a total power of 46 kw. These heaters provided a similar axial temperature distribution as the heater rods.

The heater rods were manufactured by RAMA corporation, the same company that made the FLECHT-SEASET heater rods. A chopped cosine power shape with a peak-to-average of 1.4 was used. These rods used Inconel cladding, and could have up to six thermocouples per rod installed. The axial distribution of the heater rod thermocouples and the other instrumentation is shown in Figure A-10.3. One unique feature of the ACHILLES bundle is that the instrumentation plan was developed with the idea of examining the heat transfer effects of the spacer grids both upstream and downstream of the grids.

The grids used were Inconel production 17x17 spacer grids with mixing vanes. These grids were instrumentated with 0.5 mm (0.20-inch) thermocouples which were attached to the grids using Inconel shim stock which was spot-welded to the spacer. The attachment method was designed to minimize the flow disturbance and the effects of the thermocouple lead leading to early grid rewet. Each grid had two thermocouples attached to the spacer at the top and lower edges at different radial positions. The data indicates that this installation method worked well and only one-grid thermocouples failed.

The vapor temperature was measured in the rod bundle at different axial location, up steam and down stream of spacer grids using 1 mm (0.040-inches) thermocouples which were swagged to a tip size of 0.5 mm (0.020-inches). There is an uncertainly analysis given in the report which indicates that f or the conditions used in the ACHILLES tests, the vapor temperature uncertainty is only 13 ^{0}C or 23.4 ^{0}F which is consistent with the uncertainty which was derived in the FLECHT-SEASET program. It is mentioned in Reference 2 that the vapor temperature measurements did have an effect on the entrained droplets with the probe causing additional droplet breakup and slowing down of larger droplets. There is insufficient data presented to draw an independent conclusion of these effects.

There were additional pressure taps placed along the shroud such that the pressure drops across the spacer grids were obtained as well as the frictional pressure drop in the rod bundle section. The pressure drop information was used to infer void fraction, however, there was no frictional or acceleration pressure drop corrections to the data such that the void fractions given for ACHILLES are lower then those expected.

The shroud had windows at the mid-plane for photographic purposes with the view being through specific rows of heater rods. The windows were very small such that they could be heated by the rods during heat-up before each test. The windows were set back from the inside edge to avoid direct droplet impact which would have caused the window to wet. From the report, it appears that the windows would stay dry until the quench front was within the grid span where the windows were located. One could interpret this as having the top of the froth front approaching the window before the window wetted.

Tests were performed using a four-cylinder piston pump which superimposed an oscillating flow on the forced flooding rate. The period and magnitude of the flow and oscillation frequency could be adjusted for different sensitivity tests. The bi-directional flow probe showed reverse flow, but is not clear if "real" reverse flow occurred. One significant observation is that with oscillatory flow, the grids quickly rewet as compared to constant forced injection flow. The same situation occurred for initially high injection flows.

An improved photographic droplet diameter and velocity measuring technique was developed as part of the ACHILLES program in which a pulse of green light was shined into the open camera shutter, followed by a pulse of red light. The duration of each pulse was short and there was a fixed time between the two pulses. This approach produced two images of a droplet which were of different color such that the drop size and velocity could be inferred from the prints. The filming rate was 100 frames/sec, a clips of shots were taken during a given test. Two cameras were also able to focused on different subchannels such that a reasonable droplet distribution across the bundle could be determined. It was observed that the droplet flow was not uniform with more liquid in the outermost channel near the wall. The outermost channel has the larger hydraulic diameter and hence the greater steam flow as compared to the inner regions of the bundle which could explain the observed trend. The report included droplet distribution plots for selected tests.

The test matrix for the low flooding rate tests is given in Table A-10.1. One parameter to note is that they purposely controlled the power such that very high heater rod temperatures never occurred and the maximum temperatures were very similar. Details of the reference test and the effects for the different sensitivity tests is given in Reference 3. The temperature rise values were different. Table A-10.2 gives the test numbers for the droplet distribution experiments, Table A-10.3 gives the conditions for the air flow only single phase experiments, and Table A-10.3 gives the test numbers for the voidage distribution experiments. Each series of tests is discussed in Reference 2. The test matrix for the best-estimate or realistic Reflood tests is given in Table A-10-4 from Reference 5.

The authors did perform a similar analysis as in the FLECHT and FLECHT-SEASET tests in which the actual quality was calculated at the bundle cross sections where vapor measurements existed. The same or similar exist flow measurements were made in the ACHILLES tests as in the FLECHT and FLECHT-SEASET tests such that a bundle heat and mass balance could be written. However, the authors did not attempt to separate the radiation component from the total measured heat transfer such that their estimates of the convective dispersed flow film boiling heat transfer results in higher heat transfer coefficients then would be the case in the FLECHT and FLECHT-SEASET experiments. However, very similar trends were observed, with very low vapor Reynolds number flows and enhancement of the dispersed flow film boiling heat transfer above the single phase convection heat transfer limit for the same fluid conditions.

The effects of the spacer grids were analyzed and a correlation was suggested for the convective enhancement of the local heat transfer downstream of the grid. There were also some very informative plots of the vapor temperatures and the spacer grid temperatures which showed that when the grid quenches, the vapor temperature downstream of the grid decreases.

He axial distribution of the heater rod thermocouples gave an excellent indication of the quench front along the bundle. These authors did display their data more as axial plots for different time periods such that additional information good be obtained with fewer figures. Variable reflood rates, oscillatory flooding rates, and stepped flooding rates would easily quench the spacer grids and they remained wetted throughout the transient. The very high flooding rates also quenched the miniature thermocouples used to measure the vapor temperature. Some of these thermocouples could dry out later in the tests and would indicate the presence of superheated vapor.

The best-estimate tests had more favorable test initial conditions such that the heat transfer was higher and the bundle would quench more easily. The same or similar phenomena was observed in these tests excepting that the transients were shorter and the temperatures were lower.

Single-phase heat transfer and flow tests were also conducted using air as the fluid. A specially constructed hot film probe was used for the air velocity distribution which confirmed that a bypass effect was occurring in the ACHILLES bundle due to the large excess flow area located on the outside edge of the bundle between the heater rods and the shroud. Single-phase effects of the spacer grids were also determined and compared to a previous correlation. We need to verify the axial distribution of the Thermocouples in the RBHT test to make sure that we can detect the decaying heat transfer trend downstream of the spacer grids.

One of the more unique data obtained in the ACHILLES program is the droplet or liquid distribution across the bundle using the photographic technique. Again, this distribution is distorted and shows more liquid at the edge of the bundle where the steam mass flow is higher due to the increased bypass flow at this location. The opposite would be expected in an infinite bundle since the center rods would be hotter creating a thermal syphon which should result in increased entrainment.

Conclusions

The ACHILLES Reflood experiments potentially represent some of the best Reflood data available for computer code validation. However, a two-channel model which includes crossflow should be used to represent the inner region of the bundle which has the correct flow are per rod, while an outer channel would represent the outer region of the bundle where there is excess flow area. Also, the computer code would have to model the housing or shroud which also supplies energy to the fluid. Computer codes such as the TRAC- P series, and COBRA-TF and COBRA-TRAC have the ability to model these effects. However, the flow diversion, excess flow area, and housing heat release effects must be assessed as test distortions. Also, if they are first order effects, it will be difficult to determine what models in the candidate code need improving since the test distortions could mask the model requirements resulting in compensating error being introduced into the code.

There is some unique data from the ACHILLES tests which are not available from other tests such as the subchannel droplet distribution data, spacer grid loss coefficient data, instrumentated spacer grid and local fluid temperature data, along with very finely spaced heater rod thermocouple data which shows the heat transfer effects of the spacer grids and quench front. The differential pressure data was taken using small spans both between grids and across spacer grids. This data needs to be corrected for frictional pressure drop and acceleration pressure drop in order to be used for inferring the local void fraction. Once this is performed, the local heat transfer can then be correlated with the void fraction.

The tests cover a wide range of conditions which are equally applicable to evaluation model calculations as well as best-estimate Reflood conditions such that an ample set of data is available. Also the tests include oscillating inlet flow, stepped forced flooding rate tests, and gravity Reflood tests.

It is strongly recommended that these data be screened and selected ACHILLES tests be obtained from CEGB and added to the NRC data bank and analyzed with the TRAC-M code and COBRA-TF. These tests can also be used for comparison purposes with the Rod Bundle Heat Transfer Tests.

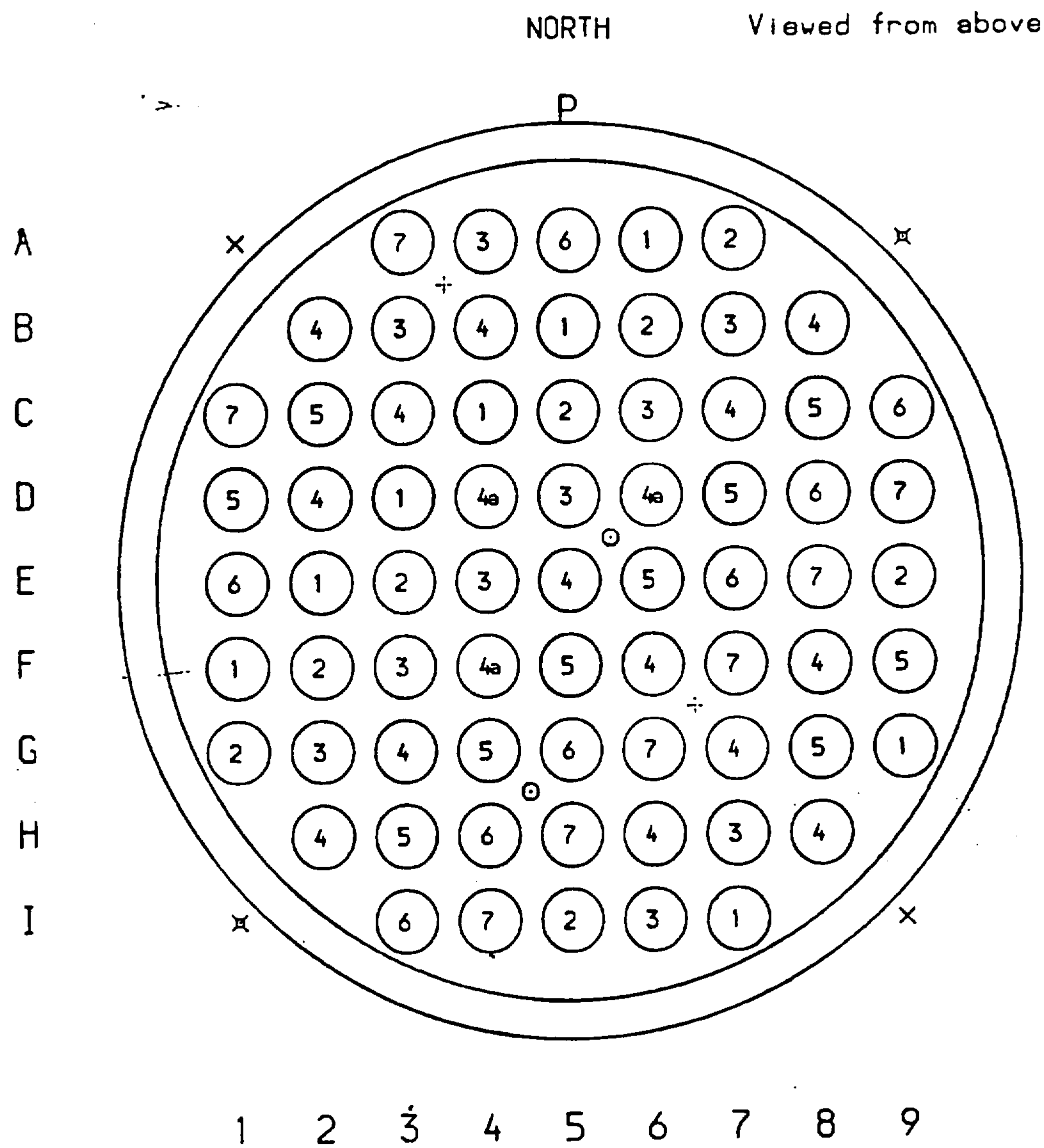

Key to Instrument Locations (for Axial Positions see Fig 3)

⊙ Instream and Grid Thermocouples
Grid Thermocouples :
bottom and top of grids 4 and 5
top of other grids only

÷ Instream Thermocouple at 2.17 m only

¤ Shroud Thermocouple at all Levels

X Shroud Thermocouple at 2.13 and 2.95 m only

P Pressure Tapping

Figure A-10-1
Cross Section of ACHILLES 69-Rod Bundle

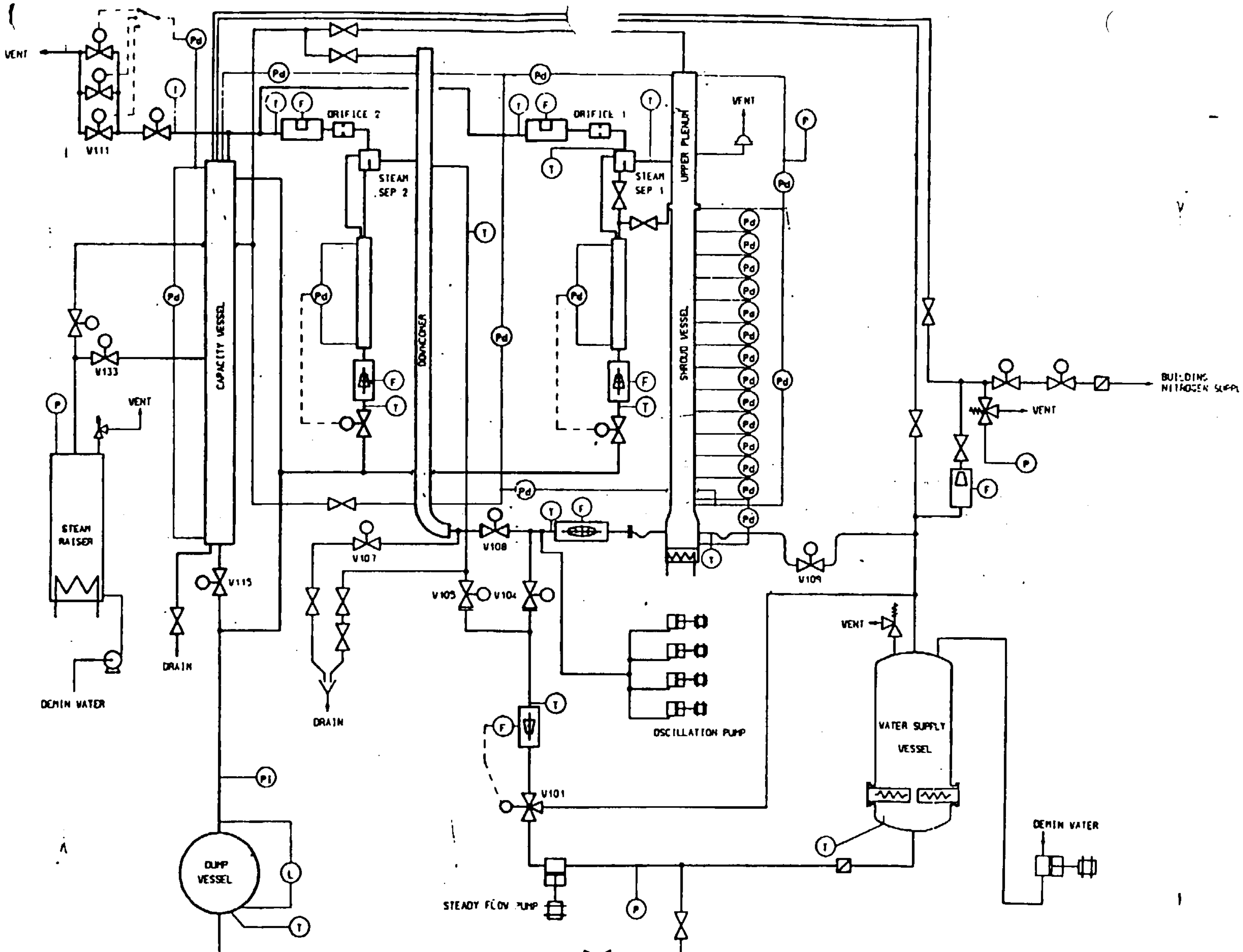

Figure A-10-2
Schematic of ACHILLES Flow Loop

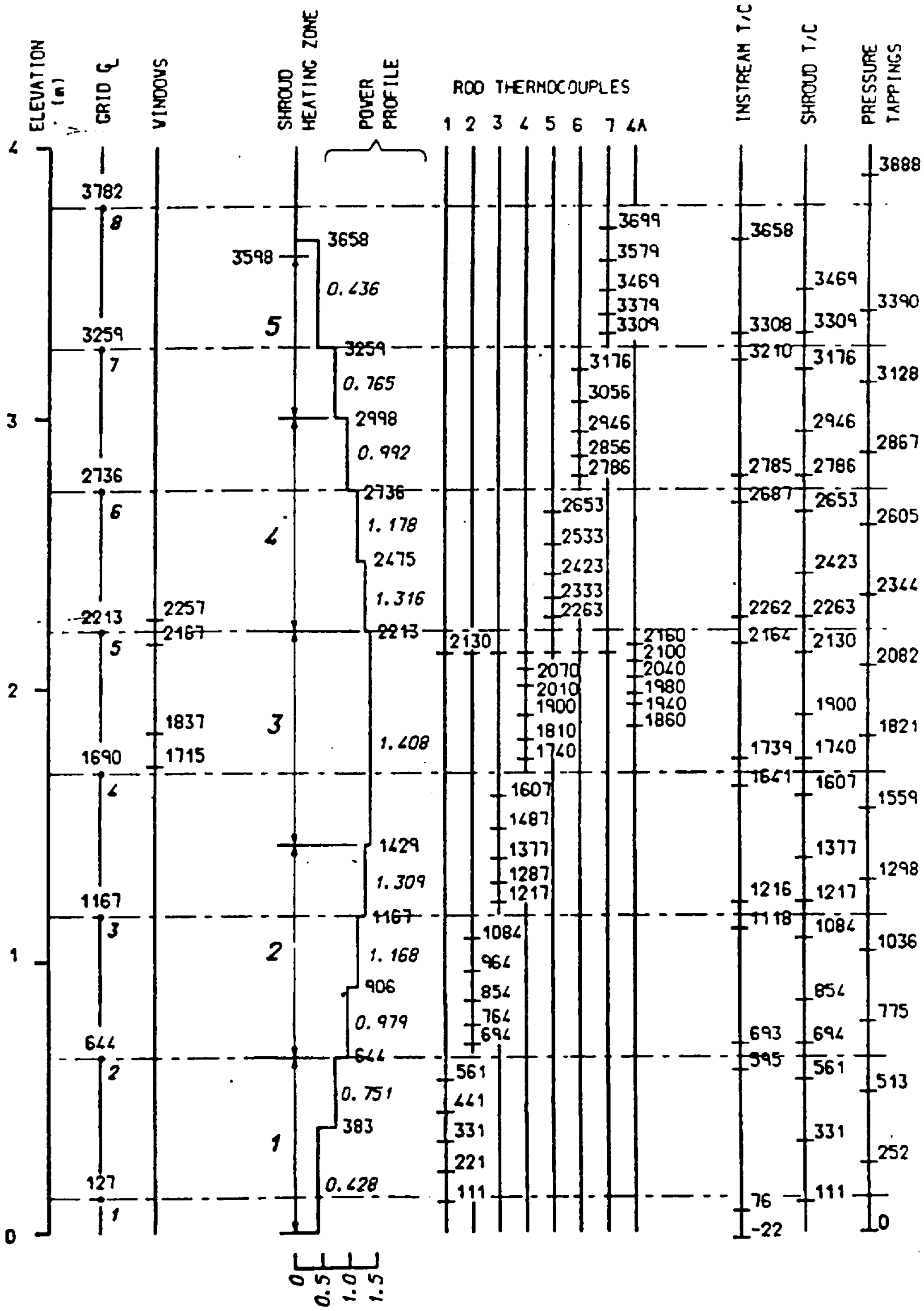

NOMINAL LOCATIONS IN mm ABOVE BOTTOM OF HEATED LENGTH

Figure A-10-3
Axial Locations in Test Section

Table A-10-1
Summary of Low Flooding Rate Reflood Experiments

Run Number	Description	Pressure bar	Steady Reflood Rate cm/s	Inlet Subcooling °C	Initial Rod Power KW	Initial Temp °C	Results at 2.13 m		Grid Centre Rewet Time		
							Max Temp (°C)	Rewet Time (s)	Grid 4 (s)	Grid 5 (s)	Grid 6 (s)
Forced Reflood											
A1R027	Medium Constant Power	2.4	2.0	28	2.0	662	879	418	120	189	207
A1R028	High Constant Power	2.1	2.0	22	2.5	654	964	606	121	283	452
A1R029	90% ANS + 2σ	2.1	2.0	24	3.9	651	1082	678	141	382	532
A1R030	Base Case (70% ANS + 2σ)	2.1	2.0	24	3.0	651	971	515	120	263	323
A1R032	50% ANS + 2σ	2.1	2.0	24	2.3	653	879	416	120	206	199
A1R033	Low Flow, Constant Power	2.1	1.0	22	1.5	654	960	589	206	416	608
A1R035	Maximum Flow	2.2	10.0	25	3.0	652	666	210	27	22	23
A1R036	Maximum Flow and Subcooling	2.1	10.0	55	3.0	649	682	154	32	24	24
A1R037	Low Flow, Decreasing Power	2.1	1.0	23	1.8	652	960	533	130	264	344
1R040	Varying Flow	2.1	Fig 56	23	3.0	648	889	571	9	3	3
A1R042	Base Case Repeat 1	2.1	2.0	23	3.0	653	974	525	125	240	304
A1R044	Low Pressure	1.4	2.0	24	3.0	652	987	687	136	312	450
A1R045	High Pressure	4.1	2.0	23	3.0	650	947	340	106	150	198
A1R046	Low Initial Temperature	2.1	2.0	23	3.0	505	878	453	90	143	91
A1R047	High Inlet Subcooling	2.1	2.0	53	3.0	653	984	460	113	183	288
A1R048	High Flow	2.1	4.0	24	3.0	654	801	355	32	31	18
A1R053	Base Case Repeat 2	2.1	2.0	24	3.0	653	974	522	96	160	272
A1R055	80% ANS + 2σ	2.1	2.0	24	3.4	655	1014	582	96	214	346
A1R056	60% ANS + 2σ	2.1	2.0	24	2.6	652	923	453	96	149	200
A1R059	4 Unpowered Rods	2.1	2.0	24	3.0	654	947	482	97	155	231
A1R061	4 Unpowered Rods, Low Shroud Temp	2.1	2.0	25	3.0	653	919	452	81	117	166
A1R063	1 Unpowered Rod	2.1	2.0	25	3.0	656	963	520	77	144	240
A1R072	High Shroud Power	2.1	2.0	24	3.0	657	963	588	90	161	287
A1R073	Low Shroud Temperature	2.1	2.0	24	3.0	667	958	475	82	73	177
A1R074	Base Case Repeat 3	2.1	2.0	25	3.0	654	969	518	102	104	226
A1R114	Combination of 40 and 61	2.1	Fig 59	16	3.0	657	828	512	2	2	2
A1R117	Very Low Shroud Temperature	2.1	2.0	24	3.0	675	909	345	68	115	227
Flow Oscillations											
A1R050	Maximum Amplitude	2.1	2.0	17	3.0	652	966	690	10	10	10
Gravity Reflood											
A1G041	Gravity Base Case	2.3	2.0	27	3.0	656	897	463	20	6	5
A1G051	High Pressure	4.2	2.0	26	3.0	651	850	313	2	2	2
A1G052	High Inlet Subcooling	2.2	2.0	53	3.0	652	907	405	2	4	3

Table A-10-2
Droplet Distribution Experiments

Run No	Description	Sub-Chan	Window	Inlet Sub-Cool (C)	Init Temp at 2.13 m Rod E5 (C)	Init Temp at 2.13 m Shroud (C)	Results at 2.13 m Max Temp (C)	Results at 2.13 m Rewet Time (s)
Hot Shroud Experiments								
A3R014		D0	3	23	647	599	960	540
A3R025		D0	3	24	645	598	947	521
A3R021		D1	3	23	644	599	947	523
A3R019		D2	3	19	647	599	953	552
A3R020		D3	3	24	648	598	952	528
A3R018		D4	3	18	645	597	940	553
A3R001	Base Case	D5	3,4	23	646	600	958	526
A3R002		D5	1,2	23	645	597	961	524
A3R006		D5	3,4	23	649	595	950	527
A3R013		D6	3	23	648	600	950	519
A3R003		D7	3,4	21	645	598	960	540
A3R012		D8	3	25	646	597	950	510
A3R005		D9	3,4	23	646	600	960	535
Cool Shroud Experiments								
A3R017		D0	3	21	657	399	940	498
A3R022		D1	3	23	656	399	946	500
A3R023		D2	3	22	656	399	947	510
A3R024		D3	3	21	656	400	941	498
A3R009	Base Case	D5	3,4	23	652	399	945	493
A3R008		D7	3,4	23	650	399	950	492
A3R011		D8	3	24	652	398	940	491
A3R010		D9	3	23	653	398	940	473

Table A-10-3
Airflow and Voidage Distribution Experiments

Air Flow Distribution Experiments

Run No	Description	Inlet Re No	Cluster Power (kW)	Cluster Temp (°C)	Scan Period (s)	Log Time (s)
Repeat Heat Transfer Experiments						
A3A015	Examined	5000	15	350	2	2000
A3A016	temperature	5000	15	350	2	2000
A3A026	asymmetry	5000	15	350	2	2000
A3A027		5000	15	350	2	2000
A3A036		1000	3	350	8	8000
A3A035		1750	5.5	350	5	5000
A3A034		3000	10	350	3	3000
A3A033		9000	25	350	1	1000
Isothermal Flow Distribution Experiments						
A3A029	Measured	3000	0	23	2	2000
A3A030	radial	3000	0	21	2	2000
A3A031	Velocity	3000	0	22	2	2000
A3A028		5000	0	23	2	2000
A3A032		5000	0	23	2	2000

Voidage Distribution Experiments

Run No	Description	Press (bar)	Flow Rate (dm^3/s)	Sub-Cool (°C)	Cluster Power (kW)
Air/Water					
A3L037	Commission	1.0	3.0	-	0
Boil-down					
A3L038		1.2	d/c	-	20
A3L039		1.0	d/c	-	20
Steady-boiling					
A3L040		1.2	d/c	4	20
A3L041		1.2	0.08	4	20
A3L042		1.2	0.08	4	40
A3L043		1.2	0.08	4	60
A3L044		1.2	0.08	4	80
A3L045	Base Case	1.2	0.08	50	40
A3L046	Power	1.2	0.08	50	60
A3L047	Flow	1.2	0.11	50	40
A3L048	Pressure	2.0	0.08	50	40
A3L049	A3R condition	2.0	0.15	86	105

d/c - downcomer connected to shroud vessel

Table A-10-4
Summary of Best Estimate Reflood Experiments

FORCED REFLOOD

Run Number	Description	Rig Pressure (bar)	Initial Flow (cm/s)	Surge Volume (dm³)	Subcooling (K)	Initial Temperature (°C)	Quench front Elevation after Initial Surge (m)	Results at 2.13 m Max Temp (°C)	Results at 2.13 m Rewet Time (s)
A1B088[1]	High Initial Temp	3	30	19.2	10	650	0.19	720	266
A1B091	High Initial Temp	3	30	20.0	10	650	0.34	716	254
A1B092	Low Initial Temp	3	30	20.1	10	500	0.56	624	172
A1B094	Base Case Repeat	3	30	20.5	10	550	0.53	658	184
A1B095	High Inlet Subcooling	3	30	20.9	50	550	0.66	621	183
A1B096	Low Initial Temp	3	30	20.8	10	400	0.70	536	115
A1B097	Low Pressure	2	30	21.4	10	550	0.42	696	333
A1B098[2]	Low Downcomer Level	3	30	10.8	10	550	0.32	683	194
A1B099	EM Comparison	3	30	20.6	20	650	0.44	737	319
A1B100	High Surge Rate	3	60	18.0	10	550	0.52	666	233
A1B101	High Surge Rate	3	100	21.4	10	550	0.53	665	223
A1B112	Base Case	3	30	21.2	10	550	0.43	666	240

Notes
All Condition as Base Case unless stated.
[1] Initial Temperature high at bottom of test-section only.
[2] Initial Downcomer Level 50%.

NATURAL REFLOOD

Run Number	Description	Rig Pressure (bar)	Surge Volume (dm³)	Subcooling (K)	Initial Temperature (°C)	OR1/OR2[1]	Quench front Elevation after Initial Surge (m)	Results at 2.13 m Max Temp (°C)	Results at 2.13 m Rewet Time (s)
A1B087	Flow Resistance	3	9.3	10	650	0/0	0.33	734	265
A1B089	Flow Resistance	3	25.9	10	650	0/300	0.42	798	308
A1B102	Flow Resistance	3	21.7	10	650	25/300	0.33	812	300
A1B103	Flow Resistance	3	18.9	10	650	35/200	0.33	796	278
A1B104	Flow Resistance	3	22.9	10	550	35/200	0.68	755	268
A1B105	High Initial Temp	3	17.1	10	650	35/100	0.33	784	275
A1B106	Base Case	3	19.0	10	550	35/100	0.38	738	248
A1B107	Low Initial Temp	3	20.8	10	400	35/100	0.74	613	169
A1B108	High Inlet Cooling	3	24.3	50	550	35/100	0.7	740	214
A1B109	Low Pressure	2	24.0	10	550	35/100	0.57	777	341
A1B110[2]	Odd Initial Temp	3	23.7	10	550	35/100	0.96	709	225
A1B111	Flow Resistance	3	10.0	10	550	35/0	0.16	711	254
A1B123	Base Case Repeat	3	18.1	10	550	35/100	0.33	732	254

Notes
All Condition as Base Case unless stated.
[1] OR1 & OR2 k values based on Area = 3578 mm².
[2] Initially, Bottom 1.0 m of Cluster at Saturation Temperature.

Appendix A
Literature Review

Appendix A11: Lehigh 9-Rod Bundle Tests

Dates When Tests Were Performed: 1982 - 1986

References:

R27. Tuzla, K., Unal C., Badr, O., Neti, S., Chen, J.C., "Thermodynamic Nonequilibrium in Post-Critical-Heat-Flux Boiling in a Rod Bundle", NUREG CR-5095 Vol. 1-4, June 1988.

R28. Unal C., Tuzla, K., Badr, O., Neti, S., Chen, J.C., "Convective Boiling in a Rod Bundle: Traverse Variation of Vapor Superheat Temperature Under Stabilized post-CHF Conditions", Int. J. Heat and Mass Transfer, Vol. 34, No. 7, pp. 1695-1706, 1991

Availability of Data:

The data for these experiments is contained in Volumes 2 - 4 of reference R27. Raw data is not available from the original source.

Test Facility Description, Types of Tests:

The rods were 0.374-inches in diameter and were arranged in a square pitch of .0496-inches. The actual test section of the facility was 4-feet long with one spacer grid located at 30-inches from the bottom. The rods had a linear power profile to provide a constant heat flux over the length of the test section. Each sub-channel had the same wetted perimeter and this resulted in ~39% of excess flow area in the bundle. The excess flow area was to account for the housing effect.

Coolant Mass Flow Rate	3.0×10^{-4} to 7.7×10^{-2} lb./sec
Inlet Subcooling	72 ^{0}F to 1 ^{0}F
Pressure	14.8 to 17.4 psi
Initial Shroud Temperature	575 ^{0}F to 750^{0}F

Initial Rod Temperature	~1100^{0}F
Heat Flux	5 to 4312 kW/m^2
Linear Heat Generation (const. Over length)	0.4 to 3.5 kW/ft
Constant Flooding Rates	0.04 to 0.16 in/sec

Instrumentation and Data From Tests:

There were 8 thermocouples imbedded in each of the 9 heater rods at 6-inch intervals. Due to limitations of the data collection system, only 80 channels could be monitored for any given test. The arrangement of thermocouple elevations has one disturbing shortcoming. There are no thermocouples located at identical elevations and angles to allow for checking of the symmetry of the test section. The pressure cells were spaced to far apart to be able to make a calculation of the void fraction. Two aspirating steam probes were located at 24 and 38-inches respectively. These probes were traversed through the bundle in several experiments to measure the traverse variation of vapor superheat. The vapor temperature difference was reduced from 120 to 40 ^oC superheat when the inlet quality was increased from 0.04 to 0.40. Effects of dispersed droplet cooling were evident after the grid as well.

The data shows a pronounced effect caused by the spacer grid located at the 30-inch elevation. This information might be used in evaluating the effects of spacer grids in two-phase - dispersed droplet flow. The data also showed a small error caused by the steam probes.

Conclusions:

This series of tests is of limited use to the Rod Bundle Program. The information gathered using a traversing steam probe is the most significant contribution.

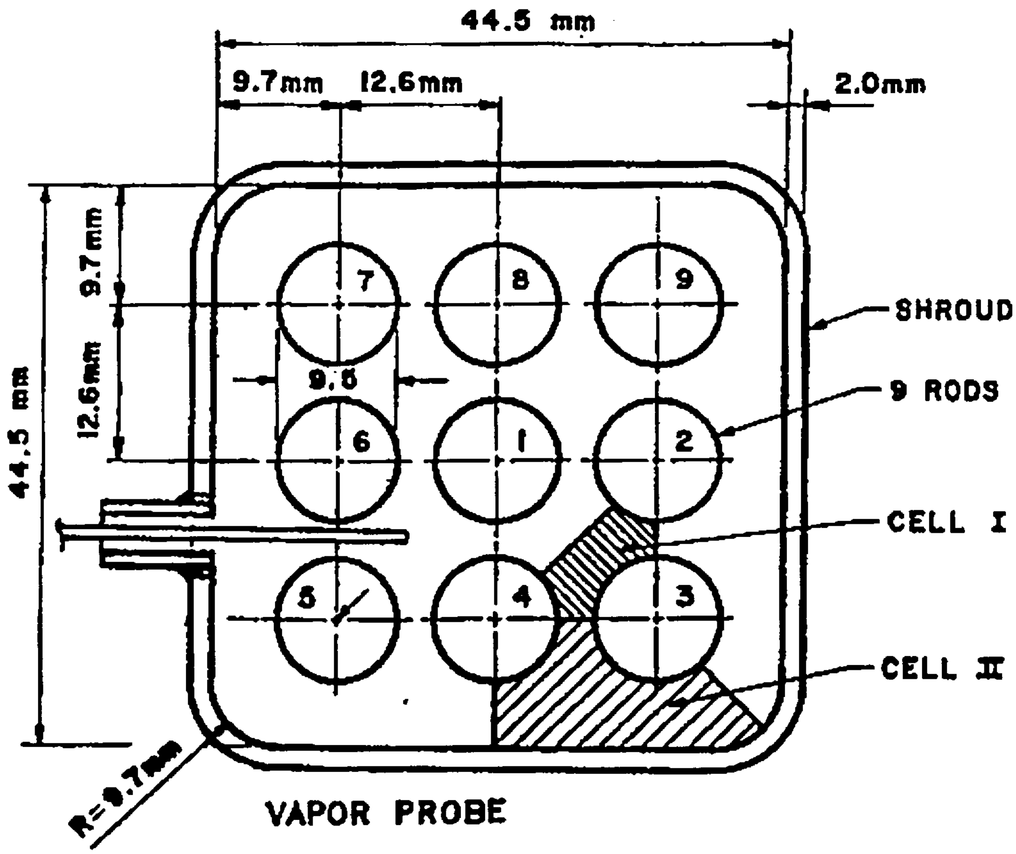

Figure A-11-1. Cross-sectional view of test bundle.

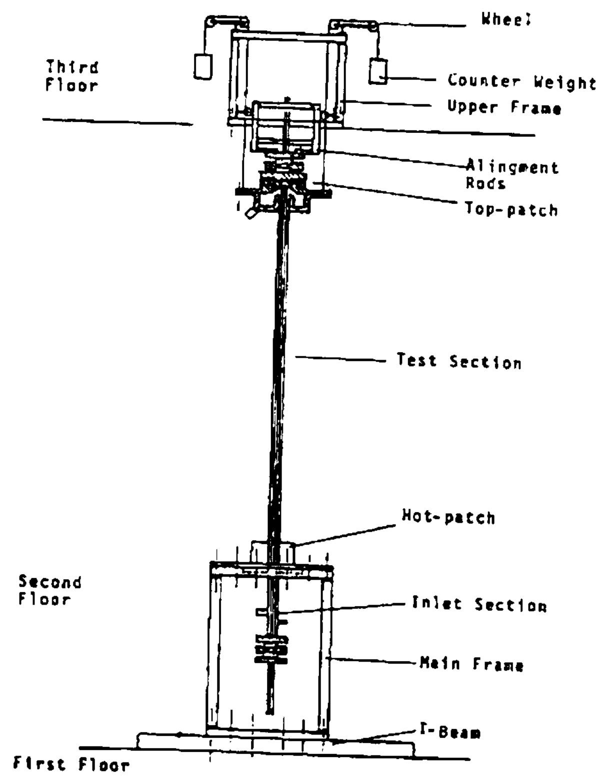

Figure A-11-2. Schematic of test section support system.

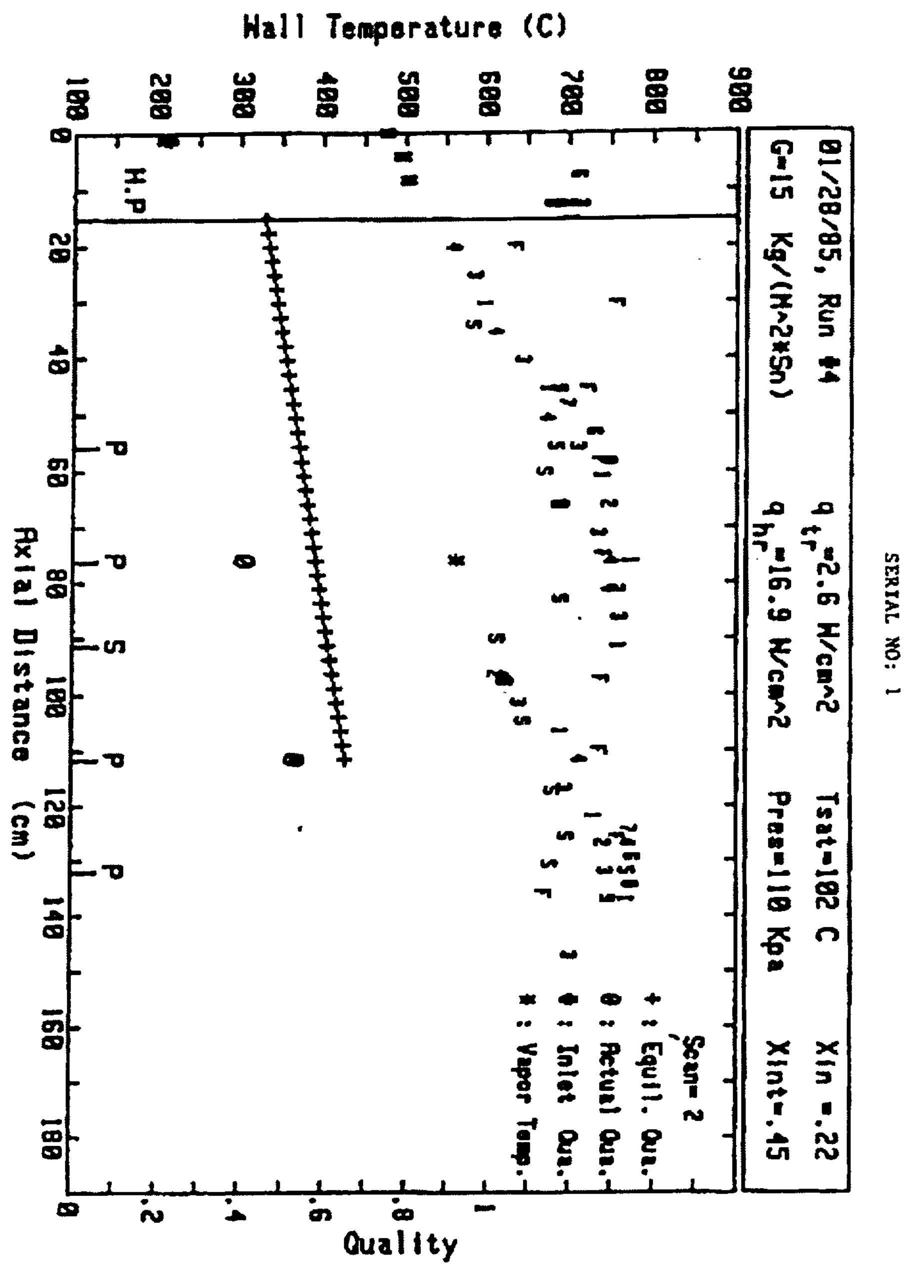

Figure A-11-3. Sample plot of temperature and steam quality data for the stabilized quench front experiments.

Table A-11-1. Sample tabulation of a stabilized quench front data point (see Table A-11-2 for nomenclature).

```
INLET QUALITY            =  .219
INLET MASS FLUX          = 15.00  Kg/M^2s
TEST-ROD  HEAT FLUX      =  2.60  W/cm^2
HOT-ROD   HEAT FLUX      = 16.89  W/cm^2
HOT-PATCH HEAT FLUX      = 12.82  W/cm^2
INLET PRESSURE           = 110.0  Kpa
SAT. TEMPERATURE         = 102.3  C
```

VAPOR SUPERHEAT TEMPERATURE

AT Z=76.2 CM TV1 = 561.0 C	AT Z=111.8 CM TV2 = 366.0 C
RATING OF TV1 = 1	RATING OF TV2 = 4
XA1 = .408	XA2 = .527
XE1 = .579	XE2 = .651

SHROUD				TEST RODS						
ZS (CM)	QRS (W/CM2)	ZS (CM)	TS (C)	ZT (CM)	XE	TR1 (C)	TR3 (C)	TR4 (C)		
18.7	.93	1.3	501.	15.2	.45	701				
25.9	1.24	5.5	495.	20.3	.46			558		
33.2	1.26	9.7	475.	25.4	.48		584			
40.4	1.21			30.5	.49	596				
47.5	1.04	34.3	582.	35.6	.50			610		
54.7	.81	60.2	669.	40.6	.51		643			
61.9	.57	66.1	689.	45.7	.52	674			TR9	687
69.0	.50	83.1	686.	48.3	.52				TR7	696
76.2	.50	90.2	611.	50.8	.53			672		
83.4	.43	97.8	619.	53.5	.53				TR6	729
90.5	1.38	104.9	643.	55.9	.54		709		TR5	683
97.7	1.25	117.4	679.	58.4	.54				TR8	746
104.9	.98	125.7	695.	61.0	.55	738				
112.1	.82	130.8	676.	66.0	.56			746		
119.2	.43			71.1	.57		734			
126.4	.20			76.2	.58	772		750		
133.6	1.06			81.3	.59			747	TR2	756
				86.4	.60		758			
				91.4	.61	757				
				96.5	.62			617	TR2	609
				101.6	.63		638			
				106.7	.64	687				
				111.8	.65			712		
				116.8			694			
				121.9		728				
				124.5					TR7	770
				127.0				770	TR2	739
				129.4					TR6	774
				132.1			743		TR5	768
				134.6					TR8	772
				137.1		768			TR9	746
				147.3			700			

Table A-11-2. Definition of parameters used in Table A-11-1.

QRS	= shroud heat flux (local)
TR 1	= surface temperature of test rod number 1
TR 3	= surface temperature of test rod number 3
TR 4	= surface temperature of test rod number 4
TR 5	= surface temperature of test rod number 5
TR 6	= surface temperature of test rod number 6
TR 7	= surface temperature of test rod number 7
TR 8	= surface temperature of test rod number 8
TR 9	= surface temperature of test rod number 9
TS	= shroud surface temperature
TV 1	= vapor temperature obtained from first probe
TV 2	= vapor temperature obtained from second probe
XA 1	= actual quality at the first vapor probe location
XA 2	= actual quality at the second vapor probe location
XE	= equilibrium quality
XE 1	= equilibrium quality at the first vapor probe location
XE 2	= equilibrium quality at the second vapor probe location
ZS	= shroud axial location (reference to hot-patch inlet)
ZT	= test section axial location (reference to hot-patch inlet)

Table A-11-3. Sample tabulation of an advancing quench front data point (see Table A-11-4 for nomenclature).

SERIAL NO: 161

INLET QUALITY	= .084		
INLET MASSFLUX	= 19.63 KG/M^2S	TEST-ROD ELEC FLUX =	3.11 W/CM^2
INLET PRESSURE	= 109.0 KPA	SCAN NUMBER =	8
SAT. TEMPERATURE	= 102.3 C	TIME OF SCAN =	22 SEC

CHF CONDITIONS, RATING=2

DEV.	DIS. CM	VEL. CM/S	QUAL.
R1	4.5	.16	.093
R4	5.1	.13	.095
R3	8.1	.08	.111
R6	6.0	.15	.100
R7	4.5	.13	.093
R8	7.9	.12	.110
SH	9.9	.11	.120

VAPOR TEMPERATURE

AT Z= 61.0 CM TV1 = 573 C
RATING OF TV1 = 1
XA1 = .149
XE1 = .213
DIST. FROM CHF = 56.4 CM

AT Z= 96.5 CM TV2 = 534 C
RATING OF TV2 = 1
XA2 = .191
XE2 = .266
DIST. FROM CHF = 92.0 CM

SHROUD

ZS CM	QRS W/CM^2	ZS CM	TS C
3.6	1.4	19.2	517
10.8	1.8	45.3	577
17.9	1.2	51.0	583
25.1	1.2	68.0	582
32.3	1.1	75.3	535
39.4	1.0	82.8	543
46.6	.9	89.8	572
53.8	.8	102.0	588
60.9	.8	110.0	589
68.1	.9	115.0	550
75.3	1.2		
82.5	1.2		
89.6	.9		
96.8	.8		
104.0	.7		
111.1	.6		
118.3	.5		

TEST RODS

ZT CM	XE	TR1 C	TR4 C	TR5 C	TR6 C	TR7 C	TR8 C
0.0	.084	106	—	—	—	—	—
2.5	.089	—	—	—	—	100	—
5.1	.095	—	122	—	—	—	—
7.6	.109	—	—	—	519	—	—
10.2	.121	—	—	521	—	—	—
12.7	.133	—	—	—	—	—	565
15.2	.141	590	—	—	—	—	—
17.8	.147	—	—	—	—	583	—
20.3	.153	—	609	—	—	—	—
22.9	.158	—	—	—	609	—	—
25.4	.163	—	—	610	—	—	—
27.9	.168	—	—	—	—	—	644
30.5	.172	635	—	—	—	—	—
33.0	.176	—	—	—	—	613	—
35.6	.180	—	645	—	—	—	—
38.1	.184	—	—	—	648	—	—
40.6	.188	—	—	638	—	—	—
43.2	.192	—	—	—	—	—	666
45.7	.195	676	—	—	—	—	—
48.3	.198	—	—	—	—	637	—
50.8	.202	—	641	—	—	—	—
53.3	.205	—	—	—	663	—	—
55.9	.207	—	—	645	—	—	—
58.4	.210	—	—	—	—	—	668
61.0	.213	659	—	—	—	—	—
63.5	.216	—	—	—	—	647	—
66.0	.219	—	663	—	—	—	—
68.6	.222	—	—	—	660	—	—
71.1	.226	—	—	650	—	—	—
73.7	.230	—	—	—	—	—	643
76.2	.234	626	—	—	—	—	—
78.7	.238	—	—	—	—	563	—
81.3	.242	—	572	—	—	—	—
83.8	.247	—	—	—	587	—	—
86.4	.251	—	—	601	—	—	—
88.9	.255	—	—	—	—	—	626
91.4	.259	619	—	—	—	—	—
94.0	.263	—	—	—	—	639	—
96.5	.267	—	651	—	—	—	—
99.1	.270	—	—	—	654	—	—
101.6		—	—	657	—	—	—
104.1		—	—	—	—	—	673
106.7		651	—	—	—	—	—
109.2		—	—	—	—	672	—
111.8		—	682	—	—	—	—
114.3		—	—	—	670	—	—
116.8		—	—	657	—	—	—
119.4		—	—	—	—	—	682
121.9		686	—	—	—	—	—

Table A-11-4. Definition of parameters used in Table A-11-3.

DEV	= device
DIS	= distance
QRS	= shroud's heat flux (local value)
QUAL	= equilibrium quality
R1	= test rod #1
R3	= test rod #3
R4	= test rod #4
R6	= test rod #6
R7	= test rod #7
R8	= test rod #8
SH	= shroud
TR 1	= surface temperature of test rod number #1
TR 3	= surface temperature of test rod number #3
TR 4	= surface temperature of test rod number #4
TR 6	= surface temperature of test rod number #6
TR 7	= surface temperature of test rod number #7
TR 8	= surface temperature of test rod number #8
TS	= surface temperature of the shroud
TV1	= vapor temperature of first vapor probe elevation
TV2	= vapor temperature of second vapor probe elevation
XA 1	= actual quality at the first vapor probe location
XA 2	= actual quality at the second vapor probe location
XE	= equilibrium quality
XE 1	= equilibrium quality at the first vapor probe location
XE 2	= equilibrium quality at the second vapor probe location
ZS	= shroud axial location (reference to hot-patch outlet)
ZT	= test section axial location (reference to hot-patch outlet)

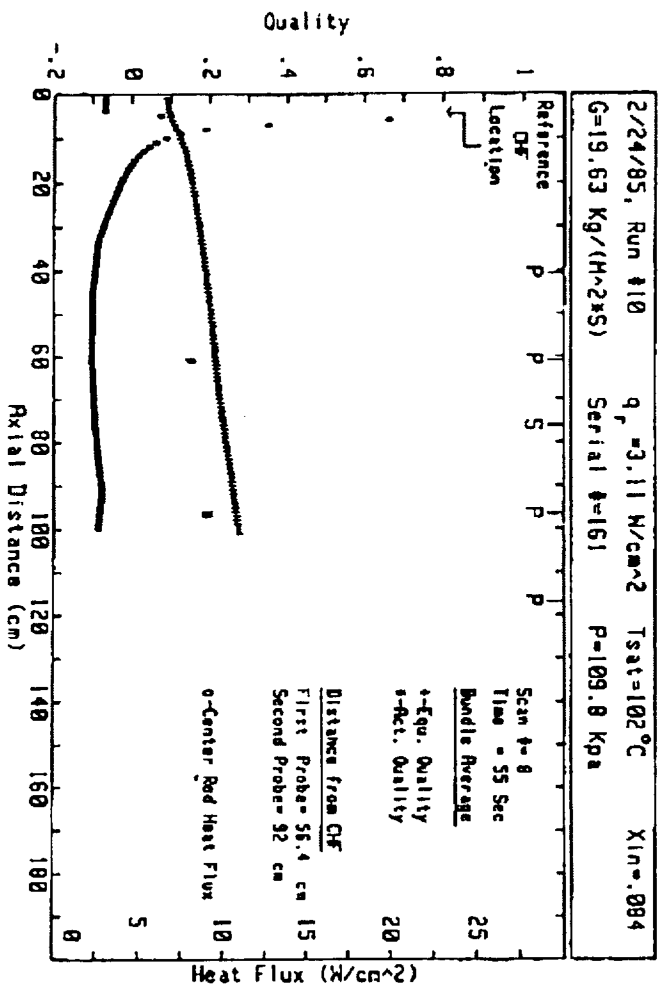

Figure A-11-4. Sample plot of heat flux and steam quality data for the advancing quench front experiments.

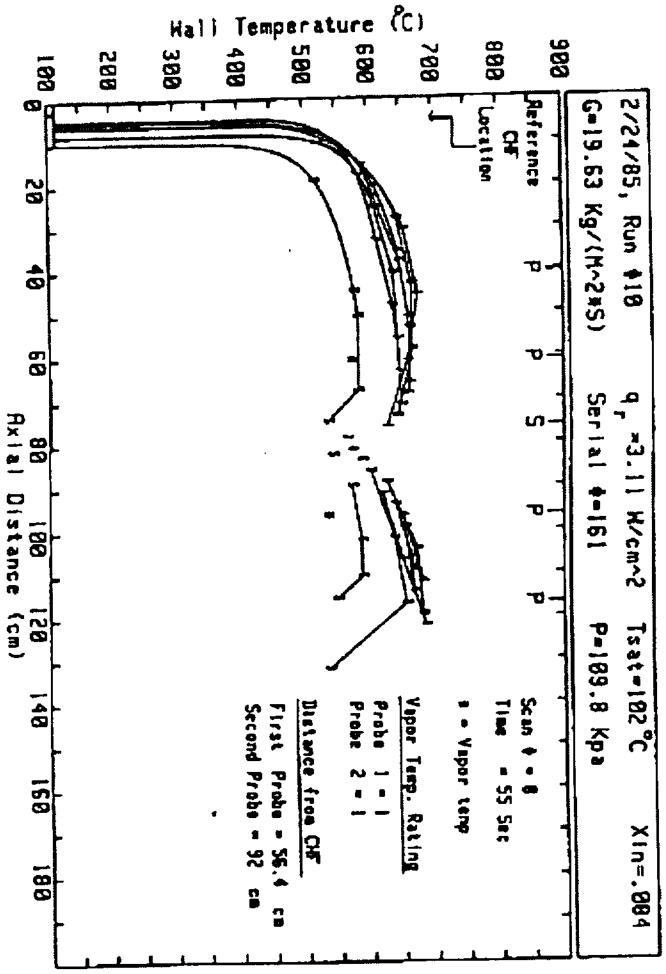

Figure A-11-5. Sample plot of rod and steam temperature data for the advancing quench front experiments.

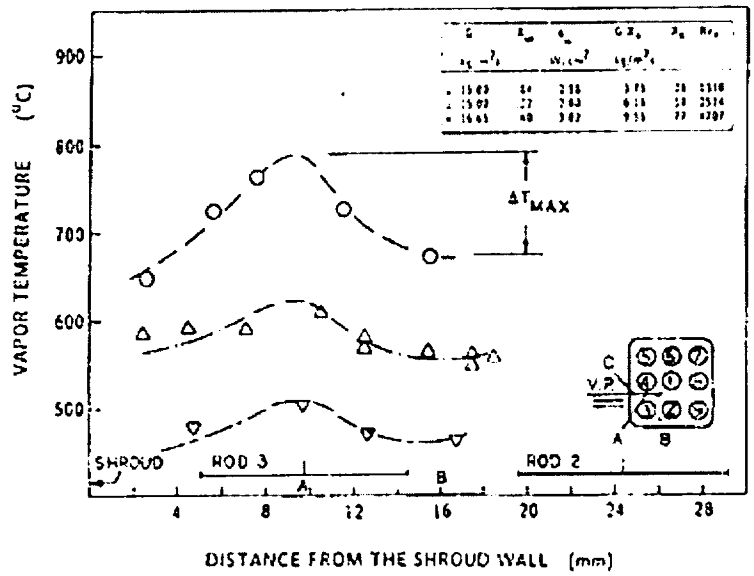

Figure A-11-6. Transverse vapor temperature profiles for various vapor qualities.

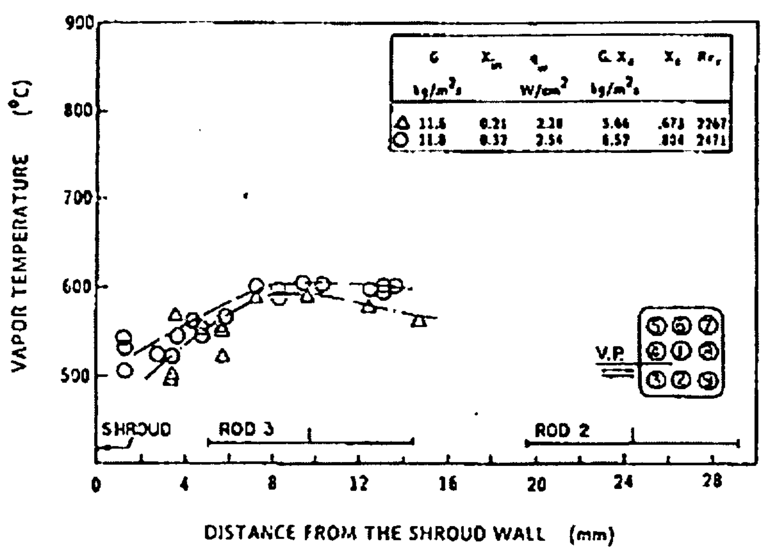

Figure A-11-7. Typical transverse vapor temperature profiles downstream of the grid spacer.

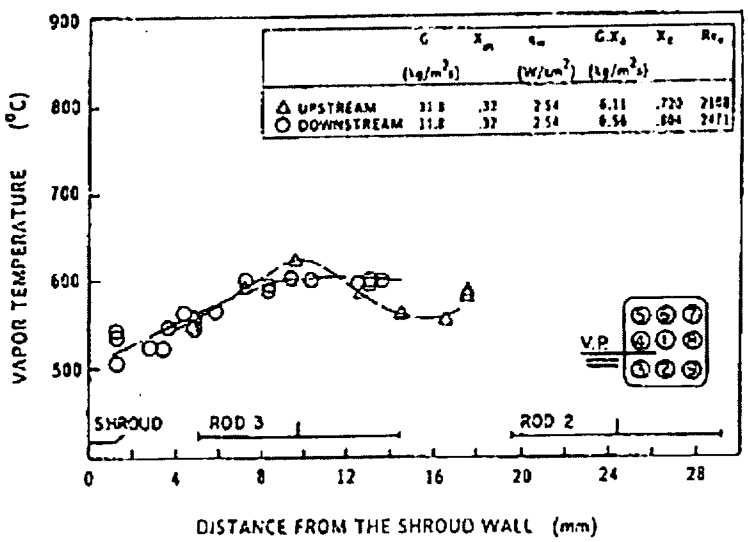

Figure A-11-8. Comparison of transverse vapor temperature profiles upstream and downstream of the grid spacer.

Appendix B.1: Radiation heat transfer network and calculation of π_i groups

In order to calculate the radiative heat transfer from the rods to the surfaces and the housing, a six node radiation network (Figure 6-3 has been developed which includes radiation heat transfer to droplets and vapor. The network resistances are defined as follows [7.2, 7.3, 7.4]:

$$\frac{1}{R_{ii}} = \frac{\varepsilon_w}{1-\varepsilon_w} A_i$$

$$\frac{1}{R_{ij}} = (1-\varepsilon_l)(1-\varepsilon_v) A_i F_{ij}$$

$$\frac{1}{R_{il}} = \varepsilon_l (1-\varepsilon_v) A_i$$

$$\frac{1}{R_{iv}} = \varepsilon_v (1-\varepsilon_l) A_i$$

$$\frac{1}{R_{lv}} = \varepsilon_l \varepsilon_v \sum_{i=1}^{4} A_i$$

where

A_i	=	radiating area per unit length for the i-th radiating wall surface
F_{ij}	=	view factor from node 'i' to node 'j'
ε_w	=	wall emissivity
$\varepsilon_l, \varepsilon_v$	=	drop and vapor emissivity

The view factors are calculated by summing up single rod-to-rod, rod-to-housing and rod-to-surfaces view factors which are calculated with the VIEWFAC subroutine of MOXY computer program[7-1]:

$$F_{12} = \sum_j \frac{\sum_{i=1}^{49} A_i F_{ij}}{\sum_{i=1}^{49} A_i}, \qquad \text{where } j = j_{CR} \text{ and } i \neq j_{CR} \quad (j_{CR} \text{ are the cold rods indices})$$

$$F_{13} = \sum_j \frac{\sum_{i=1}^{49} A_i F_{ij}}{\sum_{i=1}^{49} A_i}, \qquad \text{where } j = j_S \text{ and } i \neq j_S, j_{CR} \text{ } (j_S \text{ are surfaces indices: 1,7,43,49)}$$

$$F_{14} = \frac{\sum_{i=1}^{49} A_i F_{iN}}{\sum_{i=1}^{49} A_i} \qquad \text{where } i \neq j_S, j_{CR}$$

$$F_{23} = \sum_j \frac{\sum_{i=1}^{49} A_i F_{ij}}{\sum_{i=1}^{49} A_i}, \qquad \text{where } j = j_S \text{ and } i = j_{CR}$$

$$F_{24} = \frac{\sum_{i=1}^{49} A_i F_{iN}}{\sum_{i=1}^{49} A_i} \qquad \text{where } i = j_{CR}$$

$$F_{34} = \frac{A_1 F_{1N} + A_7 F_{7N} + A_{43} F_{43N} + A_{49} F_{49N}}{A_1 + A_7 + A_{43} + A_{49}}$$

Assuming that the droplet and vapor media are optically thin, the drop and vapor emissivities ε_l and ε_v are calculated with the following formula:

$$\varepsilon_l = 1 - e^{-a_l L_m}$$

$$\varepsilon_v = 1 - e^{-a_v L_m}$$

the beam length L_m is defined as follows for rod bundle geometry:

$$L_m = 0.85 D_h$$

Assuming the droplets in the geometric scattering regime, the liquid absorption coefficient is calculated by the following formula which is based on Ref. 7.4 with the additional assumption of considering a single drop size group (Sauter-mean diameter):

$$a_l = 0185\pi . d^2 n_d$$

where d is the drop sauter mean drop diameter (m) while the number of droplet per unit volume n_d is calculated from the void fraction:

$$n_d = \frac{6(1-\alpha)}{\pi . d^3}$$

Where the saurter-mean diameter and the void fractions are inputs in the program. The vapor absorption coefficient a_v is calculated with the following formula:

$$a_v = 9.84 \cdot 10^{-5} P \left[18.66 \left(\frac{555}{T_w} \right)^2 - \left(\frac{555}{T_w} \right)^4 \right] \qquad \text{(SI units)}$$

where P is the pressure [kPa] and T_w is the wall temperature [K].

Solution of the radiation network

The Kirchoff law is applied to nodes 1,2,3 and 4:

$$\frac{J_1 - \sigma . T_{hr}^4}{R_{11}} + \frac{J_1 - J_2}{R_{12}} + \frac{J_1 - J_3}{R_{13}} + \frac{J_1 - J_4}{R_{13}} + \frac{J_1 - \sigma . T_l^4}{R_{1l}} + \frac{J_1 - \sigma . T_v^4}{R_{1v}} = 0.0$$

$$\frac{J_2 - \sigma . T_{cr}^4}{R_{22}} + \frac{J_2 - J_1}{R_{12}} + \frac{J_2 - J_3}{R_{23}} + \frac{J_2 - J_4}{R_{24}} + \frac{J_2 - \sigma . T_l^4}{R_{2l}} + \frac{J_2 - \sigma . T_v^4}{R_{2v}} = 0.0$$

$$\frac{J_3 - \sigma . T_s^4}{R_{33}} + \frac{J_3 - J_1}{R_{13}} + \frac{J_3 - J_2}{R_{23}} + \frac{J_3 - J_4}{R_{34}} + \frac{J_3 - \sigma . T_l^4}{R_{3l}} + \frac{J_3 - \sigma . T_v^4}{R_{3v}} = 0.0$$

$$\frac{J_4 - \sigma . T_h^4}{R_{44}} + \frac{J_4 - J_1}{R_{14}} + \frac{J_4 - J_2}{R_{24}} + \frac{J_4 - J_3}{R_{34}} + \frac{J_4 - \sigma . T_l^4}{R_{4l}} + \frac{J_4 - \sigma . T_v^4}{R_{4v}} = 0.0$$

where J_i are the radiosities in the network nodes.
For a given temperature field $(T_{hr}, T_{cr}, T_s, T_h, T_l, T_v)$ the equations are solved for the unknowns J_1, J_2, J_3, J_4. Then the heat rate across each resistance in the network can be calculated as:

$$Q_{ij} = \frac{J_j - J_i}{R_{ij}}$$

The previous procedure has been implemented in the Fortran program called RADNET attached in Appendix B.5.

Another input to the RADNET computer program is how hot versus cold rods are lumped together in the bundle. It can be recognized that, for given boundary conditions, the result is dependent on how hot and cold rods are lumped together in the model. Sensitivity studies have carried out where the hot rods sub-array has been assumed to be either the central rod, the inner 3x3 or the inner 5x5. For example the group π_{30} (see later) calculated with the three different lumping approach is:

$\pi_{30,cr} = 0.567$
$\pi_{30,3x3} = 0.388$
$\pi_{30,5x5} = 0.345$

It is important to note that this is the group affected most while the effect of different lumping approach on the other groups is less important. Results from the detailed rod-to-rod model calculations (Appendix 7.1) show that the temperature is practically uniform in the inner 3x3 array while the temperature drops in the periphery as effect of the housing, thus the 3x3 hot rods lumping approach is the most appropriate and was chosen in the dimensionless groups calculation.

Appendix B.2 - Rod Grid Radiation Network for RBHT

Inputs

H grid	1.5	in	0.0381	m
N grids	6			
rod diameter	0.374	in	0.0095	m
rods pitch	0.496063	in	0.0126	m
rod power	5.6	kW		
pressure	40	psia	272.1088	kPa
liquid temperature	267	F	403.6956	K
vapor temperature	1177	F	909.2511	K
rod temperature	1650	F	1172.029	K
grid temperature	1376	F	1019.807	K
void fraction	0.995			
droplets sorter mean diameter			0.001	m
wall emissivity			0.8	

Calculation

bundle hydraulic diameter			0.01179	m
droplet density			9554140	Ndrp/m3
liquid absorption coefficient			5.55	m-1
beam length			0.010021	m
liquid emissivity			0.054101	
vapor absorption coefficient			0.182435	m-1
vapor emissivity			0.000542	
rod area (based on Hgrid) Ar	1.76154	in2	0.001136	m2
grid area (per rod) Ag	2.976	in2	0.00192	m2
1/R11			0.004546	
1/R22			0.00768	
1/R12			0.001074	
1/R1L			6.15E-05	
1/R1V			5.83E-07	
1/R2L			0.000104	
1/R2V			9.84E-07	
1/RLV			8.96E-08	
A11			0.005682	
A22			0.008859	
A12=A21			-8.96E-08	
C1			486.4733	
C2			471.1879	
det(A)			5.03E-05	

Appendix B.3 - Rod Grid Radiation Network for PWR

Inputs

H grid	1.5	in	0.0381	m
N grids	6			
rod diameter	0.374	in	0.0095	m
rods pitch	0.496063	in	0.0126	m
rod power	5.6	kW		
pressure	40	psia	272.1088	kPa
liquid temperature	267	F	403.6956	K
vapor temperature	1177	F	909.2511	K
rod temperature	1650	F	1172.029	K
grid temperature	1376	F	1019.807	K
void fraction	0.995			
droplets sorter mean diameter			0.001	m
wall emissivity			0.9	

Calculation

bundle hydraulic diameter			0.01179	m
droplet density			9554140	Ndrp/m3
liquid absorption coefficient			5.55	m-1
beam length			0.010021	m
liquid emissivity			0.054101	
vapor absorption coefficient			0.182435	m-1
vapor emissivity			0.000542	
rod area (based on Hgrid) Ar	1.76154	in2	0.001136	m2
grid area (per rod) Ag	2.976	in2	0.00192	m2
1/R11			0.010228	
1/R22			0.01728	
1/R12			0.001074	
1/R1L			6.15E-05	
1/R1V			5.83E-07	
1/R2L			0.000104	
1/R2V			9.84E-07	
1/RLV			8.96E-08	
A11			0.011365	
A22			0.018459	
A12=A21			-8.96E-08	
C1			1094.421	
C2			1059.93	
det(A)			0.00021	

Appendix B.4 - Rod Grid Radiation Network for BWR

Inputs

H grid	1.5	in	0.0381	m
N grids	6			
rod diameter	0.483071	in	0.01227	m
rods pitch	0.637795	in	0.0162	m
rod power	5.6	kW		
pressure	40	psia	272.1088	kPa
liquid temperature	267	F	403.6956	K
vapor temperature	1177	F	909.2511	K
rod temperature	1650	F	1172.029	K
grid temperature	1376	F	1019.807	K
void fraction	0.995			
droplets sorter mean diameter			0.001	m
wall emissivity			0.9	

Calculation

bundle hydraulic diameter			0.014977	m
droplet density			9554140	Ndrp/m3
liquid absorption coefficient			5.55	m-1
beam length			0.01273	m
liquid emissivity			0.068215	
vapor absorption coefficient			0.182435	m-1
vapor emissivity			0.000868	
rod area (based on Hgrid) Ar	2.275264	in2	0.001468	m2
grid area (per rod) Ag	2.976	in2	0.00192	m2
1/R11			0.013211	
1/R22			0.01728	
1/R12			0.001367	
1/R1L			0.0001	
1/R1V			1.19E-06	
1/R2L			0.000131	
1/R2V			1.55E-06	
1/RLV			2.01E-07	
A11			0.014679	
A22			0.018779	
A12=A21			-2.01E-07	
C1			1413.639	
C2			1059.992	
det(A)			0.000276	

B.5 - Program Radnet

```
program radnet
c
      dimension f(50,50),area(50)
             dimension pir(50)
      dimension ir(50)
c
      common/cgauss/ a(10,10),b(10),c(10),na
      common/temp/t(10),eb(10),tl,tv,ebl,ebv,q(10)
      common/resist/ r(10,10)
c
      data sig/5.67E-08/
      data pi/3.141592654/
c
c......input values
      nhot=9
      trmed=1650.0
             thr=2100.0
             ts=800.0
             th=800.0
             tl=267.0
             tv=1650.0
             hqch=4.0
             qrod=2296.6
c
      hcore=12.0
             qtot=qrod*45.0
             qhr=qrod*float(nhot)
      nsurf=4
      nrod=49
      ncold=nrod-nhot-nsurf
      n=nrod+1
      drod=0.0095
      dh=0.01178
             dtemp=155.0
             if (nhot.eq.9) dtemp=161.0
             if (nhot.eq.25) dtemp=170.0
             if (thr.eq.0.0) thr=trmed+ncold*dtemp/float(ncold+nhot)
             tcr=thr-dtemp
             write(6,*) thr,tcr
c
c......pressure in psia
      press=40.0
      alp=0.995
      dd=0.001
      ew=0.8
      timax=500.0
c
c......end of inputs
c
      do 301 i=1,49
      ir(i)=2
 301  continue
```

```
      if (nhot.eq.1) then
      ir(25)=1
      endif
      if (nhot.eq.9) then
      ir(17)=1
      ir(18)=1
      ir(19)=1
      ir(24)=1
      ir(26)=1
      ir(31)=1
      ir(32)=1
      ir(33)=1
      endif
      if (nhot.eq.25) then
      ir(9)=1
      ir(10)=1
      ir(11)=1
      ir(12)=1
      ir(13)=1
      ir(16)=1
      ir(20)=1
      ir(23)=1
      ir(27)=1
      ir(27)=1
      ir(30)=1
      ir(34)=1
      ir(37)=1
      ir(38)=1
      ir(39)=1
      ir(40)=1
      ir(41)=1
      endif
c
      ir(1)=3
      ir(7)=3
      ir(43)=3
      ir(49)=3
c
      shrod=float(nhot)*pi*drod
      scrod=float(ncold)*pi*drod
      ssrf=float(nsurf)*pi*drod
      shou=0.3607
      nd=6.0*(1.0-alp)/(pi*dd**3.0)
      al=0.185*nd*pi*dd**2.0
      press=press*100.0/14.7
c
c......calculate global view factors with inner hot rods array considered
c
      do 11 i=1,n
      do 12 j=1,n
      read(9,*) ni,nj,f(i,j)
   12 continue
      read(9,*) area(i)
   11 continue
c
```

```
      fhrcr=0.0
      do 101 j=1,nrod
      fsum=0.0
      asum=0.0
      if (ir(j).ne.2) goto 101
      do 102 i=1,nrod
      if (ir(i).ne.1) goto 102
      fsum=fsum+area(i)*f(i,j)
      asum=asum+area(i)
  102 continue
      fhrcr=fhrcr+fsum/asum
  101 continue
c
      fsum=0.0
      asum=0.0
      fhrh=0.0
      do 202 i=1,nrod
      if (ir(i).ne.1) goto 202
      fsum=fsum+area(i)*f(i,n)
      asum=asum+area(i)
  202 continue
      fhrh=fsum/asum
c
      fsum=0.0
      asum=0.0
      fcrh=0.0
      do 302 i=1,nrod
      if (ir(i).ne.2) goto 302
      fsum=fsum+area(i)*f(i,n)
      asum=asum+area(i)
  302 continue
      fcrh=fsum/asum
c
      fhrs=0.0
      do 401 j=1,nrod
      fsum=0.0
      asum=0.0
      if (ir(j).ne.3) goto 401
      do 402 i=1,nrod
      if (ir(i).ne.1) goto 402
      fsum=fsum+area(i)*f(i,j)
      asum=asum+area(i)
  402 continue
      fhrs=fhrs+fsum/asum
  401 continue
c
      fcrs=0.0
      do 501 j=1,nrod
      fsum=0.0
      asum=0.0
      if (ir(j).ne.3) goto 501
      do 502 i=1,nrod
      if (ir(i).ne.2) goto 502
      fsum=fsum+area(i)*f(i,j)
      asum=asum+area(i)
```

```
 502  continue
      fcrs=fcrs+fsum/asum
 501  continue
c
      asum=area(1)+area(7)+area(43)+area(49)
      fs1=area(1)*f(1,n)
      fs2=area(7)*f(7,n)
      fs3=area(43)*f(43,n)
      fs4=area(49)*f(49,n)
      fsh=(fs1+fs2+fs3+fs4)/asum
c
c......calculate network resistances
c
      ebl=sig*tl**4.0
      ebv=sig*tv**4.0
      av=9.84e-5*press*(18.66*(555.0/tv)**2.0 - (555.0/tv)**4.0)
      xlm=0.85*dh
      el=1.0-exp(-al*xlm)
      ev=1.0-exp(-av*xlm)
      r(1,1)=(1.0-ew)/(ew*shrod)
      r(1,2)=1.0/((1.0-el)*(1.0-ev)*shrod*fhrcr)
      r(1,3)=1.0/((1.0-el)*(1.0-ev)*shrod*fhrs)
      r(1,4)=1.0/((1.0-el)*(1.0-ev)*shrod*fhrh)
      r(1,5)=1.0/(el*(1.0-ev)*shrod)
      r(1,6)=1.0/(ev*(1.0-el)*shrod)
c
      r(2,1)=r(1,2)
      r(2,2)=(1.0-ew)/(ew*scrod)
      r(2,3)=1.0/((1.0-el)*(1.0-ev)*scrod*fcrs)
      r(2,4)=1.0/((1.0-el)*(1.0-ev)*scrod*fcrh)
      r(2,5)=1.0/(el*(1.0-ev)*scrod)
      r(2,6)=1.0/(ev*(1.0-el)*scrod)
c
      r(3,1)=r(1,3)
      r(3,2)=r(2,3)
      r(3,3)=(1.0-ew)/(ew*ssrf)
      r(3,4)=1.0/((1.0-el)*(1.0-ev)*ssrf*fsh)
      r(3,5)=1.0/(el*(1.0-ev)*ssrf)
      r(3,6)=1.0/(ev*(1.0-el)*ssrf)
c
      r(4,1)=r(1,4)
      r(4,2)=r(2,4)
      r(4,3)=r(3,4)
      r(4,4)=(1.0-ew)/(ew*shou)
      r(4,5)=1.0/(el*(1.0-ev)*shou)
      r(4,6)=1.0/(ev*(1.0-el)*shou)
c
      r(5,1)=r(1,5)
      r(5,2)=r(2,5)
      r(5,3)=r(3,5)
      r(5,4)=r(4,5)
      r(5,5)=0.0
      r(5,6)=1.0/(ev*el*(shrod+scrod+ssrf+shou))
c
      r(6,1)=r(1,6)
```

```
      r(6,2)=r(2,6)
      r(6,3)=r(3,6)
      r(6,4)=r(4,6)
      r(6,5)=r(5,6)
      r(6,6)=0.0
c
      na=4
c
      t(1)=273.14+(thr-32.0)/1.8
      t(2)=273.14+(tcr-32.0)/1.8
      t(3)=273.14+(ts-32.0)/1.8
      t(4)=273.14+(th-32.0)/1.8
            t(5)=273.14+(tl-32.0)/1.8
            t(6)=273.14+(tv-32.0)/1.8
      do 10 i=1,6
      eb(i)=sig*t(i)**4.0
 10   continue
c
      call matrix
      call gauss
c
      do 351 i=1,na
      q(i)=(c(i)-eb(i))/r(i,i)
 351  continue
      q(5)=0.0
      q(6)=0.0
      do 352 i=1,na
      q(5)=q(5)+(c(i)-eb(5))/r(i,5)
      q(6)=q(6)+(c(i)-eb(6))/r(i,6)
 352  continue
      qvl=(eb(6)-eb(5))/r(5,6)
      q(5)=q(5)+qvl
            q(6)=q(6)-qvl
c
            q12=(c(1)-c(2))/r(1,2)
            q13=(c(1)-c(3))/r(1,3)
            q23=(c(2)-c(3))/r(2,3)
            q14=(c(1)-c(4))/r(1,4)
      q24=(c(2)-c(4))/r(2,4)
            q1l=(c(1)-eb(5))/r(1,5)
            q1v=(c(1)-eb(6))/r(1,6)
      q2l=(c(2)-eb(5))/r(2,5)
            q2v=(c(2)-eb(6))/r(2,6)
            q3l=(c(3)-eb(5))/r(3,5)
            q3v=(c(3)-eb(6))/r(3,6)
            q4l=(c(4)-eb(5))/r(4,5)
            q4v=(c(4)-eb(6))/r(4,6)
c
c......pi groups in the flow energy equation
            pir(1)=(q1v+q2v)/qtot
            pir(2)=(q1l+q2l)/qtot
            pir(3)=q4v/qtot
            pir(4)=q4l/qtot
            pir(5)=q3v/qtot
            pir(6)=q3l/qtot
```

```
        pir(7)=qvl/qtot
c
c......pi groups in the rod energy equation
        pir(8)=q13/qhr
        pir(9)=q14/qhr
        pir(10)=q12/qhr
        pir(11)=q1l/qhr
        pir(12)=q1v/qhr
c
c......correction to account for the above quench length
      corf=(hcore-hqch)/hcore
        do 701 i=1,7
        pir(i)=pir(i)*corf
 701  continue
c
      write(6,*) 'RV = ', pir(1)
        write(6,*) 'RL = ', pir(2)
        write(6,*) 'HV = ', pir(3)
        write(6,*) 'HL = ', pir(4)
        write(6,*) 'SV = ', pir(5)
        write(6,*) 'SL = ', pir(6)
        write(6,*) 'VL = ', pir(7)
        write(6,*)
      write(6,*) 'RS = ', pir(8)
        write(6,*) 'RH = ', pir(9)
        write(6,*) 'RR = ', pir(10)
        write(6,*) 'RL = ', pir(11)
        write(6,*) 'RV = ', pir(12)
c
      stop
      end
c
c
      subroutine matrix
c
      common/cgauss/ a(10,10),b(10),c(10),na
      common/temp/t(10),eb(10),tl,tv,ebl,ebv,q(10)
      common/resist/ r(10,10)
c
      do 10 i=1,na
      b(i)=0.0
      do 10 j=1,na
      a(i,j)=0.0
  10  continue
c
      do 101 i=1,na
      b(i)=eb(i)/r(i,i)+ebl/r(i,5)+ebv/r(i,6)
      do 102 j=1,na
      if (i.ne.j) then
      a(i,j)=-1.0/r(i,j)
      else
      do 103 k=1,6
      a(i,i)=a(i,i)+1.0/r(i,k)
 103  continue
      endif
```

```
 102  continue
 101  continue
c
      return
      end
c
c
      subroutine gauss
c
      common/cgauss/ a(10,10),b(10),c(10),na
c
      k=1
  20  temp = 1.0/a(k,k)
      j=k
  30  a(k,j) = a(k,j)*temp
      if (j.eq.na) goto 40
      j=j+1
      goto 30
  40  b(k) = b(k)*temp
      j=k+1
  50  temp = a(j,k)
      l=k
  60  a(j,l) = a(j,l)-a(k,l)*temp
      if (l.eq.na) goto 70
      l=l+1
      goto 60
  70  b(j) = b(j)-b(k)*temp
      if (j.eq.na) goto 80
      j=j+1
      goto 50
  80  if (k.eq.na-1) goto 90
      k=k+1
      goto 20
  90  continue
      c(na) = b(na)/a(na,na)
      i=1
 120  sum = 0.0
      j=na-i+1
 100  sum = sum+a(na-i,j)*c(j)
      if (j.eq.na) goto 110
      j=j+1
      goto 100
 110  c(na-i) = b(na-i)-sum
      if (i.eq.na-1) goto 130
      i=i+1
      goto 120
 130  continue
c
      return
      end
c
```

Appendix C: BUNDLE MODEL Description

A full model of a square lattice rod bundle was developed to calculate the cross section temperature distribution during the reflood transient. The model includes the rod-to-rod and rod-to-housing thermal radiation heat transfer as well as the radial heat conduction in the rods and the housing. The convection heat transfer between rods and fluid as well as housing and fluid is simulated by inputting a convective heat transfer coefficient time history. The fluid temperature is another input value and it is kept constant during the transient.

The view factor matrix is calculated with the VUEFAC subroutine of MOXY computer program[7.1]. The conduction heat transfer is computed in each of the fuel rods, subject to the transient heat flux boundary condition of combined convection and radiation heat transfer. The radiative heat transfer computations are based on assumptions of gray and diffuse surfaces. The model neglects absorption, emission, or scattering of radiation by steam and droplets contained between surfaces. The radiation heat transfer between the surfaces and vapor was taken into account in the lumped model described in Section 6 (RADNET computer program).

Conductive heat transfer

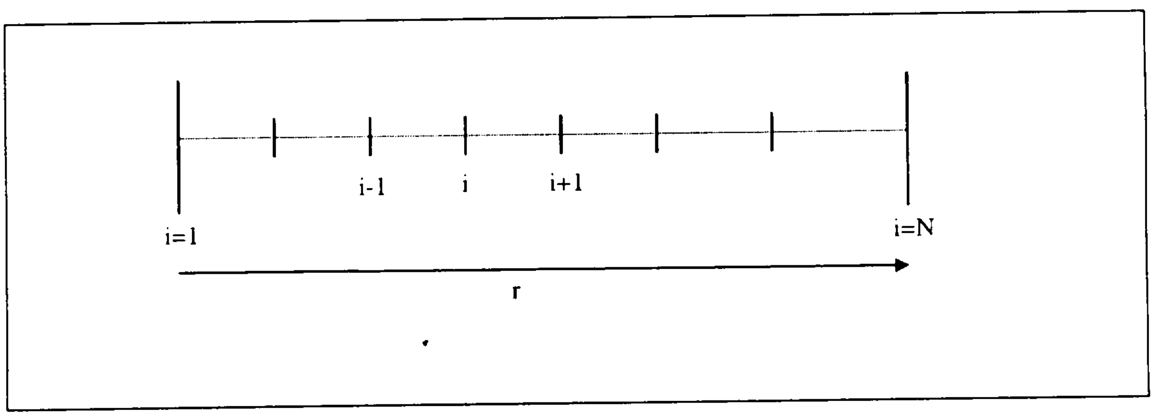

The heat conduction in fuel rods, solid inactive rods and housing is computed by numerical integration of the one-dimensional Fourier heat conduction equation:

$$\frac{1}{r}\frac{\partial}{\partial r}\left(kr\frac{\partial T}{\partial r}\right)+q'''=\rho\, C_p\frac{\partial T}{\partial t}$$

where q''' is zero for the inactive rods. The equation is discretized as follows:

$$\frac{\rho.C_{p,1}V_1}{\Delta t}\left(T_1^{n+1}-T_1^n\right)=Q_1+2\pi\left(k_1\frac{T_2^n-T_1^n}{2}\right)$$

$$\frac{\rho.C_{p,i}V_i}{\Delta t}\left(T_i^{n+1}-T_i^n\right)=Q_i+2\pi\left[k_i\left(r_i+\frac{dr_i}{2}\right)\left(\frac{T_{i+1}^n-T_i^n}{dr_i}\right)-k_{i-1}\left(r_i-\frac{dr_{i-1}}{2}\right)\left(\frac{T_i^n-T_{i-1}^n}{dr_{i-1}}\right)\right]$$

$$\frac{\rho.C_{p,N}V_N}{\Delta t}\left(T_N^{n+1}-T_N^n\right)=Q_N-2\pi\left[k_{N-1}\left(r_N-\frac{dr_{N-1}}{2}\right)\left(\frac{T_N^n-T_{N-1}^n}{dr_{N-1}}\right)\right]-2\pi r_N\left[q''_{rad}+h\left(T_N^n-T_f\right)\right]$$

where:

$$V_i=\pi\left[r_i\left(dr_{i-1}+dr_i\right)+\frac{dr_i^2-dr_{i-1}^2}{4}\right]$$

The equation for the heat conduction in the housing is:

$$\frac{\partial}{\partial x}\left(k\frac{\partial T}{\partial x}\right)+q'''=\rho.C_p\frac{\partial T}{\partial t}$$

Again, this is solved numerically with the following equations:

$$\frac{\rho.C_{p,1}dx}{\Delta t}\left(T_1^{n+1}-T_1^n\right)=k_1\left(\frac{T_2^n-T_1^n}{dx}\right)-h_{loss}\left(T_1^n-T_{out}\right)$$

$$\frac{\rho.C_{p,i}dx}{\Delta t}\left(T_i^{n+1}-T_i^n\right)=k_i\left(\frac{T_{i+1}^n-T_i^n}{dx}\right)-k_{i-1}\left(\frac{T_i^n-T_{i-1}^n}{dx}\right)$$

$$\frac{\rho.C_{p,N}dx}{\Delta t}\left(T_N^{n+1}-T_N^n\right)=-k_{N-1}\left(\frac{T_N^n-T_{N-1}^n}{dx}\right)-h\left(T_N^n-T_f\right)-q''_{rad}$$

Once the radiative heat rate q_{rad}^n is calculated form the radiation transport equations, the previous equations are solved for the temperature field at time t_{n+1}.

Radiative heat transfer

The equations governing the radiative heat transfer are the following:

$$J_i - (1-\varepsilon_i)\sum_{j=1}^{N} F_{ij} J_j = \varepsilon_i E_{b,i} \qquad i = 1,2....N$$

where:

J_i = radiosity of i-th surface
$E_{b,i}$ = blackbody emissive power of i-th surface
F_{ij} = view factor matrix
ε_i = emissivity of i-th surface

Once the temperature field is known by solving the conduction equation at time t_n, the emissive power ($E_{b,i}$) can be calculated. Then the previous system is solved for the radiosities J_i and the radiative heat fluxes at time t_n are calculated from the following equation:

$$q''_{rad,i} = \frac{\varepsilon_i}{1-\varepsilon_i}\left(E_{b,i} - J_i\right)$$

The radiative heat fluxes are applied as the wall boundary condition for the conduction equation which is used to evaluate the temperature field at time t_{n+1}.

The program herein presented can operate also in a steady state mode. In this case the conduction equation is not solved while the temperature field is calculated iteratively. The source list of the program is attached in the Appendix.

FORTRAN source list program #1

```
program bundle
c
      implicit double precision (a-h,o-z)
      dimension d(1000),pwf(1000)
      dimension a(1001,1001),b(1001)
c
      common /vf/ f(1001,1001),area(1001)
      common/heat/q(1001),qrad(1001),qconv(1001),temp(1001),
     +  emiss(1001),bs(1001),qold(1001)
      common/heat1/tfad,tenvad,h,hout,hmin,qct,qrt,qt
      common/geoint/nrod,n,nl
      common/geo/vrod(1000)
      common/temp/told(1001)
      common/converg/alfa
      common/printc/tpcv,nprt1,nprt2,imod
c
      common/trans1/regsze(4),ql(1000),qr(1000),tr(1000,100),th(100)
      common/trans2/ndreg,ndx,ndr,npc,np1,ntab,ntab2,ifrad,inuc
      common/trans3/dt,tmax,time,tft,s,tenv,hloss,qavg,htrs,trst,
     +              tdst,thst,tmin,fdcy,hgap
      common/trans4/tme(100),hft(100),tmep(100),pdcy(100),tmix(100)
c
      data pi/3.141592654/
      data sig/5.67D-08/
c
      open(unit=8,file='bd.inp')
      open(unit=11,file='bd.out')
      open(unit=12,file='bd.dmp')
      open(unit=13,file='bd.flx')
c
      write(11,800)
      write(12,600)
      write(13,700)
      read(8,*) nl
      write(11,812) nl,nl
      read(8,*) inuc
      read(8,*) dd,p,drh
      write(11,801) dd
      write(11,802) p
      write(11,803) drh
      read(8,*) pwavg
      write(11,804) pwavg
      read(8,*) emirod,emihs
      write(11,805) emirod
      write(11,806) emihs
      read(8,*) hf,tf,tmin
      write(11,807) hf
      write(11,808) tf
      hf=hf*5.679
      tf=(tf-32.0)*5.0/9.0 + 273.14
      tmin=(tmin-32.0)*5.0/9.0 + 273.14
      read(8,*) hloss,tenv
```

```
      write(11,809) hloss
      write(11,810) tenv
      hloss=hloss*5.679
      tenv=(tenv-32.0)*5.0/9.0 + 273.14
      read(8,*) s
      write(11,813) s
      s=s*0.0254
c
      hmin=0.2
c
      write(11,811)
      nrod=nl*nl
      n=nrod+1
      k1=1
      k2=k1+nl-1
      do 500 i=1,nl
      read(8,*) (pwf(k),k=k1,k2)
      write(11,903) (pwf(k),k=k1,k2)
      k1=k1+nl
      k2=k2+nl
 500  continue
c
      read(8,*) err
      read(8,*) imod,ifrad
c
      if (imod.eq.0) goto 510
c
c.....read transient data
      read(8,*) dt,tmax,nprt1,nprt2
      read(8,*) (regsze(i),i=1,4)
      do 505 i=1,4
      regsze(i)=regsze(i)*0.0254
      rsum=rsum+regsze(i)
      vrod(i)=(rsum**2.0-(rsum-regsze(i))**2.0)*pi
 505  continue
      read(8,*) hgap
      hgap=hgap*5.679
      read(8,*) ndreg,ndx
c      read(8,*) tft
c      tft=(tft-32.0)*5.0/9.0 + 273.14
      read(8,*) ntab
      do 507 i=1,ntab
      read(8,*) tme(i),hft(i),tmix(i)
      hft(i)=hft(i)*5.679
      tmix(i)=(tmix(i)-32.0)*5.0/9.0 + 273.14
 507  continue
      read(8,*) ntab2
      do 508 i=1,ntab2
      read(8,*) tmep(i),pdcy(i)
 508  continue
      read(8,*) trst,tdst,thst
      trst=(trst-32.0)*5.0/9.0 + 273.14
      tdst=(tdst-32.0)*5.0/9.0 + 273.14
      thst=(thst-32.0)*5.0/9.0 + 273.14
```

```
c
c
c....'pwavg' is the radial average power in kW/ft
c
 510   feet=0.3048
       pwl=pwavg*1000./feet
       tpcv=tf+pwl/(hf*pi*dd*0.0254)
c
       call vufac(nl,dd,p,drh)
c
       do 301 i=1,n
       do 302 j=1,n
 302   continue
       area(i)=area(i)*0.0254
 301   continue
c
       do 401 i=1,nrod
       d(i)=dd*0.0254
       ql(i)=pwf(i)*pwl
       emiss(i)=emirod
 401   continue
       emiss(n)=emihs
       qavg=pwl/(pi*d(1))
c
       if (imod.eq.1) goto 2000
c
c.....Set dimensionless variables
c
       tfad=(sig*tf**4.0d0/qavg)**0.25d0
       tenvad=(sig*tenv**4.0d0/qavg)**0.25d0
       tguess=tfad
       h=hf/(qavg**0.75d0 * sig**0.25d0)
       hout=hloss/(qavg**0.75d0 * sig**0.25d0)
       do 501 i=1,nrod
       q(i)=pwf(i)
 501   continue
       q(n)=0.0
c
c.....Start Iteration loop
c
       if (h.lt.hmin) then
       alfa=1.0
       nitmax=1000
       goto 150
       endif
c
       write(6,*) 'ALFA = ?'
       read (6,*) alfa
       write(6,*) 'NITER = ?'
       read (6,*) nitmax
c
 150   niter=0
c
c.....Initial guess for temperature
```

```
c
      do 201 i=1,n
      temp(i)=tfad
 201  continue
c
1001  niter=niter+1
c
      call rads
      call conv
c
c.....check for convergence
      eps=0.0
      elast=0.0
      do 240 i=1,n
      tnew=temp(i)
      eps=abs(tnew-told(i))
      eps=max(elast,eps)
      elast=eps
      told(i)=tnew
 240  continue
      write(6,*) niter,eps
      if (niter.gt.nitmax) goto 1002
      if (eps.gt.err) goto 1001
1002  continue
      goto 2100
c
c.....transient calculation
c
2000  call trans
      goto 9001
c
c.....print results steady state
c
2100  call print
c
c
 600  format(5x,'TIME',4x,'TCR-1',4x,'TCR-N',4x,'TWR-N',4x,'TOR-N',
     +       4x,'THO-1',4x,'THO-N',4x,'TN3x3',4x,'TN5x5',4x,'TN7x7',/)
 700  format(5x,'TIME',3x,'Q-RtoH',3x,'Q-RtoF',3x,'Q-HtoF',3x,
     +       'Q-LOSS',3x,'T-RODS',3x,'T-SURF',3x,'T-HOUS',//)
 800  format(/,40x,'CALCULATION RBHT',
     +      //,3x,'INPUT DATA')
 801  format(3x,'Rod Diameter                  (in)           = ',F8.3)
 802  format(3x,'Rods Array Pitch              (in)           = ',F8.3)
 803  format(3x,'Distance Rods-to-Housing      (in)           = ',F8.3)
 804  format(3x,'Rod Average Power             (kW)           = ',F8.3)
 805  format(3x,'Rod Surface Emissivity        (-)            = ',F8.3)
 806  format(3x,'Housing Surface Emissivity    (-)            = ',F8.3)
 807  format(3x,'Bundle Covection H.T.C.    (Btu/hr-F-ft2)= ',F8.3)
 808  format(3x,'Fluid Temperature             (F)            = ',F8.3)
 809  format(3x,'Housing Heat Losses H.T.C. (Btu/hr-F-ft2)= ',F8.3)
 810  format(3x,'Enviroment Temperature        (F)            = ',F8.3)
 811  format(//,3x,'RODS POWER FACTOR',////)
 812  format(//,3x,'Bundle Array Size            (-)            = ',3x,
```

```
     +       I2,'x',I2)
 813  format(3x,'Housing Thickness            (in)           = ',F8.3)
 903  format(20(1x,F7.2))
c
9001  stop
      end
c
c*******************************************************************
c
      subroutine trans
c
      implicit double precision (a-h,o-z)
c
      common/trans1/regsze(4),ql(1000),qr(1000),tr(1000,100),th(100)
      common/trans2/ndreg,ndx,ndr,npc,np1,ntab,ntab2,ifrad,inuc
      common/trans3/dt,tmax,time,tft,s,tenv,hloss,qavg,htrs,trst,
     +              tdst,thst,tmin,fdcy,hgap
      common/trans4/tme(100),hft(100),tmep(100),pdcy(100),tmix(100)
      common/heat/q(1001),qrad(1001),qconv(1001),temp(1001),
     +  emiss(1001),bs(1001),qold(1001)
      common/geoint/nrod,n,nl
      common /vf/ f(1001,1001),area(1001)
      common/printc/tpcv,nprt1,nprt2,imod
c
      dimension trf(1000,100),thf(100)
c
      data pi/3.141592654/
      data sig/5.67D-08/
c
      ndr=4*ndreg
      npc=ndr+1
      ndt1=0
      ndt2=0
      ic=(nl**2.0+1)/2.0
      iw=ic-(nl-1)/2.0
c
c.....initial condition
c
      do 10 j=1,nrod
      qr(j)=0.0
      do 10 i=1,npc
      tr(j,i)=trst
     if (ql(j).eq.0.0) tr(j,i)=tdst
  10  continue
      do 11 i=1,ndx+1
      th(i)=thst
  11  continue
      qr(n)=0.0
c
 100  call interp(tme,hft,time,htrs,ntab)
     if (tr(ic,npc).lt.tmin) htrs=5600.0
     call interp(tme,tmix,time,tft,ntab)
      call interp(tmep,pdcy,time,fdcy,ntab2)
      call trod
```

```
      call thous
c
      qrf=0.0
      do 102 i=1,nrod
      tw=tr(i,npc)
      temp(i)=(sig*tw**4.0d0/qavg)**0.25d0
      qrf=qrf+htrs*area(i)*(tw-tft)
 102  continue
      temp(n)=(sig*th(np1)**4.0d0/qavg)**0.25d0
      qhf=htrs*area(n)*(th(ndx+1)-tft)
      qloss=hloss*area(n)*(th(1)-tenv)
c
      if(ifrad.eq.0) goto 210
c
c.....turn off radiation after quench
      if(htrs.ge.5600.0) then
      qrh=0.0
      do 141 i=1,n
      qr(i)=0.0
 141  continue
      goto 210
      endif
c
      call rads
c
c.....calculate new radiation fluxes qrad
c
      do 201 i=1,n
      qr(i)=(temp(i)**4.0d0 - bs(i))*qavg*emiss(i)/(1.0d0-emiss(i))
 201  continue
      qrh=-qr(n)*area(n)
c
 210  time=time+dt
      ndt1=ndt1+1
      ndt2=ndt2+1
      if(ndt1.eq.nprt1) then
      write(6,*) time,htrs,tr(ic,npc)
      do 301 i=1,nrod
      do 302 j=1,npc
      trf(i,j)=(tr(i,j)-273.14)*9.0/5.0 + 32.0
 302  continue
 301  continue
      do 303 i=1,np1
      thf(i)=(th(i)-273.14)*9.0/5.0 + 32.0
 303  continue
c
c.....3x3 Taverage
      tsum=0.0
      is3=ic-nl-1
      do 402 k=1,3
      do 401 i=is3,is3+2
      tsum=tsum+trf(i,npc)
 401  continue
      is3=is3+nl
```

```
 402   continue
       t33=tsum/9.0
c
c.....5x5 Taverage
       tsum=0.0
       is5=ic-2*nl-2
       do 404 k=1,5
       do 403 i=is5,is5+4
       tsum=tsum+trf(i,npc)
 403   continue
       is5=is5+nl
 404   continue
       t55=tsum/25.0
c
c.....7x7 Taverage
       tsum=0.0
       n7=0
       is7=ic-3*nl-3
       do 406 k=1,7
       do 405 i=is7,is7+6
       if (ql(i).eq.0.0) goto 405
       tsum=tsum+trf(i,npc)
       n7=n7+1
 405   continue
       is7=is7+nl
 406   continue
       t77=tsum/n7
c
c.....Hot-Rods Taverage
       tsum1=0.0
       tsum2=0.0
       ndum=0
       do 407 i=1,nrod
       if (ql(i).eq.0.0) then
       tsum2=tsum2+trf(i,npc)
       ndum=ndum+1
       goto 407
       endif
       tsum1=tsum1+trf(i,npc)
 407   continue
       thot=tsum1/float(nrod-ndum)
       tcold=tsum2/float(ndum)
c
       write(12,601) time,trf(ic,1),trf(ic,npc),trf(22,npc),
     +                     trf(1,npc),thf(1),thf(np1),t33,t55,t77
       write(13,701) time,qrh,qrf,qhf,qloss,thot,tcold,thf(np1)
       ndt1=0
       endif
       if(ndt2.eq.nprt2) then
       call print
       ndt2=0
       endif
c
       if(time.lt.tmax) goto 100
```

```
c
      return
c
 601  format(10(1x,F8.2))
 701  format(8(1x,F9.0))
c
      end
c
c*****************************************************************
c
      subroutine rads
c
      implicit double precision (a-h,o-z)
c
      common /vf/ f(1001,1001),area(1001)
      common/heat/q(1001),qrad(1001),qconv(1001),temp(1001),
     +  emiss(1001),bs(1001),qold(1001)
      common/geoint/nrod,n,nl
c
      dimension a(1001,1001),b(1001),c(1001)
c
      do 205 i=1,n
      do 204 j=1,n
 204  a(i,j) =-f(i,j)*(1.0d0-emiss(i))
      a(i,i)=a(i,i)+1.0
 205  continue
      do 206 i=1,n
      b(i)=emiss(i)*temp(i)**4.0d0
 206  continue
c
      call gauss(a,n,b,bs)
c
      return
      end
c
c*****************************************************************
c
      subroutine conv
c
      implicit double precision (a-h,o-z)
c
      common /vf/ f(1001,1001),area(1001)
      common/heat/q(1001),qrad(1001),qconv(1001),temp(1001),
     +  emiss(1001),bs(1001),qold(1001)
      common/heat1/tfad,tenvad,h,hout,hmin,qct,qrt,qt
      common/geoint/nrod,n,nl
      common/temp/told(1001)
      common/converg/alfa
c
      data sig/5.67D-08/
c
      qct=0.0
      qrt=0.0
      qt=0.0
```

```
c
      do 102 i=1,n
      sumbs=0.0d0
      do 101 j=1,n
      sumbs=sumbs+f(i,j)*bs(j)
 101  continue
c
c.....special case: radiation dominated cases
      if (h.lt.hmin) then
      eb=q(i)*(1.0d0-emiss(i))/emiss(i) + bs(i)
      temp(i)=eb**0.25d0
      goto 102
      endif
c
      temp(i)=tfad + (q(i)-bs(i)+sumbs)/h
 102  continue
      c1=(h*tfad+hout*tout)/(h+hout)
      c2=1.0d0/(h+hout)
      temp(n)=c1+c2*(sumbs-bs(n))
c
c.....underrelaxation
      do 103 i=1,n
      temp(i)=(1.0d0-alfa)*told(i) + alfa*temp(i)
 103  continue
c
      do 105 i=1,n
      qconv(i)=h*(temp(i)-tfad)
      qrad(i)=q(i)-qconv(i)
      qrt=qrt+qrad(i)*area(i)
      qt=qt+q(i)*area(i)
      qct=qct+qconv(i)*area(i)
 105  continue
      if (h.lt.hmin) temp(n)=tenvad+qt/(hout*area(n))
c
      return
      end
c
c*******************************************************************
c
       subroutine gauss(a,na,b,c)
c
       implicit double precision (a-h,o-z)
       dimension a(1001,1001),b(1001),c(1001)
c
       k=1
   20  tmp = 1.d0/a(k,k)
       j=k
   30  a(k,j) = a(k,j)*tmp
       if (j.eq.na) goto 40
       j=j+1
       goto 30
   40  b(k) = b(k)*tmp
       j=k+1
   50  tmp = a(j,k)
```

```
      l=k
   60 a(j,l) = a(j,l)-a(k,l)*tmp
      if (l.eq.na) goto 70
      l=l+1
      goto 60
   70 b(j) = b(j)-b(k)*tmp
      if (j.eq.na) goto 80
      j=j+1
      goto 50
   80 if (k.eq.na-1) goto 90
      k=k+1
      goto 20
   90 continue
      c(na) = b(na)/a(na,na)
      i=1
  120 sum = 0.0
      j=na-i+1
  100 sum = sum+a(na-i,j)*c(j)
      if (j.eq.na) goto 110
      j=j+1
      goto 100
  110 c(na-i) = b(na-i)-sum
      if (i.eq.na-1) goto 130
      i=i+1
      goto 120
  130 continue
c
      return
      end
c
c*********************************************************************
c
      subroutine trod
c
      implicit double precision (a-h,o-z)
c
      common/trans1/regsze(4),ql(1000),qr(1000),tr(1000,100),th(100)
      common/trans2/ndreg,ndx,ndr,npc,np1,ntab,ntab2,ifrad,inuc
      common/trans3/dt,tmax,time,tft,s,tenv,hloss,qavg,htrs,trst,
     +              tdst,thst,tmin,fdcy,hgap
      common/trans4/tme(100),hft(100),tmep(100),pdcy(100),tmix(100)
      common/heat/q(1001),qrad(1001),qconv(1001),temp(1001),
     +              emiss(1001),bs(1001),qold(1001)
      common/geoint/nrod,n,nl
      common/geo/vrod(1000)
c
      dimension cd(100),cp(100),t(100),qh(100),ddr(100)
c
      data pi/3.141592654/
c
      do 201 j=1,nrod
c
      do 10 i=1,npc
      t(i)=tr(j,i)
```

```
      qh(i)=0.0
  10  continue
      i1=ndreg+2
      i2=ndreg*2
     do 20 i=i1,i2
      qh(i)=ql(j)*fdcy/float(ndreg-1)
  20  continue
      qvnuc=0.0
      if (inuc.ne.0) qvnuc=fdcy*ql(j)/(vrod(1)+vrod(2)+vrod(3))

c
c.....calculation properties
c
      ireg=1
      jr=1
      do 50 i=1,ndr
      ddr(i)=regsze(ireg)/float(ndreg)
      tn=t(i)
      call prop(tn,ireg,cnd,cpm,inuc)
     if (ql(j).eq.0.0) call prop(tn,4,cnd,cpm,inuc)
     if (i.eq.(ndreg*3+1).and.hgap.ne.0)
     +     cnd=cnd*hgap*ddr(i)/(cnd+hgap*ddr(i))
     cd(i)=cnd
     cp(i)=cpm
      if (jr.eq.ndreg) then
      jr=0
      ireg=ireg+1
      endif
      jr=jr+1
  50  continue
c
c.....calculation conduction in rod
c.....centerline, inner regions, clad surface
c
      r=0.0
c
      dr=ddr(1)
      vol=0.25*pi*dr**2.0
      a=cd(1)*0.5*(t(2)-t(1))
      c=dt/(cp(1)*vol)
      if (inuc.ne.0) qh(1)=qvnuc*vol
      t(1)=t(1)+(qh(1)+2.0*pi*a)*c
c
      r=ddr(1)
      do 101 i=2,ndr
      drm1=ddr(i-1)
      dr=ddr(i)
      vol=pi*(r*(drm1+dr) + (dr**2.0-drm1**2.0)/4.0)
     vol2=pi*(r*drm1-(drm1**2.0)/4.0)
      if (inuc.ne.0) then
     qh(i)=qvnuc*vol
      if (i.gt.ndreg*3) qh(i)=qvnuc*vol2
      if (i.gt.ndreg*3+1) qh(i)=0.0
      endif
```

```
      a=cd(i)*(r+dr/2.0)*(t(i+1)-t(i))/dr
      b=cd(i-1)*(r-drm1/2.0)*(t(i)-t(i-1))/drm1
      c=dt/(cp(i)*vol)
      t(i)=t(i)+(qh(i)+2.0*pi*(a-b))*c
      r=r+dr
 101  continue
c
      vol=pi*(r*dr - 0.25*dr**2.0)
      a=-cd(ndr)*(r-dr/2.0)*(t(npc)-t(npc-1))/dr
      b=r*(qr(j) + htrs*(t(npc)-tft))
      c=dt/(cp(ndr)*vol)
      t(npc)=t(npc)+(qh(npc)+2.0*pi*(a-b))*c
c
      do 151 i=1,npc
      tr(j,i)=t(i)
 151  continue
c
 201  continue
c
      return
      end
c
c*******************************************************************
c
      subroutine thous
c
      implicit double precision (a-h,o-z)
c
      common/trans1/regsze(4),ql(1000),qr(1000),tr(1000,100),th(100)
      common/trans2/ndreg,ndx,ndr,npc,np1,ntab,ntab2,ifrad,inuc
      common/trans3/dt,tmax,time,tft,s,tenv,hloss,qavg,htrs,trst,
     +              tdst,thst,tmin,fdcy,hgap
      common/trans4/tme(100),hft(100),tmep(100),pdcy(100),tmix(100)
      common/heat/q(1001),qrad(1001),qconv(1001),temp(1001),
     +  emiss(1001),bs(1001),qold(1001)
      common/geoint/nrod,n,nl
c
      dimension cd(100),cp(100),t(100)
c
      data pi/3.141592654/
c
      dx=s/float(ndx)
      np1=ndx+1
c
c.....calculation properties
c
      ireg=4
      do 50 i=1,ndx
      tt=th(i)
      call prop(tt,ireg,cnd,cpm,inuc)
      cd(i)=cnd
      cp(i)=cpm
   50 continue
c
```

```
c.....calculation conduction in the housing wall
c
      a=2.0*cd(1)*(th(2)-th(1))/dx
      b=hloss*(th(1)-tenv)
      c=dt/(cp(1)*dx)
      th(1)=th(1)+(a-b)*c
c
      do 101 i=2,ndx
      a=2.0*cd(i)*(th(i+1)-th(i))/dx
      b=2.0*cd(i-1)*(th(i)-th(i-1))/dx
      c=dt/(cp(i)*dx)
      th(i)=th(i)+(a-b)*c
      r=r+dr
 101  continue
c
      a=-2.0*cd(ndx)*(th(np1)-th(np1-1))/dx
      b=htrs*(th(np1)-tft)
      c=dt/(cp(ndx)*dx)
      th(np1)=th(np1)+(a-b-qr(n))*c
c
      return
      end
c
c*******************************************************************
c
      subroutine prop(tk,ireg,cnd,cpm,inuc)
c
      implicit double precision (a-h,o-z)
c
      t=tk-273.14
c
c.....nuclear rod
c
      if (inuc.eq.0) goto 100
      if (ireg.eq.4) goto 110
c
c.....uranium dioxide
      rho=9649.0
      cnd=2.45
      cpm=333.0*rho
      return
c
c.....zircalloy
 110  rho=6560.0
      a=1.461e-2
      b=12.092
      cnd=a*t+b
      cpm=347.0*rho
      return
c
c.....region 1 and 3 - BN
c
 100  if (ireg.ne.3.and.ireg.ne.1) goto 101
      rho=1910.0
```

```
      a=-0.061356
      b=122.734
      cnd=a*t + b
      cpm=1500*rho
      return
c
c.....region 2 - Heater
 101  if (ireg.ne.2) goto 102
      rho=8470.0
      a=4.7742e-10
      b=-1.1151e-6
      c=5.2571e-4
      d=4.0755e-1
      cpm=1000.0*(a*t**3.0+b*t**2.0+c*t+d)*rho
      a=2.8263e-2
      b=17.583

      cnd=a*t+b
      return
c
c.....region 4 - Clad - Inconel 600
c
 102  rho=8270.0
      a=4.7427e-4
      b=4.1430e-1
      cpm=1000.0*(a*t+b)*rho
      a=1.6972e-2
      b=14.599
      cnd=a*t+b
      cnd=15.0
      return
c
      end
c
c
c*************************************************************
c
      subroutine print
c
      implicit double precision (a-h,o-z)
c
      common/heat/q(1001),qrad(1001),qconv(1001),temp(1001),
     +  emiss(1001),bs(1001),qold(1001)
      common/trans3/dt,tmax,time,tft,s,tenv,hloss,qavg,htrs,trst,
     +                tdst,thst,tmin,fdcy,hgap
      common/trans4/tme(100),hft(100),tmep(100),pdcy(100),tmix(100)
      common/printc/tpcv,nprt1,nprt2,imod
      common/geoint/nrod,n,nl
c
      data sig/5.67D-08/
c
c.....print results
      if (imod.eq.0) write(11,900)
      if (imod.eq.1) write(11,904) time
```

```
      do 250 i=1,n
      temp(i)=temp(i)/(sig/qavg)**0.25d0
c
c.....conversion to british units
      temp(i)=(temp(i)-273.14)*9.0/5.0 + 32.0
c
 250  continue
c
      k1=1
      k2=k1+nl-1
      do 600 i=1,nl
      write(11,903) (temp(k),k=k1,k2)
      k1=k1+nl
      k2=k2+nl
 600  continue
      write(11,901) temp(n)
      tpcv=(tpcv-273.14)*9.0/5.0 + 32.0
      if (imod.eq.0) write(11,902) tpcv
c
      return
c
 900  format(///,3x,'RESULTS STEADY STATE',
     +       //,3x,'RODS SURFACE TEMPERATURE (F)',//)
 904  format(///,'**********************************************',
     +       /,3x,'RESULTS AT TIME (sec) = ',F7.2,
     +       //,3x,'RODS SURFACE TEMPERATURE (F)',//)
 901  format(/,3x,'HOUSING TEMPERATURE (INSIDE WALL) (F)  = ',F7.2)
 902  format(//,3x,'Rod Surf. Temp. for infinite array at SS (F) = ',
     +       F7.2)
 903  format(20(1x,F7.2))
c
      end
c
c
c*********************************************************************
c
      subroutine vufac(nmx,dd,p,drh)
C
c     the subroutine is based
C     VUFAC   12/06/78 D.R.EVANS
c     and modified by C. Frepoli 3/10/98
c     the symmentry logic (MIRRIM, ISWAP etc.) is deleted
c
      implicit double precision (a-h,o-z)
C
c      DIMENSION AREA(226),R0(225)
      dimension r0(1000)
      COMMON /VF/ F(1001,1001),area(1001)
      COMMON /RI/ RIJ(1001,1001)
c
      data nf,npt,n,na/1001,200,37,37/
      data pi/3.14159265358979323846/

c
```

```
      xlh=p*float(nmx-1)+dd+2.0*drh
c
      nlim=nmx
      n2=nmx*nmx +1
      nl=nmx
      nl=8
      nl1=nmx
      ahs=xlh*4.0
c
      NP=N2-1
      TWOPI=2.*PI
      DO 1700 I=1,NP
      r0(i)=dd/2.0
      AREA(I)=TWOPI*R0(I)
1700  CONTINUE
      AREA(N2)=ahs
c
      CALL VFAC(F,AREA,AEA,SCALFC,BB,R0,IROW,JCOL,MIRRIM,P,PI,N,
     1NF,NLIM,N2,NA,NSYM,NL,NL1,NPT)
c
       do 998 i=1,n2
       do 997 j=1,n2
       write(9,*) i,j,f(i,j)
  997  continue
       write(9,*) area(i)
  998  continue
c
      return
      END
c
C******       FIJ      12/12/78 D.R.EVANS
       SUBROUTINE FIJ(F,R,P,PI,M,NPT,L,SOURCE,IX,IY,L1,L2,IRC,IA)
      implicit double precision (a-h,o-z)
       DIMENSION F(M,1),R(1),XA(2,100),YA(2,100),RA(2,100)
      COMMON /RI/ RIJ(1001,1001)
       INTEGER SOURCE,TARGET,UPPER(14),LOWER(14)
       LOGICAL SKIP
       DATA XA(1,1),YA(1,1)/2*0.D0/
       DATA SKIP/.FALSE./
       IF(SKIP) GO TO 10
       SKIP=.TRUE.
       RNPT=1.D0/NPT
       DELTA=2.D0*PI*RNPT
       RDELT=1.D0/DELTA
       PIO2=.5D0*PI
   10  CONTINUE
       IF(IRC-2) 12,16,20
   12  CONTINUE
C         ROWS
       IF(IA.EQ.2) GO TO 14
C         ADJACENT ROW
       IXY=IX
       K2=L
       K3=1
```

```
      GO TO 24
   14 CONTINUE
C       ROWS BEYOND ADJACENT ROW
      IXY=IY
      IYX=IX
      I3=1
      K2=0
      K3=L
      GO TO 24
   16 CONTINUE
C       HIGHER-NUMBERED COLUMNS
      IF(IA.EQ.2) GO TO 18
C       ADJACENT COLUMN
      K2=1
      GO TO 22
   18 CONTINUE
C       COLUMNS BEYOND ADJACENT COLUMN
      IXY=IX
      IYX=IY
      I3=L
      K2=0
      K3=1
      GO TO 24
   20 CONTINUE
C       LOWER-NUMBERED COLUMNS
      K2=-1
   22 CONTINUE
      IXY=IY
      K3=L
   24 CONTINUE
C       COMPUTE SHADOWING ROD NUMBERS
      KMI=L2-IXY
      IF(KMI.LT.0) KMI=L1-IXY
      KMIABS=IABS(KMI)
      TARGET=SOURCE+K2+K3*KMI
      I2=K3*ISIGN(1,KMI)
      IF(IA.EQ.2) GO TO 30
C       ADJACENT ROW AND COLUMNS
      K4=KMIABS
      GO TO 40
   30 CONTINUE
C       ROWS AND COLUMNS BEYOND ADJACENT
      K4=KMIABS-1
      UPPER(1)=0
      LOWER(KMIABS)=0
      K5=0
   40 CONTINUE
      DO 70 I=1,K4
      LOWER(I)=SOURCE+I2*I
      IF(IA.EQ.2) GO TO 60
      UPPER(I)=TARGET-I2*(KMIABS-I+1)
      GO TO 70
   60 CONTINUE
      UPPER(I+1)=LOWER(I)+I3
```

```
      IF(IYX.EQ.L) UPPER(I+1)=0
   70 CONTINUE
      K=KMIABS+1
C       SET RADII AND COORDINATES OF SOURCE,TARGET, AND ALL POTENTIAL
C       SHADOWING RODS
      R1=R(SOURCE)
      RA(1,1)=R1
      RA(2,K)=R(TARGET)
C     XA(2,1)=0.D0
      XA(2,1)=0.E0
      YA(2,1)=P
      DO 230 I=1,KMIABS
      FI=I
      PTFI=P*FI
      IP1=I+1
      XA(1,IP1)=PTFI
C     YA(1,IP1)=0.D0
      YA(1,IP1)=0.E0
      XA(2,IP1)=PTFI
      YA(2,IP1)=P
      IF(LOWER(I).EQ.0) GO TO 200
      RA(1,IP1)=R(LOWER(I))
      GO TO 210
  200 CONTINUE
C     RA(1,IP1)=0.D0
      RA(1,IP1)=0.E0
  210 CONTINUE
      IF(UPPER(I).EQ.0) GO TO 220
      RA(2,I)=R(UPPER(I))
      GO TO 230
  220 CONTINUE
C     RA(2,I)=0.D0
      RA(2,I)=0.E0
  230 CONTINUE
      DO 700 K1=L1,L2
      KMI=K1-IXY
      KMIABS=IABS(KMI)
      TARGET=SOURCE+K2+K3*KMI
      K=KMIABS+1
      IF(IA.EQ.2) GO TO 235
      Y1=YA(2,K)
      R2=RA(2,K)
      K4=KMIABS
      GO TO 238
  235 CONTINUE
      IF(R(SOURCE).LE.R(LOWER(1)).AND.
     * R(LOWER(KMIABS-1)).GE.R(TARGET)) GO TO 700
C     Y1=0.D0
      Y1=0.E0
      R2=R(TARGET)
      K4=KMIABS-1
  238 CONTINUE
      X1=XA(2,K)
      FKMI=KMIABS-1
```

```
C     DIAG=FKMI**2+1.D0
      DIAG=FKMI**2+1.E0
C     RR12=1.D0/(P*DSQRT(DIAG))
      RR12=1.E0/(P* SQRT(DIAG))
      TEMP=P*SQRT((FLOAT(KMIABS))**2+1.)
      RIJ(SOURCE,TARGET)=TEMP-0.5*(R(SOURCE)+R(TARGET))
C     I1=RDELT*(PI-DARCOS((R1+R2)*RR12)-DATAN2(1.D0,FKMI))
      I1=RDELT*(PI-  ACOS((R1+R2)*RR12)- ATAN2(1.E0,FKMI))
  240 CONTINUE
C       COMPUTE VIEW FACTOR
      VIEWFC=0.
      DO 500 IPT=I1,NPT
      XIPT = IPT - 1
      THETA = DELTA * XIPT
C     XV=-R1*DCOS(THETA)
      XV=-R1* COS(THETA)
C     YV=R1*DSIN(THETA)
      YV=R1* SIN(THETA)
C       DETERMINE IF (XV,YV) CAN SEE THE TARGET ROD
      IF(XV*X1+YV*Y1.LE.R1*(R1-R2)) GO TO 500
C       TS IS THE TANGENT TO THE SOURCE ROD AT (XV,YV)
C     TS=DATAN2(-XV,YV)
      TS= ATAN2(-XV,YV)
C       COMPUTE TANGENTS TO TARGET ROD
C       T1 IS THE LOWER TANGENT TO THE TARGET ROD
C       T2 IS THE UPPER TANGENT TO THE TARGET ROD
      X1MXP=X1-XV
      Y1MYP=Y1-YV
      RSQ=X1MXP**2+Y1MYP**2
C     S=DSQRT(RSQ-R2**2)
      S= SQRT(RSQ-R2**2)
C     RRSQ=1.D0/RSQ
      RRSQ=1.E0/RSQ
      SORSQ=S*RRSQ
      R1ORSQ=R2*RRSQ
      A=SORSQ*X1MXP
      B=R1ORSQ*Y1MYP
      C=SORSQ*Y1MYP
      D=R1ORSQ*X1MXP
      XTAMXP=S*(A-B)
      YTAMYP=S*(C+D)
      XTBMXP=S*(A+B)
      YTBMYP=S*(C-D)
C     T2=DATAN2(YTAMYP,XTAMXP)
      T2= ATAN2(YTAMYP,XTAMXP)
C     T1=DATAN2(YTBMYP,XTBMXP)
      T1= ATAN2(YTBMYP,XTBMXP)
C       COMPUTE TANGENTS THROUGH (XV,YV) TO SHADOWING RODS
C       FIND MINIMUM UPPER SHADOWING AND MAXIMUM LOWER SHADOWING
      DO 300 J=1,2
      DO 300 I=1,K4
      RB=RA(J,I+2-J)
      IF(RB.EQ.0.) GO TO 300
      XB=XA(J,I+2-J)
```

```
      YB=YA(J,I+2-J)
      X1MXP=XB-XV
      Y1MYP=YB-YV
      RSQ=X1MXP**2+Y1MYP**2
C     S=DSQRT(RSQ-RB**2)
      S= SQRT(RSQ-RB**2)
      IF(S.EQ.0.) GO TO 260
C     RRSQ=1.D0/RSQ
      RRSQ=1.E0/RSQ
      SORSQ=S*RRSQ
      R1ORSQ=RB*RRSQ
      A=SORSQ*X1MXP
      B=R1ORSQ*Y1MYP
      C=SORSQ*Y1MYP
      D=R1ORSQ*X1MXP
      IF(J.EQ.2) GO TO 250
C       UPPER TANGENTS TO LOWER SHADOWING RODS
      XTAMXP=S*(A-B)
      YTAMYP=S*(C+D)
      TA=DATAN2(YTAMYP,XTAMXP)
c     TA= ATAN2(YTAMYP,XTAMXP)
      T1=DMAX1(TA,T1)
c      T1=AMAX1(TA,T1)
      GO TO 300
  250 CONTINUE
C       LOWER TANGENTS TO UPPER SHADOWING RODS
      XTBMXP=S*(A+B)
      YTBMYP=S*(C-D)
      TB=DATAN2(YTBMYP,XTBMXP)
c     TB= ATAN2(YTBMYP,XTBMXP)
      T2=DMIN1(TB,T2)
c     T2=AMIN1(TB,T2)
      GO TO 300
  260 CONTINUE
      IF(J.EQ.2) GO TO 270
      T1=DMAX1(PIO2,T1)
c     T1=AMAX1(PIO2,T1)
      GO TO 300
  270 CONTINUE
      T2=DMIN1(0.D0,T2)
c     T2=AMIN1(0.E0,T2)
  300 CONTINUE
      IF (T1 .GE. T2) GO TO 490
      IF (T1 .LT. TS .OR.  T1 .GE. TS + PI) GO TO 320
      PHI1 = T1 - TS
      GO TO 350
  320 CONTINUE
      PHI1 = 0.
      IF (T1 .GE. TS) PHI1 = PI
  350 CONTINUE
      IF (T2 .LT. TS .OR. T2 .GE. TS + PI) GO TO 370
      PHI2 = T2 - TS
      GO TO 380
  370 CONTINUE
```

```
      PHI2 = 0.
      IF  (T2 .GE. TS) PHI2 = PI
 380  CONTINUE
C     CONFIG=.5D0*(DCOS(PHI1)-DCOS(PHI2))
      CONFIG=.5E0*( COS(PHI1)- COS(PHI2))
      VIEWFC=VIEWFC+CONFIG
      GO TO 500
 490  CONTINUE
      IF(VIEWFC.NE.0.) GO TO 510
 500  CONTINUE
 510  CONTINUE
      IF(IA.EQ.1) GO TO 550
      IF(K5.EQ.1) GO TO 540
      FSAVE=VIEWFC
      K5=K5+1
      DO 530 I=1,K4
      IF(IYX.EQ.1) GO TO 520
      UPPER(I+1)=LOWER(I)-I3
      RA(2,I+1)=R(UPPER(I+1))
      GO TO 530
 520  CONTINUE
C     RA(2,I+1)=0.D0
      RA(2,I+1)=0.E0
 530  CONTINUE
      GO TO 240
 540  CONTINUE
      VIEWFC=VIEWFC+FSAVE
      K5=0
      DO 545 I=1,K4
      IF(IYX.EQ.L) GO TO 542
      UPPER(I+1)=LOWER(I)+I3
      RA(2,I+1)=R(UPPER(I+1))
      GO TO 545
 542  CONTINUE
C     RA(2,I+1)=0.D0
      RA(2,I+1)=0.E0
 545  CONTINUE
 550  CONTINUE
      F(SOURCE,TARGET)=VIEWFC*RNPT
 700  CONTINUE
      RETURN
      END
C
C******       PATHLEN 12/14/78 D.R.EVANS
      SUBROUTINE PATHLEN(R,DELTAX,P,N2,L)
      implicit double precision (a-h,o-z)
      DIMENSION F(15),R(1)
      COMMON /RI/ RIJ(1001,1001)
      INTEGER SOURCE
      REAL L1,L2,L3,L4
      DATA F/0.5,0.086740,0.013966,0.001517,0.000424,0.000172,
     1      0.000088,0.000048,0.000034,6*0./
C        COMPUTE PATH LENGTHS FROM RODS TO CANISTER
      DO 100 IX=1,L
```

```
      DO 100 IY=1,L
      SOURCE=IY+(IX-1)*L
      HALFR1=0.5*R(SOURCE)
C        PATH OND
      L1=P*FLOAT(IX-1)+DELTAX-HALFR1
C        PATH TWO
      L2=P*FLOAT(L-IX)+DELTAX-HALFR1
C        PATH THREE
      L3=P*FLOAT(IY-1)+DELTAX-HALFR1
C        PATH FOUR
      L4=P*FLOAT(L-IY)+DELTAX-HALFR1
C        PATH LENGTH IS THE VIEW-FACTOR-WEIGHTED MEAN OF FOUR
C        CONTRIBUTIONS
      RIJ(SOURCE,N2)=(L1*F(IX)
     1              +L2*F(L-IX+1)
     2              +L3*F(IY)
     3              +L4*F(L-IY+1)) /
     4              (F(IX)
     5              +F(L-IX+1)
     6              +F(IY)
     7              +F(L-IY+1))
100   CONTINUE
      RETURN
      END
c
C******       STRING  12/12/78 D.R.EVANS
      SUBROUTINE STRING(F,R,P,PI,M,L,SOURCE,IX,IY)
      implicit double precision (a-h,o-z)
      DIMENSION F(M,1),R(1)
      COMMON /RI/ RIJ(1001,1001)
      DIMENSION TIN(1000,4),THET(1000,4),TEX(1000,2),ALPH(1000,2)
      INTEGER SOURCE,TARGET
      LOGICAL SKIP
      DATA SKIP/.FALSE./,PP/0./
      IF(SKIP) GO TO 10
      SKIP=.TRUE.
C     RPI=1.D0/PI
      RPI=1.E0/PI
C     PIO2=.5D0*PI
      PIO2=.5E0*PI
C     PIO4=.5D0*PIO2
      PIO4=.5E0*PIO2
   10 CONTINUE
      IF(PP.EQ.P) GO TO 20
      PP=P
      PSQ=P**2
C     R13SQ=2.D0*PSQ
      R13SQ=2.E0*PSQ
C     RR13=1.D0/DSQRT(R13SQ)
      RR13=1.E0/ SQRT(R13SQ)
C     RP=1.D0/P
      RP=1.E0/P
   20 CONTINUE
C       COMPUTE TANGENT LENGTHS AND ANGLES FOR CROSSED STRING METHOD
```

```
      IF(IX.GT.1.OR.IY.EQ.L) GO TO 145
      J1=SOURCE
      J2=SOURCE+L-2
      DO 140 I=J1,J2
      R1=R(I)
      R2=R(I+1)
      R3=R(I+1+L)
      R4=R(I+L)
      R2MR3=R2-R3
      R4MR3=R4-R3
C     TIN13=DSQRT(R13SQ-(R1+R3)**2)
      TIN13= SQRT(R13SQ-(R1+R3)**2)
C     TIN23=DSQRT(PSQ-(R2+R3)**2)
      TIN23= SQRT(PSQ-(R2+R3)**2)
C     TIN34=DSQRT(PSQ-(R3+R4)**2)
      TIN34= SQRT(PSQ-(R3+R4)**2)
C     TIN24=DSQRT(R13SQ-(R2+R4)**2)
      TIN24= SQRT(R13SQ-(R2+R4)**2)
      TIN(I,2)=TIN13
      TIN(I+1,3)=TIN23
      TIN(I+L,1)=TIN34
      TIN(I+1,4)=TIN24
C     THET(I,2)=DARSIN(TIN13*RR13)
      THET(I,2)=  ASIN(TIN13*RR13)
C     THET(I+1,3)=DARSIN(TIN23*RP)
      THET(I+1,3)=  ASIN(TIN23*RP)
C     THET(I+L,1)=DARSIN(TIN34*RP)
      THET(I+L,1)=  ASIN(TIN34*RP)
C     THET(I+1,4)=DARSIN(TIN24*RR13)
      THET(I+1,4)=  ASIN(TIN24*RR13)
      IF(R2MR3.EQ.0.) GO TO 100
C     ALPH(I+1,2)=DARCOS(R2MR3*RP)
      ALPH(I+1,2)=  ACOS(R2MR3*RP)
C     TEX(I+1,2)=DSQRT(PSQ-R2MR3**2)
      TEX(I+1,2)= SQRT(PSQ-R2MR3**2)
      GO TO 105
  100 CONTINUE
      ALPH(I+1,2)=PIO2
      TEX(I+1,2)=P
  105 CONTINUE
      IF(R4MR3.EQ.0.) GO TO 110
C     ALPH(I+L,1)=DARCOS(R4MR3*RP)
      ALPH(I+L,1)=  ACOS(R4MR3*RP)
C     TEX(I+L,1)=DSQRT(PSQ-R4MR3**2)
      TEX(I+L,1)= SQRT(PSQ-R4MR3**2)
      GO TO 115
  110 CONTINUE
      ALPH(I+L,1)=PIO2
      TEX(I+L,1)=P
  115 CONTINUE
      IF(I.GT.J1) GO TO 130
      R1MR4=R1-R4
C     TIN14=DSQRT(PSQ-(R1+R4)**2)
      TIN14= SQRT(PSQ-(R1+R4)**2)
```

```
      TIN(I,3)=TIN14
C     THET(I,3)=DARSIN(TIN14*RP)
      THET(I,3)=  ASIN(TIN14*RP)
      IF(R1MR4.EQ.0.) GO TO 120
C     ALPH(I,2)=DARCOS(R1MR4*RP)
      ALPH(I,2)=  ACOS(R1MR4*RP)
C     TEX(I,2)=DSQRT(PSQ-R1MR4**2)
      TEX(I,2)= SQRT(PSQ-R1MR4**2)
      GO TO 125
  120 CONTINUE
      ALPH(I,2)=PIO2
      TEX(I,2)=P
  125 CONTINUE
  130 CONTINUE
      IF(IY.GT.1) GO TO 140
      R1MR2=R1-R2
C     TIN12=DSQRT(PSQ-(R1+R2)**2)
      TIN12= SQRT(PSQ-(R1+R2)**2)
      TIN(I,1)=TIN12
C     THET(I,1)=DARSIN(TIN12*RP)
      THET(I,1)=  ASIN(TIN12*RP)
      IF(R1MR2.EQ.0.) GO TO 135
C     ALPH(I,1)=DARCOS(R1MR2*RP)
      ALPH(I,1)=  ACOS(R1MR2*RP)
C     TEX(I,1)=DSQRT(PSQ-R1MR2**2)
      TEX(I,1)= SQRT(PSQ-R1MR2**2)
      GO TO 140
  135 CONTINUE
      ALPH(I,1)=PIO2
      TEX(I,1)=P
  140 CONTINUE
  145 CONTINUE
C       COMPUTE ADJACENT AND DIAGONAL ROD VIEW FACTORS
C       USING CROSSED STRING METHOD
C       COMPUTE ADJACENT ROD VIEW FACTORS
      R1=R(SOURCE)
      DO 150 I=1,2
      IF(IX.EQ.L.AND.I.EQ.1) GO TO 150
      IF(IY.EQ.L.AND.I.EQ.2) GO TO 150
      TARGET=SOURCE+L**(I-1)
      R2=R(TARGET)
      CROLEN=TIN(SOURCE,2**I-1)+R1*ALPH(SOURCE,I)
     * +R2*(PI-ALPH(SOURCE,I))-(R1+R2)*THET(SOURCE,2**I-1)
      CROMUN=CROLEN-TEX(SOURCE,I)
C     F(SOURCE,TARGET)=.5D0*RPI*CROMUN/R1
      F(SOURCE,TARGET)=.5E0*RPI*CROMUN/R1
      RIJ(SOURCE,TARGET)=P-0.5*(R1+R2)
      IF(IY.NE.IX) GO TO 150
      F(SOURCE,SOURCE+L)=F(SOURCE,TARGET)
      RIJ(SOURCE,SOURCE+L)=RIJ(SOURCE,TARGET)
      GO TO 152
  150 CONTINUE
  152 CONTINUE
      IF(IY.EQ.L) GO TO 190
```

```
C         COMPUTE DIAGONAL ROD VIEW FACTORS
      DO 185 I=1,2
      IF(IX.EQ.1.AND.I.EQ.1) GO TO 185
      IF(IX.EQ.L.AND.I.EQ.2) GO TO 185
      MORP1=(-1)**I
      M1ORZ=I-2
      TARGET=SOURCE+L+MORP1
      R2=R(SOURCE+MORP1)
      R3=R(TARGET)
      R4=R(SOURCE+L)
      TIN12=TIN(SOURCE+M1ORZ,1)
      THET12=THET(SOURCE+M1ORZ,1)
      TIN13=TIN(SOURCE,2**(3-I))
      THET13=THET(SOURCE,2**(3-I))
      TIN14=TIN(SOURCE,3)
      THET14=THET(SOURCE,3)
      TIN23=TIN(SOURCE+MORP1,3)
      THET23=THET(SOURCE+MORP1,3)
      TIN34=TIN(SOURCE+L+M1ORZ,1)
      THET34=THET(SOURCE+L+M1ORZ,1)
      PSI2=PIO2-THET12-THET23
      PSI4=PIO2-THET14-THET34
      IF(PSI2.GT.0.) GO TO 155
      R1MR3=R1-R3
C     ALPH31=DARCOS(R1MR3*RR13)
      ALPH31=  ACOS(R1MR3*RR13)
      PSI312=ALPH31-THET13
      PSI132=PI-ALPH31-THET13
C     TIN12=DSQRT(R13SQ-R1MR3**2)
      TIN12= SQRT(R13SQ-R1MR3**2)
C     TIN23=0.D0
      TIN23=0.E0
C     PSI2=0.D0
      PSI2=0.E0
      GO TO 160
  155 CONTINUE
      PSI312=PIO4+THET12-THET13
      PSI132=PIO4+THET23-THET13
  160 CONTINUE
      IF(PSI4.GT.0.) GO TO 175
      IF(PSI2.LE.0.) GO TO 165
      R1MR3=R1-R3
C     ALPH31=DARCOS(R1MR3*RR13)
      ALPH31=  ACOS(R1MR3*RR13)
      PSI314=ALPH31-THET13
      PSI134=PI-ALPH31-THET13
C     TIN14=DSQRT(R13SQ-R1MR3**2)
      TIN14= SQRT(R13SQ-R1MR3**2)
      GO TO 170
  165 CONTINUE
      PSI314=PSI312
      PSI134=PSI132
      TIN14=TIN12
  170 CONTINUE
```

```
C       TIN34=0.D0
        TIN34=0.E0
C       PSI4=0.D0
        PSI4=0.E0
        GO TO 180
  175   CONTINUE
        PSI314=PIO4+THET14-THET13
        PSI134=PIO4+THET34-THET13
  180   CONTINUE
C       CROLEN=2.D0*TIN13+R1*(PSI312+PSI314)+R3*(PSI132+PSI134)
        CROLEN=2.E0*TIN13+R1*(PSI312+PSI314)+R3*(PSI132+PSI134)
        UNCLEN=TIN12+TIN23+TIN34+TIN14+R2*PSI2+R4*PSI4
        CROMUN=CROLEN-UNCLEN
C       F(SOURCE,TARGET)=.25D0*RPI*CROMUN/R1
        F(SOURCE,TARGET)=.25E0*RPI*CROMUN/R1
        RIJ(SOURCE,TARGET)=SQRT(R13SQ)-0.5*(R1+R3)
  185   CONTINUE
  190   CONTINUE
        RETURN
        END
c
C******        VFAC     12/12/78 D.R.EVANS
        SUBROUTINE VFAC(F,AREA,E,SCALFC,B,R0,IROW,JCOL,MIRRIM,P,PI,N,
     1  M,L,N2,NA,NSYM,NL,NL1,NPT)
       implicit double precision (a-h,o-z)
        DIMENSION F(M,1),AREA(1),E(1),SCALFC(1),B(NA,1),IROW(1),
     1  JCOL(1),MIRRIM(20,1),R0(1)
       COMMON /RI/ RIJ(1001,1001)
        INTEGER ROD,TARGET
        NP=N2-1
        SL=0.25*AREA(N2)
C          SL IS THE DISTANCE BETWEEN OPPOSITE SIDES OF THE CANISTER
        DELTAX=0.5*(SL-P*FLOAT(L-1))
C          DELTAX IS THE DISTANCE FROM THE CENTER OF AN EDGE ROD TO
C          THE ADJACENT FACE OF THE CANISTER
C          CALCULATE THE PATH LENGTH FROM ROD TO CANISTER
        CALL PATHLEN(R0,DELTAX,P,N2,L)
C
C         GENERATE UPPER DIAGONAL PORTION OF VIEW FACTOR MATRIX
        DO 50 IY=1,L
        IYP2=IY+2
        IYP1=IY+1
        DO 45 IX=1,L
        IYMIX=IY-IX
        IXP2=IX+2
        ROD=IX+L*(IY-1)
C         ZERO OUT MATRIX
        DO 10 KK=ROD,NP
        F(ROD,KK)=0.
        RIJ(ROD,KK)=0.
   10   CONTINUE
C         ADJACENT AND DIAGONAL ROD VIEW FACTORS BY CROSSED STRING
C         METHOD
        CALL STRING(F,R0,P,PI,M,L,ROD,IX,IY)
```

```
      IF(IY.EQ.L) GO TO 40
C       MORE-DISTANT VIEW FACTORS BY MODIFIED VIEWPIN METHOD
C       HIGHER-NUMBERED ROWS
C       ADJACENT ROW
      K1=IX-NL
      IF(K1.LE.0) K1=1
      IXM2=IX-2
      IF(IXM2.LT.K1) GO TO 12
      CALL FIJ(F,R0,P,PI,M,NPT,L,ROD,IX,IY,K1,IXM2,1,1)
   12 CONTINUE
      K2=IX+NL
      IF(K2.GT.L) K2=L
      IF(K2.LT.IXP2) GO TO 14
      CALL FIJ(F,R0,P,PI,M,NPT,L,ROD,IX,IY,IXP2,K2,1,1)
   14 CONTINUE
      IF(IYMIX.NE.0) GO TO 20
      DO 15 KK=K1,K2
      IF(KK.LT.IX.OR.KK.EQ.IYP1) GO TO 15
      TARGET=KK+L*IY
      ITARG2=IYP1+(KK-1)*L
      RIJ(ROD,ITARG2)=RIJ(ROD,TARGET)
      F(ROD,ITARG2)=F(ROD,TARGET)
   15 CONTINUE
   20 CONTINUE
      IF(IYP1.GE.L) GO TO 40
C       ROWS BEYOND ADJACENT ROW
      K2=IY+NL1
      IF(K2.GT.L) K2=L
      IF(K2.LT.IYP2) GO TO 24
      CALL FIJ(F,R0,P,PI,M,NPT,L,ROD,IX,IY,IYP2,K2,1,2)
      IF(IYMIX.NE.0) GO TO 24
      DO 21 KK=IYP2,K2
      TARGET=ROD+(KK-IY)*L
      ITARG2=ROD+KK-IY
      F(ROD,ITARG2)=F(ROD,TARGET)
   21 CONTINUE
   24 CONTINUE
      IF(IX.EQ.1) GO TO 34
C       LOWER-NUMBERED ADJACENT COLUMN
      K2=IY+NL
      IF(K2.GT.L) K2=L
      IF(K2.LT.IYP2) GO TO 40
      CALL FIJ(F,R0,P,PI,M,NPT,L,ROD,IX,IY,IYP2,K2,3,1)
   34 CONTINUE
      IF(IYMIX.EQ.0) GO TO 45
      IF(IX.EQ.L) GO TO 45
C       HIGHER-NUMBERED COLUMNS
C       ADJACENT COLUMN
      CALL FIJ(F,R0,P,PI,M,NPT,L,ROD,IX,IY,IYP2,K2,2,1)
   40 CONTINUE
      IF(IX.EQ.L-1) GO TO 45
C       COLUMNS BEYOND ADJACENT COLUMN
      K2=IX+NL1
      IF(K2.GT.L) K2=L
```

```
      IF(K2.LT.IXP2) GO TO 44
      CALL FIJ(F,RO,P,PI,M,NPT,L,ROD,IX,IY,IXP2,K2,2,2)
   44 CONTINUE
   45 CONTINUE
   50 CONTINUE
C
C          FILL VIEW FACTOR MATRIX
      DO 225 I=1,NP
      DO 225 J=I,NP
      RIJ(J,I)=RIJ(I,J)
  225 F(J,I)=F(I,J)*AREA(I)/AREA(J)
      SUMA=1.
      DO 230 I=1,NP
      SUM=1.
      DO 235 J=1,NP
  235 SUM=SUM-F(I,J)
      F(I,N2)=SUM
      RIJ(N2,I)=RIJ(I,N2)
      F(N2,I)=F(I,N2)*AREA(I)/AREA(N2)
  230 SUMA=SUMA-F(N2,I)
      F(N2,N2)=SUMA
      RIJ(N2,N2)=0.25*SL
C
      RETURN
      END
C
C
C*************************************************
C
      SUBROUTINE INTERP(X,Y,X1,Y1,N)
C
      implicit double precision (a-h,o-z)
C
      dimension x(100),y(100)
C
      DO 100 I=1,n
      I1=I
      IF(X(I1)-X1) 100,100,200
  100 CONTINUE
  200 Y1=Y(I1-1)+((X1-X(I1-1))/(X(I1)-X(I1-1)))*(Y(I1)-Y(I1-1))
      RETURN
      END
```

4. LISTINGS FOR COBRA-TF

D.1 Introduction

Appendix D contains an input listing from the two-channel model of COBRA-TF and associated input processing as well as the output for time zero. A full listing of the sub-channel model is not given because the listing is too large because the file is too large, instead only the input file is given here.

D.2 Two-Channel Model Listing

```
1********************************* input file listing *********************************
       1234567890123456789012345678901234567890123456789012345678901234567890
           0
           0          0.0
         .001          10          40
         1                   **** RBHT Bundle 7x7 Rods    ****
     1   1
      40.0    1170.     0.0    0.466     124.      0.0    .9999    1.0
 air         .0001
     2   5
     144.8671.74   0 7.22
     27.22071.74
     32.17918.79
     45.04052.95
     550.2471.74 7.22    0
     3   1
     1   3   41.952 1.38  2.0  0.0   0    0 1.0    0   0
   16.  0.0
     0
     4   4   1   0
     1   1   2   4.0
     1   2                           1
     2   1   1  5.75
     2   3   4                       1
     3   2  22   2.51  10
     2     2.51  3     7.72   4     7.72   5    7.72   6     6.85
    20     6.85  21    6.85  22     6.85  22    6.85  23     6.85
     3   5                           2
     4   5                           2
     4   1   3   4.0
     5   5                           3   4
     2
       1234567890123456789012345678901234567890123456789012345678901234567890
    50
     7   8   1   1   1   1   1   0   0   0
   1.2   2   2   3
   1.2   5   2   3
   1.2   8   2   3
   1.2  11   2   3
   1.2  14   2   3
   1.2  17   2   3
   1.2  20   2   3
   1.2  23   2   3
     1   8   2   1     1.4    .2952      1.5    1.984
     2   5   8  11  14  17  20  23
     3  16.      1   1
     4  33.      2   1
     8   3   1   2   2   0   0   0   1
     1   1   1   2    0.05    16.      1.0    5000.   1
```

```
    3  1.0
    2    1    1    2      0.05      29.0      1.0     5000.    1
    4  1.0
    3    2    0    2      0.05       4.       0.0     5000.    1
    4  1.0
    1    3     14.20     14.20       1.0    4             0.      90.0
    1    2    0    4
    1    2
     13.75     521.0    121.75     1563.    157.75     502.0    169.76     502.0
    2    1    1    2
    3
   -1
     13.75     521.0     169.0      521.
    9    3
1234567890123456789012345678901234567890123456789012345678901234567890123456789890
    1 hrod       .374       0.0    4    0
    1     2.0685  0.0     1    3 .044  1.0    3     2.0545  0.0    3    1  .02  0.0
    2 tube       .374      .209    1    0
    3     1.0825  0.0
    3 wall     14.20       .250    1         0
    3    1 .250
   10    3
    1   17     516.7
       32.     .1010    8.1400       70.      .1030     8.340
      212.     .1110     9.090      392.      .1210     10.04
      500.     .1270     10.60      572.      0.131     10.98
      752.     .1410     11.93      932.      0.151     12.88
     1000.     0.158     13.23     1112.      0.166     13.82
     1292.     0.178     14.77     1472.      0.191     15.72
     1500.     0.193     15.86     1652.      0.204     16.66
     1832.     0.216     17.61     2012.      0.229     18.56
     2192.     0.241     19.50
    2   14      119.
      212.    .16587     67.37      392.     .22014    63.827
      572.    .26263     60.28      752.     .29590    56.737
      932.    .32194     53.19     1112.     .34233    49.646
     1292.    .35829     46.10     1472.     .37078    42.555
     1652.    .38056     39.01     1832.     .38822    35.464
     2012.    .39421     31.92     2192.     .39891    28.375
     2372.    .40259     24.83     2552.     .40546    21.284
    3   10     528.8
      70.0    .10000    10.083      200.      0.107    11.333
      400.    .11400     13.00      600.      0.117    14.833
      800.      .120     16.50     1000.      0.125    18.333
     1200.      .132     20.00     1400.      0.141    21.833
1234567890123456789012345678901234567890123456789012345678901234567890123456789890
     1600.     0.157     23.50     1800.      0.186    25.167
   11    1    25
    1    5
     13.75       0.5    121.75      1.50     157.75       0.5    157.76       0.0
     168.0       0.0
       0.0        1.      17.5      .921       35.0     .8704      52.5     .8326
```

```
       70.        .803      87.5      .7755      105.0      .7512      122.5      .7302
      140.        .714     157.5      .6973      175.0      .6837      192.5      .6710
      220.        .652     255.0      .6332      290.0      .6167      325.0      .6017
      360.        .588     395.0      .5769      430.0      .5656      465.0      .5562
      500.        .547     535.0      .5444      570.0      .5304      605.0      .5243
     1000.        .002
   13    2    0    2    0    0
    3    3
  0.0       0.0  0.1       .801500.       .80
  0.0       1.0  0.2       1.01500.       1.0
    1    1    2    1    0       .260      92.05       40.0
 124.  1.0.9999.0001
    5    5    1    0    0       40.0     1170.0       40.0
 124.  1.0.9999.0001
   14    5    0    0    0    0    1    2
    0
    0
 500    0    0
          .0002          .015          500.           1.0        99999.
             5.            1.          800.          800.
          -.001          .005          5.0           1.0          200.
1234567890123456789012345678901234567890123456789012345678901234567890123456789012345678901234567890
            10.           10.          500.          500.
1

          cobra_tf        date 19980803      time 00:00:00
1                     main control parameters are:

                     restart time step . . . . . . . . . . .     0
                     simulation start time . . . . . . . . .       .000
                     outer iteration convergence limit . . .   .0010000
                     maximum number of inner iterations . .   40
                     maximum number of outer iterations  . .   10

    1    1    0    0    0    0    0    0    0    0    0
    2    5    0    0    0    0    0    0    0    0    0
    3    1    0    0    0    0    0    0    0    0    0
    4    4    1    0    0    0    0    0    0    0    0
    7    8    1    1    1    1    1    0    0    0    0
    8    3    1    2    2    0    0    0    1    0    0
    9    3    0    0    0    0    0    0    0    0    0
```

10	3	0	0	0	0	0	0	0	0	0
11	1	25	0	0	0	0	0	0	0	0
13	2	0	2	0	0	0	0	0	0	0
14	5	0	0	0	0	1	2	0	0	0
0	0	0	0	0	0	0	0	0	0	0

1 input summary

**** Test 31504 Bundle Rod 7x7 ****

general information
****

0

```
initial system operating pressure (psi)  . . .        40.00000
initial system steam/water enthalpy    . . . . .1170.00000
initial noncondensable gas enthalpy    . . . . .  124.00000
initial liquid volume fraction          . . . . .     .00000
mass flux for initialization (lb/ft**2 sec) . .       .00000
average linear heat rate (kw/ft) . . . . . . .        .46600
total axial length (inches). . . . . . . . . .    174.71997
total no. of axial nodes . . . . . . . . . . .           28
```

1

initial volume fractions of vapor and noncondensable gases

1

100.00000 percent of the total system volume is initially filled with vapor and/or noncondensable gases. the fraction of this gas volume occupied by water vapor and each noncondensable gas is as follows:

steam .9999 air .00010

1

subchannel data

subchannel id. no.	nominal channel area (in**2)	wetted perimeter (in.)	momentum area (bottom)	momentum area (top)	axial variation tables continuity area	momentum area	wetted perimeter
1	44.8600	71.740	44.8600	7.2200	0	0	0
2	7.2200	71.740	7.2200	7.2200	0	0	0
3	2.1790	18.790	2.1790	2.1790	0	0	0
4	5.0400	52.950	5.0400	5.0400	0	0	0
5	50.2400	71.740	7.2200	50.2400	0	0	0

0

1 **

grid spacer data

model selection (0=off,1=on)	grid quench front heat transfer to fluid	1
	drop breakup at grid spacer	1
	grid enhancement of single phase vapor convection	1

grid type 1	material type index,	1
	grid length [in]	1.500
	grid perimeter [in]	1.984
	fraction of channel blocked	.295
	loss coefficient multiplier	1.400

axial levels containing grid type 1

2 5 8 11 14 17 20 23

grid located in channel	no. of grids in channel	fuel rod surface index pairs surrounding grid					
3	16.000	1 - 1	0 0	0 - 0	0 - 0	0 - 0	0 - 0
4	33.000	2 - 1	0 - 0	0 - 0	0 - 0	0 - 0	0 - 0

0

0 data for lateral momentum convected by axial velocities at section boundries

channel no.	node no.	gap below	gap above	area	node no.	gap below	gap above	area	node no.	gap below	gap above	area	node no.	gap below	gap above	area

0

****

channel thermal connection input data

channel no.	fuel rod surface index pairs	heat slab indices

3	1	1	0	0	0	0	0	0	0	0	0	0	0	0	0	0	0	0	0	0
4	2	1	3	1	0	0	0	0	0	0	0	0	1	0	0	0	0	0	0	0

****

0

gap data

gap no.	ik	jk	gap width	centroid distance	loss coeff.	frict. flag	gap below	gap above	sign modifier	gaps which face this gap ii side			jj side			variation table
1	3	4	1.952	1.380	2.000	.00	0	0	1.000	0	0	0	0	0	0	0

1

channel splitting data - axial level 1 of 4

number of channels	no. of nodes	cell length (nominal)
1	2	.3333

channel	channels above						channels below					
1	2	0	0	0	0	0	1	0	0	0	0	0

1

channel splitting data - axial level 2 of 4

number of channels	no. of nodes	cell length (nominal)
1	1	.4792

channel	channels above						channels below					
2	3	4	0	0	0	0	1	0	0	0	0	0

variable axial noding

node no.	length (ft)	node no.	length (ft)	node no.	length (ft)	node no.	length (ft)	node no.	length (ft)
2	.4792								

1

channel splitting data axial level 3 of 4

number of channels	no. of nodes	cell length (nominal)
2	22	.5643

channel	channels above						channels below					
3	5	0	0	0	0	0	2	0	0	0	0	0
4	5	0	0	0	0	0	2	0	0	0	0	0

variable axial noding

node no.	length (ft)	node no.	length (ft)	node no.	length (ft)	node no.	length (ft)	node no.	length (ft)
2	.2092	3	.6433	4	.6433	5	.6433	6	.5708
7	.5708	8	.5708	9	.5708	10	.5708	11	.5708
12	.5708	13	.5708	14	.5708	15	.5708	16	.5708
17	.5708	18	.5708	19	.5708	20	.5708	21	.5708
22	.5708	23	.5708						

1

channel splitting data axial level 4 of 4

number of channels	no. of nodes	cell length (nominal)
1	3	.3333

channel	channels above						channels below					
5	5	0	0	0	0	0	3	4	0	0	0	0

variable axial noding

node no.	length (ft)	node no.	length (ft)	node no.	length (ft)	node no.	length (ft)	node no.	length (ft)
2	.3333	3	.3333	4	.3333				

simultaneous solution group information

no. of groups	last cell number in each group
1	50

1

****

fuel rod and heat slab model input

no. of fuel rods = 3 no. of fuel rod surfaces = 3
no. of heat slabs = 1

****

fuel rod model input

fuel rod index	axial (in.)	location (in.)	geometry type	conductor type	radial power factor	axial power profile	renoding flag	minimum node size	rod multiplier
1	13.75 -	162.72	hrod	1	1.000	1	2	.0500	16.000
2	13.75 -	162.72	hrod	1	1.000	1	2	.0500	29.000
3	13.75 -	162.72	tube	2	.000	0	2	.0500	4.000

heat slab model input

heat slab index	ch	annel connection inside	heated perimeter	outside	geometry type	conductor type	slab multiplier
1	4	14.20	0	14.20	wall	3	1.000

conductor geometry description
no. of geometry types = 3

type 1 - hrod   cylindrical heater rod

rod diameter .3740 (in.)
inside diameter .0000 (in.)
no. of nodes (total) 8
material index (oxide) 0

radial noding information

node no.	material index	radial location	node boundaries (inside)	node boundaries (outside)	power fraction
1	2	.0484	.0000	.0685	.00000
2	3	.0931	.0685	.1125	1.00000
3	2	.1219	.1125	.1307	.00000
4	2	.1400	.1307	.1488	.00000
5	2	.1582	.1488	.1670	.00000
6	1	.1710	.1670	.1750	.00000
7	1	.1790	.1750	.1830	.00000
8	1	.1870	.1830	.1870	.00000

type 2   tube   tube conductor geometry

outside diameter .3740 (in.)
inside diameter .2090 (in.)
no. of nodes (total) 3
material index (inside) 0
material index (outside) 0

radial noding information

node no.	material index	radial location	node boundaries (inside)	node boundaries (outside)	power fraction
1	1	.1045	.1045	.1251	.00000
2	1	.1472	.1251	.1664	.00000
3	1	.1870	.1664	.1870	.00000

type 3 - wall flat plate conductor geometry

```
wall perimeter              14.2000 (in.)
wall thickness                .2500 (in.)
no. of nodes (total)         3
material index (inside)      0
material index(outside)      0
```

radial noding information

node no.	material index	radial location	node boundaries (inside)	node boundaries (outside)	power fraction
1	1	.0000	.0000	.0625	.00000
2	1	.1250	.0625	.1875	.00000
3	1	.2500	.1875	.2500	.00000

material property tables

material type 1 cold state density = 516.700 (lbm/ft3)

temperature (f)	specific heat (btu/lbm-f)	conductivity (btu/hr ft-f)
32.0	.10100	8.140
70.0	.10300	8.340
212.0	.11100	9.090
392.0	.12100	10.040
500.0	.12700	10.600
572.0	.13100	10.980
752.0	.14100	11.930
932.0	.15100	12.880
1000.0	.15800	13.230
1112.0	.16600	13.820
212.0	.16587	67.370
392.0	.22014	63.827
572.0	.26263	60.280
752.0	.29590	56.737
932.0	.32194	53.190
1112.0	.34233	49.646
1292.0	.35829	46.100

material type 2 cold state density = 119.000 (lbm/ft3)

temperature (f) specific heat (btu/lbm-f) conductivity (btu/hr-ft-f)

212.0	.16587	67.370
392.0	.22014	63.827
572.0	.26263	60.280
752.0	.29590	56.737
932.0	.32194	53.190
1112.0	.34233	49.646
1292.0	.35829	46.100
1472.0	.37078	42.555
1652.0	.38056	39.010
1832.0	.38822	35.464
70.0	.10000	10.083
200.0	.10700	11.333
400.0	.11400	13.000
600.0	.11700	14.833

material type - 3 cold state density = 528.800 (lbm/ft3)

temperature (f)	specific heat (btu/lbm-f)	conductivity (btu/hr-ft-f)
70.0	.10000	10.083
200.0	.10700	11.333
400.0	.11400	13.000
600.0	.11700	14.833
800.0	.12000	16.500
1000.0	.12500	18.333
1200.0	.13200	20.000
1400.0	.14100	21.833
1600.0	.15700	23.500
1800.0	.18600	25.167

axial power profile tables

axial profile no. 1 used by rod nos. = 1 2

rod node no.	axial location (in.)	fluid node no.	axial power factor
1	13.75	5	.5029
2	15.01	5	.5145
3	20.12	6	.5590
4	27.84	7	.6305
5	35.56	8	.7019
6	42.84	9	.7694
7	49.69	10	.8328
8	56.54	11	.8962
9	63.39	12	.9597
10	70.24	13	1.0231

11	77.09	14	1.0865
12	83.94	15	1.1500
13	90.79	16	1.2134
14	97.64	17	1.2768
15	104.49	18	1.3402
16	111.34	19	1.4037
17	118.19	20	1.4671
18	125.04	21	1.4084
19	131.89	22	1.2182
20	138.74	23	1.0279
21	145.59	24	.8376
22	152.44	25	.6474
23	159.29	26	.1930
24	162.72	26	.0000

this table integrates to .9689 over a heated length of 148.97 (in.)

power forcing function table

transient time (secs)	power factor
.0000	1.0000
17.5000	.9210
35.0000	.8704
52.5000	.8326
70.0000	.8030
87.5000	.7755
105.0000	.7512
122.5000	.7302
140.0000	.7140
157.5000	.6973
175.0000	.6837
192.5000	.6710
220.0000	.6520
255.0000	.6332
290.0000	.6167
325.0000	.6017
360.0000	.5880
395.0000	.5769
430.0000	.5656
465.0000	.5562
500.0000	.5470
535.0000	.5444
570.0000	.5304
605.0000	.5243
1000.0000	.0020

1 forcing function tables

0 table 1

time coord.	forcing factor	time coord.	forcing factor	time coord.	forcing factor	time coord.	forcing factor	time coord.	forcing factor
.000	.000	.100	.800	1500.000	.800				

0 table 2

time coord.	forcing factor	time coord.	forcing factor	time coord.	forcing factor	time coord.	forcing factor	time coord.	forcing factor
.000	1.000	.200	1.000	1500.000	1.000				

1 axial and/or injection boundary conditions

boundary type	property specification
1= pressure and enthalpy (axial)	pressure
2= flow and ehthalpy (axial)	mass flow
3= zero axial flow	zero
4= injected flow and enthalpy	injected flow
5= pressure sink and enthalpy	sink pressure

channel index	axial node	boundary type (see above)	specified property (see above)	enthalpy
1	1	2	.26	92.05
5	5	1	40.00	1170.00

0

zero crossflow boundary conditions

gap index	axial node

5 channels will be printed

1 2 3 4 5

0 3 rods will be printed

1 2 3

```
0                  1     gaps will be printed

                                              1
0    ***** graphics dump data *************************************************************************************

          initial run

               maximum number of graphics                  (check against dimension of indcmp array
               dumps  . . . . . . . . . . . . . . .    500   must not exceed it.)

               normal vessel dump selected
1 trac major edit

    time =   0.000E+00 seconds      delt =  0.000E+00 seconds      time steps -      0   oitno=        0

     last minimum number of inner iterations was  0 at step      0
     current convergence limits and limitation counts
         delamx       delemx       delrmx       delvmx       delcmx       delpmx
       0.000E+00    0.000E+00    0.000E+00    0.000E+00    0.000E+00    0.000E+00
           0            0            0            0            0            0
     cptime = 0.000E+00
0      channel results      date 19980803  time 00:00:00                         **** Test 31504 Bundle Rod 7x7  ****
*******************************************************************************************************************************
            simulation time =         .00000  seconds           fluid properties for channel    1
 node  dist.    pressure          velocity                   void fraction                     flow rate           flow     heat added       gama
  no.  (ft.)     (psi)            (ft/sec)                                                     (lbm/s)             reg.       (btu/s)       (lbm/s)
                             liquid  vapor   entr.       liquid  vapor   entr.        liquid     vapor      entr.         liquid     vapor

   3    .67      40.009       .00     .00     .00       .0000 1.0000  .0000        .00000    .00000    .00000   0    .000E+00   .000E+00     .00
   2    .33      40.010       .00     .00     .00       .0000 1.0000  .0000        .00000    .00000    .00000   0    .000E+00   .000E+00     .00
   1    .00      40.010       .00     .00     .00       .0000 1.0000  .0000        .00000    .00000    .00000   0    .000E+00   .000E+00     .00

 node  dist.                                      enthalpy                                                      density               net
  no.  (ft.)                                      (btu/lbm)                                                    (lbm/ft3)            entrain

                  vapor        hg      vapor-hg     liquid        hf     liq.  hf     mixture        liquid     vapor    mixture

   3    .67      1170.00    1169.77       .23      236.13      236.14        .01     1169.25      58.29915    .09446     .0945      .000
   2    .33      1170.00    1169.77       .23      236.13      236.14       -.01     1169.25      58.29915    .09446     .0945      .000
   1    .00      1170.00    1169.77       .23      236.13      236.15       -.02     1169.25      58.29915    .09446     .0945      .000

* * * * * * * * * * * * * * * * * * * * * * * * * * * * * * * * * * * * * * * * * * * * * * * * * * * * * * * * * * * * * * * * * *
```

node no.	dist.	mixture flow rate	mixture velocity	relative velocities vap. - liq.	relative velocities vap. - entr.	area	vap./liq. interfacial drag	vap./drop interfacial drag	grid spacers grid type	grid spacers temperature degf	grid spacers percent quenched
3	.67	.00	.00	.00	.00	.0501	.0010	.0010	0	.00	.000
2	.33	.00	.00	.00	.00	.3115	.0010	.0010	0	.00	.000
1	.00	.00	.00	.00	.00	.3115	.0010	.0010	0	.00	.000

* *

node	dist.	hashl	hascl	hashv	hascv	drop ai	ai source	sent	sdent	qradd	gradv	snkld	gamsd
3	.67	347.3965	34.7397	3.4740	34.7397	.1000E-09	.0000E+00	.0000E+00	.0000E+00	.0000E+00	.0000E+00	.0000E+00	.0000E+00
2	.33	347.3965	34.7397	3.4740	34.7397	.1000E-09	.0000E+00	.0000E+00	.0000E+00	.0000E+00	.0000E+00	.0000E+00	.0000E+00
1	.00	347.3965	34.7397	3.4740	34.7397	.1000E-09	.0000E+00	.0000E+00	.0000E+00	.0000E+00	.0000E+00	.0000E+00	.0000E+00

0 ---------- gas volumetric analysis ----------

		hmgas	rmgas	steam	air					diam-ld	diam-sd	flow-sd	veloc-sd	gamsd
3	.67	124.00	.00001	99.990	.010	.000	.000	.000	.000	.0000	.00000	.0000E+00	.00	.0000E+00
2	.33	124.00	.00001	99.990	.010	.000	.000	.000	.000	.0000	.00000	.0000E+00	.00	.0000E+00
1	.00	124.00	.00001	99.990	.010	.000	.000	.000	.000	.0000	.00000	.0000E+00	.00	.0000E+00

****

0 channel results date 19980803 time 00:00:00 **** Test 31504 Bundle Rod 7x7 ****

****

simulation time = .00000 seconds — fluid properties for channel 2

node no.	dist. (ft.)	pressure (psi)	velocity (ft/sec) liquid	velocity vapor	velocity entr.	void fraction liquid	void fraction vapor	void fraction entr.	flow rate (lbm/s) liquid	flow rate vapor	flow rate entr.	flow reg.	heat added (btu/s) liquid	heat added vapor	gama (lbm/s)
2	1.15	40.009	.00	.00	.00	.0000	1.0000	.0000	.00000	.00000	.00000	0	.000E+00	.000E+00	.00
1	.67	40.009	.00	.00	.00	.0000	1.0000	.0000	.00000	.00000	.00000	0	.000E+00	.000E+00	.00

node no.	dist. (ft.)	enthalpy (btu/lbm) vapor	hg	vapor hg	liquid	hf	liq. - hf	mixture	density (lbm/ft3) liquid	vapor	mixture	net entrain
2	1.15	1170.00	1169.77	.23	236.13	236.14	-.01	1169.25	58.29915	.09446	.0945	.000
1	.67	1170.00	1169.77	.23	236.13	236.14	-.01	1169.22	58.29915	.09446	.0945	.000

* *

node no.	dist.	mixture flow rate	mixture velocity	relative velocities vap. liq.	relative velocities vap. entr.	area	vap./liq. interfacial drag	vap./drop interfacial drag	grid spacers grid type	grid spacers temperature degf	grid spacers percent quenched

2	1.15	.00	.00	.00	.00	.0501	.0010	.0010	0	.00	.000
1	.67	.00	.00	.00	.00	.0501	.0010	.0010	0	.00	.000

* *

node	dist.	hashl	hascl	hashv	hascv	drop ai	ai source	sent	sdent	qradd	qradv	snkld	gamsd
2	1.15	80.3732	8.0373	.8037	8.0373	.1000E-09	.0000E+00	.0000E+00	.0000E+00	.0000E+00	.0000E+00	.0000E+00	.0000E+00
1	.67	80.3732	8.0373	.8037	8.0373	.1000E-09	.0000E+00	.0000E+00	.0000E+00	.0000E+00	.0000E+00	.0000E+00	.0000E+00

0 gas volumetric analysis

		hmgas	rmgas	steam	air					diam ld	diam-sd	flow sd	veloc-sd	gamsd
2	1.15	124.00	.00001	99.990	.010	.000	.000	.000	.000	.0000	.00000	.0000E+00	.00	.0000E+00
1	.67	124.00	.00001	99.990	.010	.000	.000	.000	.000	.0000	.00000	.0000E+00	.00	.0000E+00

****

0 channel results date 19980803 time 00:00:00 **** Test 31504 Bundle Rod 7x7 ****

****

simulation time = .00000 seconds fluid properties for channel 3

node no.	dist. (ft.)	pressure (psi)	velocity (ft/sec) liquid	vapor	entr.	void fraction liquid	vapor	entr.	flow rate (lbm/s) liquid	vapor	entr.	flow reg.	heat added (btu/s) liquid	vapor	gama (lbm/s)
23	13.56	40.001	.00	.00	.00	.0000	1.0000	.0000	.00000	.00000	.00000	0	.000E+00	.000E+00	.00
22	12.99	40.001	.00	.00	.00	.0000	1.0000	.0000	.00000	.00000	.00000	0	.000E+00	.000E+00	.00
21	12.42	40.002	.00	.00	.00	.0000	1.0000	.0000	.00000	.00000	.00000	0	.000E+00	.000E+00	.00
20	11.85	40.002	.00	.00	.00	.0000	1.0000	.0000	.00000	.00000	.00000	0	.000E+00	.000E+00	.00
19	11.28	40.003	.00	.00	.00	.0000	1.0000	.0000	.00000	.00000	.00000	0	.000E+00	.000E+00	.00
18	10.71	40.003	.00	.00	.00	.0000	1.0000	.0000	.00000	.00000	.00000	0	.000E+00	.000E+00	.00
17	10.13	40.003	.00	.00	.00	.0000	1.0000	.0000	.00000	.00000	.00000	0	.000E+00	.000E+00	.00
16	9.56	40.004	.00	.00	.00	.0000	1.0000	.0000	.00000	.00000	.00000	0	.000E+00	.000E+00	.00
15	8.99	40.004	.00	.00	.00	.0000	1.0000	.0000	.00000	.00000	.00000	0	.000E+00	.000E+00	.00
14	8.42	40.004	.00	.00	.00	.0000	1.0000	.0000	.00000	.00000	.00000	0	.000E+00	.000E+00	.00
13	7.85	40.005	.00	.00	.00	.0000	1.0000	.0000	.00000	.00000	.00000	0	.000E+00	.000E+00	.00
12	7.28	40.005	.00	.00	.00	.0000	1.0000	.0000	.00000	.00000	.00000	0	.000E+00	.000E+00	.00
11	6.71	40.006	.00	.00	.00	.0000	1.0000	.0000	.00000	.00000	.00000	0	.000E+00	.000E+00	.00
10	6.14	40.006	.00	.00	.00	.0000	1.0000	.0000	.00000	.00000	.00000	0	.000E+00	.000E+00	.00
9	5.57	40.006	.00	.00	.00	.0000	1.0000	.0000	.00000	.00000	.00000	0	.000E+00	.000E+00	.00
8	5.00	40.007	.00	.00	.00	.0000	1.0000	.0000	.00000	.00000	.00000	0	.000E+00	.000E+00	.00
7	4.43	40.007	.00	.00	.00	.0000	1.0000	.0000	.00000	.00000	.00000	0	.000E+00	.000E+00	.00
6	3.86	40.007	.00	.00	.00	.0000	1.0000	.0000	.00000	.00000	.00000	0	.000E+00	.000E+00	.00
5	3.28	40.008	.00	.00	.00	.0000	1.0000	.0000	.00000	.00000	.00000	0	.000E+00	.000E+00	.00
4	2.64	40.008	.00	.00	.00	.0000	1.0000	.0000	.00000	.00000	.00000	0	.000E+00	.000E+00	.00
3	2.00	40.009	.00	.00	.00	.0000	1.0000	.0000	.00000	.00000	.00000	0	.000E+00	.000E+00	.00
2	1.36	40.009	.00	.00	.00	.0000	1.0000	.0000	.00000	.00000	.00000	0	.000E+00	.000E+00	.00
1	1.15	40.009	.00	.00	.00	.0000	1.0000	.0000	.00000	.00000	.00000	0	.000E+00	.000E+00	.00

node no.	dist. (ft.)	enthalpy (btu/lbm)	density (lbm/ft3)	net entrain

		vapor	hg	vapor-hg	liquid	hf	liq. - hf	mixture	liquid	vapor	mixture	
23	13.56	1170.00	1169.77	.23	236.13	236.13	.00	1169.25	58.29915	.09444	.0945	.000
22	12.99	1170.00	1169.77	.23	236.13	236.13	.00	1169.25	58.29915	.09444	.0945	.000
21	12.42	1170.00	1169.77	.23	236.13	236.13	.00	1169.25	58.29915	.09444	.0945	.000
20	11.85	1170.00	1169.77	.23	236.13	236.13	.00	1169.25	58.29915	.09444	.0945	.000
19	11.28	1170.00	1169.77	.23	236.13	236.13	.00	1169.25	58.29915	.09444	.0945	.000
18	10.71	1170.00	1169.77	.23	236.13	236.13	.00	1169.25	58.29915	.09444	.0945	.000
17	10.13	1170.00	1169.77	.23	236.13	236.14	-.01	1169.25	58.29915	.09444	.0945	.000
16	9.56	1170.00	1169.77	.23	236.13	236.14	-.01	1169.25	58.29915	.09444	.0945	.000
15	8.99	1170.00	1169.77	.23	236.13	236.14	-.01	1169.25	58.29915	.09444	.0945	.000
14	8.42	1170.00	1169.77	.23	236.13	236.14	-.01	1169.25	58.29915	.09444	.0945	.000
13	7.85	1170.00	1169.77	.23	236.13	236.14	-.01	1169.25	58.29915	.09445	.0945	.000
12	7.28	1170.00	1169.77	.23	236.13	236.14	-.01	1169.25	58.29915	.09445	.0945	.000
11	6.71	1170.00	1169.77	.23	236.13	236.14	-.01	1169.25	58.29915	.09445	.0945	.000
10	6.14	1170.00	1169.77	.23	236.13	236.14	-.01	1169.25	58.29915	.09445	.0945	.000
9	5.57	1170.00	1169.77	.23	236.13	236.14	-.01	1169.25	58.29915	.09445	.0945	.000
8	5.00	1170.00	1169.77	.23	236.13	236.14	-.01	1169.25	58.29915	.09445	.0945	.000
7	4.43	1170.00	1169.77	.23	236.13	236.14	-.01	1169.25	58.29915	.09445	.0945	.000
6	3.86	1170.00	1169.77	.23	236.13	236.14	-.01	1169.25	58.29915	.09445	.0945	.000
5	3.28	1170.00	1169.77	.23	236.13	236.14	-.01	1169.25	58.29915	.09445	.0945	.000
4	2.64	1170.00	1169.77	.23	236.13	236.14	-.01	1169.25	58.29915	.09445	.0945	.000
3	2.00	1170.00	1169.77	.23	236.13	236.14	-.01	1169.25	58.29915	.09445	.0945	.000
2	1.36	1170.00	1169.77	.23	236.13	236.14	-.01	1169.25	58.29915	.09446	.0945	.000
1	1.15	1170.00	1169.77	.23	236.13	236.14	-.01	1169.25	58.29915	.09446	.0945	.000

* *

node no.	dist.	mixture flow rate	mixture velocity	-- relative velocities -- vap. - liq.	vap. - entr.	area	vap./liq. interfacial drag	vap./drop interfacial drag	-------- grid spacers -------- grid type	temperature degf	percent quenched
23	13.56	.00	.00	.00	.00	.0151	.0010	.0010	1	.00	.000
22	12.99	.00	.00	.00	.00	.0151	.0010	.0010	0	.00	.000
21	12.42	.00	.00	.00	.00	.0151	.0010	.0010	0	.00	.000
20	11.85	.00	.00	.00	.00	.0151	.0010	.0010	1	502.00	.000
19	11.28	.00	.00	.00	.00	.0151	.0010	.0010	0	.00	.000
18	10.71	.00	.00	.00	.00	.0151	.0010	.0010	0	.00	.000
17	10.13	.00	.00	.00	.00	.0151	.0010	.0010	1	1062.12	.000
16	9.56	.00	.00	.00	.00	.0151	.0010	.0010	0	.00	.000
15	8.99	.00	.00	.00	.00	.0151	.0010	.0010	0	.00	.000
14	8.42	.00	.00	.00	.00	.0151	.0010	.0010	1	1528.70	.000
13	7.85	.00	.00	.00	.00	.0151	.0010	.0010	0	.00	.000
12	7.28	.00	.00	.00	.00	.0151	.0010	.0010	0	.00	.000
11	6.71	.00	.00	.00	.00	.0151	.0010	.0010	1	1330.43	.000
10	6.14	.00	.00	.00	.00	.0151	.0010	.0010	0	.00	.000
9	5.57	.00	.00	.00	.00	.0151	.0010	.0010	0	.00	.000
8	5.00	.00	.00	.00	.00	.0151	.0010	.0010	1	1132.16	.000
7	4.43	.00	.00	.00	.00	.0151	.0010	.0010	0	.00	.000

6	3.86	.00	.00	.00	.00	.0151	.0010	.0010	0	.00	.000
5	3.28	.00	.00	.00	.00	.0151	.0010	.0010	1	933.89	.000
4	2.64	.00	.00	.00	.00	.0151	.0010	.0010	0	.00	.000
3	2.00	.00	.00	.00	.00	.0151	.0010	.0010	0	.00	.000
2	1.36	.00	.00	.00	.00	.0151	.0010	.0010	1	731.43	.000
1	1.15	.00	.00	.00	.00	.0151	.0010	.0010	0	.00	.000

* *

node	dist.	hashl	hascl	hashv	hascv	drop ai	ai source	sent	sdent	qradd	qradv	snkld	gamsd
23	13.56	110.3287	11.0329	1.1033	11.0329	.1000E-09	.0000E+00	.0000E+00	.0000E+00	.0000E+00	.0000E+00	.0000E+00	.0000E+00
22	12.99	110.3287	11.0329	1.1033	11.0329	.1000E-09	.0000E+00	.0000E+00	.0000E+00	.0000E+00	.0000E+00	.0000E+00	.0000E+00
21	12.42	110.3287	11.0329	1.1033	11.0329	.1000E-09	.0000E+00	.0000E+00	.0000E+00	.0000E+00	.0000E+00	.0000E+00	.0000E+00
20	11.85	110.3287	11.0329	1.1033	11.0329	.1000E 09	.0000E+00	.0000E+00	.0000E+00	.0000E+00	.0000E+00	.0000E+00	.0000E+00
19	11.28	110.3287	11.0329	1.1033	11.0329	.1000E-09	.0000E+00	.0000E+00	.0000E+00	.0000E+00	.0000E+00	.0000E+00	.0000E+00
18	10.71	110.3287	11.0329	1.1033	11.0329	.1000E-09	.0000E+00	.0000E+00	.0000E+00	.0000E+00	.0000E+00	.0000E+00	.0000E+00
17	10.13	110.3287	11.0329	1.1033	11.0329	.1000E-09	.0000E+00	.0000E+00	.0000E+00	.0000E+00	.0000E+00	.0000E+00	.0000E+00
16	9.56	110.3287	11.0329	1.1033	11.0329	.1000E-09	.0000E+00	.0000E+00	.0000E+00	.0000E+00	.0000E+00	.0000E+00	.0000E+00
15	8.99	110.3287	11.0329	1.1033	11.0329	.1000E-09	.0000E+00	.0000E+00	.0000E+00	.0000E+00	.0000E+00	.0000E+00	.0000E+00
14	8.42	110.3287	11.0329	1.1033	11.0329	.1000E-09	.0000E+00	.0000E+00	.0000E+00	.0000E+00	.0000E+00	.0000E+00	.0000E+00
13	7.85	110.3287	11.0329	1.1033	11.0329	.1000E 09	.0000E+00	.0000E+00	.0000E+00	.0000E+00	.0000E+00	.0000E+00	.0000E+00
12	7.28	110.3287	11.0329	1.1033	11.0329	.1000E-09	.0000E+00	.0000E+00	.0000E+00	.0000E+00	.0000E+00	.0000E+00	.0000E+00
11	6.71	110.3287	11.0329	1.1033	11.0329	.1000E-09	.0000E+00	.0000E+00	.0000E+00	.0000E+00	.0000E+00	.0000E+00	.0000E+00
10	6.14	110.3287	11.0329	1.1033	11.0329	.1000E-09	.0000E+00	.0000E+00	.0000E+00	.0000E+00	.0000E+00	.0000E+00	.0000E+00
9	5.57	110.3287	11.0329	1.1033	11.0329	.1000E-09	.0000E+00	.0000E+00	.0000E+00	.0000E+00	.0000E+00	.0000E+00	.0000E+00
8	5.00	110.3287	11.0329	1.1033	11.0329	.1000E-09	.0000E+00	.0000E+00	.0000E+00	.0000E+00	.0000E+00	.0000E+00	.0000E+00
7	4.43	110.3287	11.0329	1.1033	11.0329	.1000E-09	.0000E+00	.0000E+00	.0000E+00	.0000E+00	.0000E+00	.0000E+00	.0000E+00
6	3.86	110.3287	11.0329	1.1033	11.0329	.1000E 09	.0000E+00	.0000E+00	.0000E+00	.0000E+00	.0000E+00	.0000E+00	.0000E+00
5	3.28	124.3412	12.4341	1.2434	12.4341	.1000E 09	.0000E+00	.0000E+00	.0000E+00	.0000E+00	.0000E+00	.0000E+00	.0000E+00
4	2.64	124.3412	12.4341	1.2434	12.4341	.1000E-09	.0000E+00	.0000E+00	.0000E+00	.0000E+00	.0000E+00	.0000E+00	.0000E+00
3	2.00	124.3412	12.4341	1.2434	12.4341	.1000E-09	.0000E+00	.0000E+00	.0000E+00	.0000E+00	.0000E+00	.0000E+00	.0000E+00
2	1.36	40.4270	4.0427	.4043	4.0427	.1000E-09	.0000E+00	.0000E+00	.0000E+00	.0000E+00	.0000E+00	.0000E+00	.0000E+00
1	1.15	40.4270	4.0427	.4043	4.0427	.1000E-09	.0000E+00	.0000E+00	.0000E+00	.0000E+00	.0000E+00	.0000E+00	.0000E+00

0 ----- ---------------- gas volumetric analysis ---------------------

		hmgas	rmgas	steam	air					diam ld	diam sd	flow sd	veloc sd	gamsd
23	13.56	124.00	.00001	99.990	.010	.000	.000	.000	.000	.0000	.00000	.0000E+00	.00	.0000E+00
22	12.99	124.00	.00001	99.990	.010	.000	.000	.000	.000	.0000	.00000	.0000E+00	.00	.0000E+00
21	12.42	124.00	.00001	99.990	.010	.000	.000	.000	.000	.0000	.00000	.0000E+00	.00	.0000E+00
20	11.85	124.00	.00001	99.990	.010	.000	.000	.000	.000	.0000	.00000	.0000E+00	.00	.0000E+00
19	11.28	124.00	.00001	99.990	.010	.000	.000	.000	.000	.0000	.00000	.0000E+00	.00	.0000E+00
18	10.71	124.00	.00001	99.990	.010	.000	.000	.000	.000	.0000	.00000	.0000E+00	.00	.0000E+00
17	10.13	124.00	.00001	99.990	.010	.000	.000	.000	.000	.0000	.00000	.0000E+00	.00	.0000E+00
16	9.56	124.00	.00001	99.990	.010	.000	.000	.000	.000	.0000	.00000	.0000E+00	.00	.0000E+00
15	8.99	124.00	.00001	99.990	.010	.000	.000	.000	.000	.0000	.00000	.0000E+00	.00	.0000E+00
14	8.42	124.00	.00001	99.990	.010	.000	.000	.000	.000	.0000	.00000	.0000E+00	.00	.0000E+00
13	7.85	124.00	.00001	99.990	.010	.000	.000	.000	.000	.0000	.00000	.0000E+00	.00	.0000E+00
12	7.28	124.00	.00001	99.990	.010	.000	.000	.000	.000	.0000	.00000	.0000E+00	.00	.0000E+00
11	6.71	124.00	.00001	99.990	.010	.000	.000	.000	.000	.0000	.00000	.0000E+00	.00	.0000E+00
10	6.14	124.00	.00001	99.990	.010	.000	.000	.000	.000	.0000	.00000	.0000E+00	.00	.0000E+00
9	5.57	124.00	.00001	99.990	.010	.000	.000	.000	.000	.0000	.00000	.0000E+00	.00	.0000E+00

8	5.00	124.00	.00001	99.990	.010	.000	.000	.000	.000	.0000	.00000	.0000E+00	.00	.0000E+00
7	4.43	124.00	.00001	99.990	.010	.000	.000	.000	.000	.0000	.00000	.0000E+00	.00	.0000E+00
6	3.86	124.00	.00001	99.990	.010	.000	.000	.000	.000	.0000	.00000	.0000E+00	.00	.0000E+00
5	3.28	124.00	.00001	99.990	.010	.000	.000	.000	.000	.0000	.00000	.0000E+00	.00	.0000E+00
4	2.64	124.00	.00001	99.990	.010	.000	.000	.000	.000	.0000	.00000	.0000E+00	.00	.0000E+00
3	2.00	124.00	.00001	99.990	.010	.000	.000	.000	.000	.0000	.00000	.0000E+00	.00	.0000E+00
2	1.36	124.00	.00001	99.990	.010	.000	.000	.000	.000	.0000	.00000	.0000E+00	.00	.0000E+00
1	1.15	124.00	.00001	99.990	.010	.000	.000	.000	.000	.0000	.00000	.0000E+00	.00	.0000E+00

****

0 channel results date 19980803 time 00:00:00 **** Test 31504 Bundle Rod 7x7 ****

****

simulation time = .00000 seconds fluid properties for channel 4

node no.	dist. (ft.)	pressure (psi)	velocity (ft/sec)			void fraction			flow rate (lbm/s)			flow reg.	heat added (btu/s)		gama (lbm/s)
			liquid	vapor	entr.	liquid	vapor	entr.	liquid	vapor	entr.		liquid	vapor	
23	13.56	40.001	.00	.00	.00	.0000	1.0000	.0000	.00000	.00000	.00000	0	.000E+00	.000E+00	.00
22	12.99	40.001	.00	.00	.00	.0000	1.0000	.0000	.00000	.00000	.00000	0	.000E+00	.000E+00	.00
21	12.42	40.002	.00	.00	.00	.0000	1.0000	.0000	.00000	.00000	.00000	0	.000E+00	.000E+00	.00
20	11.85	40.002	.00	.00	.00	.0000	1.0000	.0000	.00000	.00000	.00000	0	.000E+00	.000E+00	.00
19	11.28	40.003	.00	.00	.00	.0000	1.0000	.0000	.00000	.00000	.00000	0	.000E+00	.000E+00	.00
18	10.71	40.003	.00	.00	.00	.0000	1.0000	.0000	.00000	.00000	.00000	0	.000E+00	.000E+00	.00
17	10.13	40.003	.00	.00	.00	.0000	1.0000	.0000	.00000	.00000	.00000	0	.000E+00	.000E+00	.00
16	9.56	40.004	.00	.00	.00	.0000	1.0000	.0000	.00000	.00000	.00000	0	.000E+00	.000E+00	.00
15	8.99	40.004	.00	.00	.00	.0000	1.0000	.0000	.00000	.00000	.00000	0	.000E+00	.000E+00	.00
14	8.42	40.004	.00	.00	.00	.0000	1.0000	.0000	.00000	.00000	.00000	0	.000E+00	.000E+00	.00
13	7.85	40.005	.00	.00	.00	.0000	1.0000	.0000	.00000	.00000	.00000	0	.000E+00	.000E+00	.00
12	7.28	40.005	.00	.00	.00	.0000	1.0000	.0000	.00000	.00000	.00000	0	.000E+00	.000E+00	.00
11	6.71	40.006	.00	.00	.00	.0000	1.0000	.0000	.00000	.00000	.00000	0	.000E+00	.000E+00	.00
10	6.14	40.006	.00	.00	.00	.0000	1.0000	.0000	.00000	.00000	.00000	0	.000E+00	.000E+00	.00
9	5.57	40.006	.00	.00	.00	.0000	1.0000	.0000	.00000	.00000	.00000	0	.000E+00	.000E+00	.00
8	5.00	40.007	.00	.00	.00	.0000	1.0000	.0000	.00000	.00000	.00000	0	.000E+00	.000E+00	.00
7	4.43	40.007	.00	.00	.00	.0000	1.0000	.0000	.00000	.00000	.00000	0	.000E+00	.000E+00	.00
6	3.86	40.007	.00	.00	.00	.0000	1.0000	.0000	.00000	.00000	.00000	0	.000E+00	.000E+00	.00
5	3.28	40.008	.00	.00	.00	.0000	1.0000	.0000	.00000	.00000	.00000	0	.000E+00	.000E+00	.00
4	2.64	40.008	.00	.00	.00	.0000	1.0000	.0000	.00000	.00000	.00000	0	.000E+00	.000E+00	.00
3	2.00	40.009	.00	.00	.00	.0000	1.0000	.0000	.00000	.00000	.00000	0	.000E+00	.000E+00	.00
2	1.36	40.009	.00	.00	.00	.0000	1.0000	.0000	.00000	.00000	.00000	0	.000E+00	.000E+00	.00
1	1.15	40.009	.00	.00	.00	.0000	1.0000	.0000	.00000	.00000	.00000	0	.000E+00	.000E+00	.00

node no.	dist. (ft.)	enthalpy (btu/lbm)							density (lbm/ft3)			net entrain
		vapor	hg	vapor-hg	liquid	hf	liq. - hf	mixture	liquid	vapor	mixture	
23	13.56	1170.00	1169.77	.23	236.13	236.13	.00	1169.25	58.29915	.09444	.0945	.000
22	12.99	1170.00	1169.77	.23	236.13	236.13	.00	1169.25	58.29915	.09444	.0945	.000
21	12.42	1170.00	1169.77	.23	236.13	236.13	.00	1169.25	58.29915	.09444	.0945	.000
20	11.85	1170.00	1169.77	.23	236.13	236.13	.00	1169.25	58.29915	.09444	.0945	.000

19	11.28	1170.00	1169.77	.23	236.13	236.13	.00	1169.25	58.29915	.09444	.0945	.000
18	10.71	1170.00	1169.77	.23	236.13	236.13	.00	1169.25	58.29915	.09444	.0945	.000
17	10.13	1170.00	1169.77	.23	236.13	236.14	-.01	1169.25	58.29915	.09444	.0945	.000
16	9.56	1170.00	1169.77	.23	236.13	236.14	.01	1169.25	58.29915	.09444	.0945	.000
15	8.99	1170.00	1169.77	.23	236.13	236.14	.01	1169.25	58.29915	.09444	.0945	.000
14	8.42	1170.00	1169.77	.23	236.13	236.14	.01	1169.25	58.29915	.09444	.0945	.000
13	7.85	1170.00	1169.77	.23	236.13	236.14	-.01	1169.25	58.29915	.09445	.0945	.000
12	7.28	1170.00	1169.77	.23	236.13	236.14	.01	1169.25	58.29915	.09445	.0945	.000
11	6.71	1170.00	1169.77	.23	236.13	236.14	.01	1169.25	58.29915	.09445	.0945	.000
10	6.14	1170.00	1169.77	.23	236.13	236.14	.01	1169.25	58.29915	.09445	.0945	.000
9	5.57	1170.00	1169.77	.23	236.13	236.14	-.01	1169.25	58.29915	.09445	.0945	.000
8	5.00	1170.00	1169.77	.23	236.13	236.14	-.01	1169.25	58.29915	.09445	.0945	.000
7	4.43	1170.00	1169.77	.23	236.13	236.14	.01	1169.25	58.29915	.09445	.0945	.000
6	3.86	1170.00	1169.77	.23	236.13	236.14	.01	1169.25	58.29915	.09445	.0945	.000
5	3.28	1170.00	1169.77	.23	236.13	236.14	.01	1169.25	58.29915	.09445	.0945	.000
4	2.64	1170.00	1169.77	.23	236.13	236.14	-.01	1169.25	58.29915	.09445	.0945	.000
3	2.00	1170.00	1169.77	.23	236.13	236.14	.01	1169.25	58.29915	.09445	.0945	.000
2	1.36	1170.00	1169.77	.23	236.13	236.14	.01	1169.25	58.29915	.09446	.0945	.000
1	1.15	1170.00	1169.77	.23	236.13	236.14	.01	1169.25	58.29915	.09446	.0945	.000

* *

node no.	dist.	mixture flow rate	mixture velocity	-- relative velocities vap.	liq.	vap. - entr.	area	vap./liq. interfacial drag	vap./drop interfacial drag	-------- grid spacers -------- grid type	temperature degf	percent quenched
23	13.56	.00	.00		.00	.00	.0350	.0010	.0010	1	.00	.000
22	12.99	.00	.00		.00	.00	.0350	.0010	.0010	0	.00	.000
21	12.42	.00	.00		.00	.00	.0350	.0010	.0010	0	.00	.000
20	11.85	.00	.00		.00	.00	.0350	.0010	.0010	1	502.00	.000
19	11.28	.00	.00		.00	.00	.0350	.0010	.0010	0	.00	.000
18	10.71	.00	.00		.00	.00	.0350	.0010	.0010	0	.00	.000
17	10.13	.00	.00		.00	.00	.0350	.0010	.0010	1	1062.12	.000
16	9.56	.00	.00		.00	.00	.0350	.0010	.0010	0	.00	.000
15	8.99	.00	.00		.00	.00	.0350	.0010	.0010	0	.00	.000
14	8.42	.00	.00		.00	.00	.0350	.0010	.0010	1	1528.70	.000
13	7.85	.00	.00		.00	.00	.0350	.0010	.0010	0	.00	.000
12	7.28	.00	.00		.00	.00	.0350	.0010	.0010	0	.00	.000
11	6.71	.00	.00		.00	.00	.0350	.0010	.0010	1	1330.43	.000
10	6.14	.00	.00		.00	.00	.0350	.0010	.0010	0	.00	.000
9	5.57	.00	.00		.00	.00	.0350	.0010	.0010	0	.00	.000
8	5.00	.00	.00		.00	.00	.0350	.0010	.0010	1	1132.16	.000
7	4.43	.00	.00		.00	.00	.0350	.0010	.0010	0	.00	.000
6	3.86	.00	.00		.00	.00	.0350	.0010	.0010	0	.00	.000
5	3.28	.00	.00		.00	.00	.0350	.0010	.0010	1	933.89	.000
4	2.64	.00	.00		.00	.00	.0350	.0010	.0010	0	.00	.000
3	2.00	.00	.00		.00	.00	.0350	.0010	.0010	0	.00	.000
2	1.36	.00	.00		.00	.00	.0350	.0010	.0010	1	731.43	.000
1	1.15	.00	.00		.00	.00	.0350	.0010	.0010	0	.00	.000

* *

node	dist.	hashl	hascl	hashv	hascv	drop ai	ai source	sent	sdent	qradd	qradv	snkld	gamsd
23	13.56	90.5571	9.0557	.9056	9.0557	.1000E-09	.0000E+00	.0000E+00	.0000E+00	.0000E+00	.0000E+00	.0000E+00	.0000E+00
22	12.99	90.5571	9.0557	.9056	9.0557	.1000E-09	.0000E+00	.0000E+00	.0000E+00	.0000E+00	.0000E+00	.0000E+00	.0000E+00
21	12.42	90.5571	9.0557	.9056	9.0557	.1000E-09	.0000E+00	.0000E+00	.0000E+00	.0000E+00	.0000E+00	.0000E+00	.0000E+00
20	11.85	90.5571	9.0557	.9056	9.0557	.1000E-09	.0000E+00	.0000E+00	.0000E+00	.0000E+00	.0000E+00	.0000E+00	.0000E+00
19	11.28	90.5571	9.0557	.9056	9.0557	.1000E-09	.0000E+00	.0000E+00	.0000E+00	.0000E+00	.0000E+00	.0000E+00	.0000E+00
18	10.71	90.5571	9.0557	.9056	9.0557	.1000E-09	.0000E+00	.0000E+00	.0000E+00	.0000E+00	.0000E+00	.0000E+00	.0000E+00
17	10.13	90.5571	9.0557	.9056	9.0557	.1000E-09	.0000E+00	.0000E+00	.0000E+00	.0000E+00	.0000E+00	.0000E+00	.0000E+00
16	9.56	90.5571	9.0557	.9056	9.0557	.1000E-09	.0000E+00	.0000E+00	.0000E+00	.0000E+00	.0000E+00	.0000E+00	.0000E+00
15	8.99	90.5571	9.0557	.9056	9.0557	.1000E-09	.0000E+00	.0000E+00	.0000E+00	.0000E+00	.0000E+00	.0000E+00	.0000E+00
14	8.42	90.5571	9.0557	.9056	9.0557	.1000E-09	.0000E+00	.0000E+00	.0000E+00	.0000E+00	.0000E+00	.0000E+00	.0000E+00
13	7.85	90.5571	9.0557	.9056	9.0557	.1000E-09	.0000E+00	.0000E+00	.0000E+00	.0000E+00	.0000E+00	.0000E+00	.0000E+00
12	7.28	90.5571	9.0557	.9056	9.0557	.1000E-09	.0000E+00	.0000E+00	.0000E+00	.0000E+00	.0000E+00	.0000E+00	.0000E+00
11	6.71	90.5571	9.0557	.9056	9.0557	.1000E-09	.0000E+00	.0000E+00	.0000E+00	.0000E+00	.0000E+00	.0000E+00	.0000E+00
10	6.14	90.5571	9.0557	.9056	9.0557	.1000E-09	.0000E+00	.0000E+00	.0000E+00	.0000E+00	.0000E+00	.0000E+00	.0000E+00
9	5.57	90.5571	9.0557	.9056	9.0557	.1000E-09	.0000E+00	.0000E+00	.0000E+00	.0000E+00	.0000E+00	.0000E+00	.0000E+00
8	5.00	90.5571	9.0557	.9056	9.0557	.1000E-09	.0000E+00	.0000E+00	.0000E+00	.0000E+00	.0000E+00	.0000E+00	.0000E+00
7	4.43	90.5571	9.0557	.9056	9.0557	.1000E-09	.0000E+00	.0000E+00	.0000E+00	.0000E+00	.0000E+00	.0000E+00	.0000E+00
6	3.86	90.5571	9.0557	.9056	9.0557	.1000E-09	.0000E+00	.0000E+00	.0000E+00	.0000E+00	.0000E+00	.0000E+00	.0000E+00
5	3.28	102.0585	10.2059	1.0206	10.2059	.1000E-09	.0000E+00	.0000E+00	.0000E+00	.0000E+00	.0000E+00	.0000E+00	.0000E+00
4	2.64	102.0585	10.2059	1.0206	10.2059	.1000E-09	.0000E+00	.0000E+00	.0000E+00	.0000E+00	.0000E+00	.0000E+00	.0000E+00
3	2.00	102.0585	10.2059	1.0206	10.2059	.1000E-09	.0000E+00	.0000E+00	.0000E+00	.0000E+00	.0000E+00	.0000E+00	.0000E+00
2	1.36	33.1822	3.3182	.3318	3.3182	.1000E-09	.0000E+00	.0000E+00	.0000E+00	.0000E+00	.0000E+00	.0000E+00	.0000E+00
1	1.15	33.1822	3.3182	.3318	3.3182	.1000E-09	.0000E+00	.0000E+00	.0000E+00	.0000E+00	.0000E+00	.0000E+00	.0000E+00

0

------------------------------------ gas volumetric analysis ------------------------------------

		hmgas	rmgas	steam	air					diam-ld	diam-sd	flow sd	veloc-sd	gamsd
23	13.56	124.00	.00001	99.990	.010	.000	.000	.000	.000	.0000	.00000	.0000E+00	.00	.0000E+00
22	12.99	124.00	.00001	99.990	.010	.000	.000	.000	.000	.0000	.00000	.0000E+00	.00	.0000E+00
21	12.42	124.00	.00001	99.990	.010	.000	.000	.000	.000	.0000	.00000	.0000E+00	.00	.0000E+00
20	11.85	124.00	.00001	99.990	.010	.000	.000	.000	.000	.0000	.00000	.0000E+00	.00	.0000E+00
19	11.28	124.00	.00001	99.990	.010	.000	.000	.000	.000	.0000	.00000	.0000E+00	.00	.0000E+00
18	10.71	124.00	.00001	99.990	.010	.000	.000	.000	.000	.0000	.00000	.0000E+00	.00	.0000E+00
17	10.13	124.00	.00001	99.990	.010	.000	.000	.000	.000	.0000	.00000	.0000E+00	.00	.0000E+00
16	9.56	124.00	.00001	99.990	.010	.000	.000	.000	.000	.0000	.00000	.0000E+00	.00	.0000E+00
15	8.99	124.00	.00001	99.990	.010	.000	.000	.000	.000	.0000	.00000	.0000E+00	.00	.0000E+00
14	8.42	124.00	.00001	99.990	.010	.000	.000	.000	.000	.0000	.00000	.0000E+00	.00	.0000E+00
13	7.85	124.00	.00001	99.990	.010	.000	.000	.000	.000	.0000	.00000	.0000E+00	.00	.0000E+00
12	7.28	124.00	.00001	99.990	.010	.000	.000	.000	.000	.0000	.00000	.0000E+00	.00	.0000E+00
11	6.71	124.00	.00001	99.990	.010	.000	.000	.000	.000	.0000	.00000	.0000E+00	.00	.0000E+00
10	6.14	124.00	.00001	99.990	.010	.000	.000	.000	.000	.0000	.00000	.0000E+00	.00	.0000E+00
9	5.57	124.00	.00001	99.990	.010	.000	.000	.000	.000	.0000	.00000	.0000E+00	.00	.0000E+00
8	5.00	124.00	.00001	99.990	.010	.000	.000	.000	.000	.0000	.00000	.0000E+00	.00	.0000E+00
7	4.43	124.00	.00001	99.990	.010	.000	.000	.000	.000	.0000	.00000	.0000E+00	.00	.0000E+00
6	3.86	124.00	.00001	99.990	.010	.000	.000	.000	.000	.0000	.00000	.0000E+00	.00	.0000E+00
5	3.28	124.00	.00001	99.990	.010	.000	.000	.000	.000	.0000	.00000	.0000E+00	.00	.0000E+00
4	2.64	124.00	.00001	99.990	.010	.000	.000	.000	.000	.0000	.00000	.0000E+00	.00	.0000E+00
3	2.00	124.00	.00001	99.990	.010	.000	.000	.000	.000	.0000	.00000	.0000E+00	.00	.0000E+00
2	1.36	124.00	.00001	99.990	.010	.000	.000	.000	.000	.0000	.00000	.0000E+00	.00	.0000E+00

1	1.15	124.00	.00001	99.990	.010	.000	.000	.000	.000	.0000	.00000	.0000E+00	.00	.0000E+00

****

0 channel results date 19980803 time 00:00:00 **** Test 31504 Bundle Rod 7x7 ****

****

simulation time = .00000 seconds fluid properties for channel 5

node no.	dist. (ft.)	pressure (psi)	velocity (ft/sec) liquid	vapor	entr.	void fraction liquid	vapor	entr.	flow rate (lbm/s) liquid	vapor	entr.	flow reg.	heat added (btu/s) liquid	vapor	gama (lbm/s)
4	14.56	40.000	.00	.00	.00	.0000	1.0000	.0000	.00000	.00000	.00000	0	.000E+00	.000E+00	.00
3	14.23	40.000	.00	.00	.00	.0000	1.0000	.0000	.00000	.00000	.00000	0	.000E+00	.000E+00	.00
2	13.89	40.001	.00	.00	.00	.0000	1.0000	.0000	.00000	.00000	.00000	0	.000E+00	.000E+00	.00
1	13.56	40.001	.00	.00	.00	.0000	1.0000	.0000	.00000	.00000	.00000	0	.000E+00	.000E+00	.00

node no.	dist. (ft.)	enthalpy (btu/lbm) vapor	hg	vapor-hg	liquid	hf	liq. - hf	mixture	density (lbm/ft3) liquid	vapor	mixture	net entrain
4	14.56	1170.00	1169.77	.23	236.13	236.13	.00	1169.25	58.29915	.09443	.0945	.000
3	14.23	1170.00	1169.77	.23	236.13	236.13	.00	1169.25	58.29915	.09444	.0945	.000
2	13.89	1170.00	1169.77	.23	236.13	236.13	.00	1169.25	58.29915	.09444	.0945	.000
1	13.56	1170.00	1169.77	.23	236.13	236.13	.00	1169.29	58.29915	.09444	.0945	.000

* *

node no.	dist.	mixture flow rate	mixture velocity	relative velocities vap. liq.	vap. entr.	area	vap./liq. interfacial drag	vap./drop interfacial drag	grid type	grid spacers temperature degf	percent quenched
4	14.56	.00	.00	.00	.00	.3489	.0010	.0010	0	.00	.000
3	14.23	.00	.00	.00	.00	.3489	.0010	.0010	0	.00	.000
2	13.89	.00	.00	.00	.00	.3489	.0010	.0010	0	.00	.000
1	13.56	.00	.00	.00	.00	.0501	.0010	.0010	0	.00	.000

* *

node	dist.	hashl	hascl	hashv	hascv	drop ai	ai source	sent	sdent	qradd	qradv	snkld	gamsd
4	14.56	389.0593	38.9059	3.8906	38.9059	.1000E-09	.0000E+00	.0000E+00	.0000E+00	.0000E+00	.0000E+00	.0000E+00	.0000E+00
3	14.23	389.0593	38.9059	3.8906	38.9059	.1000E-09	.0000E+00	.0000E+00	.0000E+00	.0000E+00	.0000E+00	.0000E+00	.0000E+00
2	13.89	389.0593	38.9059	3.8906	38.9059	.1000E-09	.0000E+00	.0000E+00	.0000E+00	.0000E+00	.0000E+00	.0000E+00	.0000E+00
1	13.56	389.0593	38.9059	3.8906	38.9059	.1000E-09	.0000E+00	.0000E+00	.0000E+00	.0000E+00	.0000E+00	.0000E+00	.0000E+00

0 ---------------- gas volumetric analysis --------------------------------

hmgas rmgas steam air diam-ld diam-sd flow-sd veloc-sd gamsd

4	14.56	124.00	.00001	99.990	.010	.000	.000	.000	.000	.0000	.00000	.0000E+00	.00	.0000E+00
3	14.23	124.00	.00001	99.990	.010	.000	.000	.000	.000	.0000	.00000	.0000E+00	.00	.0000E+00
2	13.89	124.00	.00001	99.990	.010	.000	.000	.000	.000	.0000	.00000	.0000E+00	.00	.0000E+00
1	13.56	124.00	.00001	99.990	.010	.000	.000	.000	.000	.0000	.00000	.0000E+00	.00	.0000E+00

1 rod results date 1998 0803 time 00:0 0:00

**** Test 31504 Bundle Rod 7x7 ****

heater rod number 1

surface no. 1 of 1

simulation time = .00 seconds

conducts heat to channels 3 0 0 0 0 0

and azimuthally to surfaces 1 and 1

geometry type = 1

no. of radial nodes = 8

rod node no.		axial location (in.)	fluid temperatures (deg-f) liquid	vapor	surface heat flux (b/h-ft2)	heat transfer mode	heater rod temperatues, (deg f) surface	center	
24		162.72	.0	.0	.0000E+00		502.00	502.00	.0000E+00
23	*	159.29	.0	.0	.0000E+00		502.00	502.00	.0000E+00
22	*	152.44	.0	.0	.0000E+00		658.35	658.35	.0000E+00
21	*	145.59	.0	.0	.0000E+00		860.24	860.24	.0000E+00
20	*	138.74	.0	.0	.0000E+00		1062.12	1062.12	.0000E+00
19	*	131.89	.0	.0	.0000E+00		1264.00	1264.00	.0000E+00
18	*	125.04	.0	.0	.0000E+00		1465.89	1465.89	.0000E+00
17	*	118.19	.0	.0	.0000E+00		1528.70	1528.70	.0000E+00
16	*	111.34	.0	.0	.0000E+00		1462.61	1462.61	.0000E+00
15	*	104.49	.0	.0	.0000E+00		1396.52	1396.52	.0000E+00
14	*	97.64	.0	.0	.0000E+00		1330.43	1330.43	.0000E+00
13	*	90.79	.0	.0	.0000E+00		1264.34	1264.34	.0000E+00
12	*	83.94	.0	.0	.0000E+00		1198.25	1198.25	.0000E+00
11	*	77.09	.0	.0	.0000E+00		1132.16	1132.16	.0000E+00
10	*	70.24	.0	.0	.0000E+00		1066.07	1066.07	.0000E+00
9	*	63.39	.0	.0	.0000E+00		999.98	999.98	.0000E+00
8	*	56.54	.0	.0	.0000E+00		933.89	933.89	.0000E+00
7	*	49.69	.0	.0	.0000E+00		867.80	867.80	.0000E+00
6	*	42.84	.0	.0	.0000E+00		801.71	801.71	.0000E+00
5	*	35.56	.0	.0	.0000E+00		731.43	731.43	.0000E+00
4	*	27.84	.0	.0	.0000E+00		656.94	656.94	.0000E+00
3	*	20.12	.0	.0	.0000E+00		582.46	582.46	.0000E+00
2	*	15.01	.0	.0	.0000E+00		533.11	533.11	.0000E+00
1		13.75	.0	.0	.0000E+00		521.00	521.00	.0000E+00

rod node | axial location | --rod temperatures (deg-f)-- radii in inches

no.		(in.)	.0484	.0931	.1219	.1400	.1582	.1710	.1790	.1870
23	*	159.29	502.0	502.0	502.0	502.0	502.0	502.0	502.0	502.0
22	*	152.44	658.4	658.4	658.4	658.4	658.4	658.4	658.4	658.4
21	*	145.59	860.2	860.2	860.2	860.2	860.2	860.2	860.2	860.2
20	*	138.74	1062.1	1062.1	1062.1	1062.1	1062.1	1062.1	1062.1	1062.1
19	*	131.89	1264.0	1264.0	1264.0	1264.0	1264.0	1264.0	1264.0	1264.0
18	*	125.04	1465.9	1465.9	1465.9	1465.9	1465.9	1465.9	1465.9	1465.9
17	*	118.19	1528.7	1528.7	1528.7	1528.7	1528.7	1528.7	1528.7	1528.7
16	*	111.34	1462.6	1462.6	1462.6	1462.6	1462.6	1462.6	1462.6	1462.6
15	*	104.49	1396.5	1396.5	1396.5	1396.5	1396.5	1396.5	1396.5	1396.5
14	*	97.64	1330.4	1330.4	1330.4	1330.4	1330.4	1330.4	1330.4	1330.4
13	*	90.79	1264.3	1264.3	1264.3	1264.3	1264.3	1264.3	1264.3	1264.3
12	*	83.94	1198.3	1198.3	1198.3	1198.3	1198.3	1198.3	1198.3	1198.3
11	*	77.09	1132.2	1132.2	1132.2	1132.2	1132.2	1132.2	1132.2	1132.2
10	*	70.24	1066.1	1066.1	1066.1	1066.1	1066.1	1066.1	1066.1	1066.1
9	*	63.39	1000.0	1000.0	1000.0	1000.0	1000.0	1000.0	1000.0	1000.0
8	*	56.54	933.9	933.9	933.9	933.9	933.9	933.9	933.9	933.9
7	*	49.69	867.8	867.8	867.8	867.8	867.8	867.8	867.8	867.8
6	*	42.84	801.7	801.7	801.7	801.7	801.7	801.7	801.7	801.7
5	*	35.56	731.4	731.4	731.4	731.4	731.4	731.4	731.4	731.4
4	*	27.84	656.9	656.9	656.9	656.9	656.9	656.9	656.9	656.9
3	*	20.12	582.5	582.5	582.5	582.5	582.5	582.5	582.5	582.5
2	*	15.01	533.1	533.1	533.1	533.1	533.1	533.1	533.1	533.1

****

heater rod number 2
surface no. 1 of 1

simulation time = .00 seconds

conducts heat to channels 4 0 0 0 0 0
and azimuthally to surfaces 1 and 1

geometry type = 1
no. of radial nodes = 8

****

rod node no.		axial location (in.)	fluid temperatures (deg-f) liquid	vapor	surface heat flux (b/h-ft2)	heat transfer mode	heater rod temperatues, (deg-f) surface	center	
24		162.72	.0	.0	.0000E+00		502.00	502.00	.0000E+00
23	*	159.29	.0	.0	.0000E+00		502.00	502.00	.0000E+00
22	*	152.44	.0	.0	.0000E+00		658.35	658.35	.0000E+00
21	*	145.59	.0	.0	.0000E+00		860.24	860.24	.0000E+00
20	*	138.74	.0	.0	.0000E+00		1062.12	1062.12	.0000E+00
19	*	131.89	.0	.0	.0000E+00		1264.00	1264.00	.0000E+00
18	*	125.04	.0	.0	.0000E+00		1465.89	1465.89	.0000E+00
17	*	118.19	.0	.0	.0000E+00		1528.70	1528.70	.0000E+00
16	*	111.34	.0	.0	.0000E+00		1462.61	1462.61	.0000E+00
15	*	104.49	.0	.0	.0000E+00		1396.52	1396.52	.0000E+00

14	*	97.64	.0	.0	.0000E+00	1330.43	1330.43	.0000E+00
13	*	90.79	.0	.0	.0000E+00	1264.34	1264.34	.0000E+00
12	*	83.94	.0	.0	.0000E+00	1198.25	1198.25	.0000E+00
11	*	77.09	.0	.0	.0000E+00	1132.16	1132.16	.0000E+00
10	*	70.24	.0	.0	.0000E+00	1066.07	1066.07	.0000E+00
9	*	63.39	.0	.0	.0000E+00	999.98	999.98	.0000E+00
8	*	56.54	.0	.0	.0000E+00	933.89	933.89	.0000E+00
7	*	49.69	.0	.0	.0000E+00	867.80	867.80	.0000E+00
6	*	42.84	.0	.0	.0000E+00	801.71	801.71	.0000E+00
5	*	35.56	.0	.0	.0000E+00	731.43	731.43	.0000E+00
4	*	27.84	.0	.0	.0000E+00	656.94	656.94	.0000E+00
3	*	20.12	.0	.0	.0000E+00	582.46	582.46	.0000E+00
2	*	15.01	.0	.0	.0000E+00	533.11	533.11	.0000E+00
1		13.75	.0	.0	.0000E+00	521.00	521.00	.0000E+00

rod node no.		axial location (in.)	rod temperatures (deg-f) radii in inches .0484	.0931	.1219	.1400	.1582	.1710	.1790	.1870
23	*	159.29	502.0	502.0	502.0	502.0	502.0	502.0	502.0	502.0
22	*	152.44	658.4	658.4	658.4	658.4	658.4	658.4	658.4	658.4
21	*	145.59	860.2	860.2	860.2	860.2	860.2	860.2	860.2	860.2
20	*	138.74	1062.1	1062.1	1062.1	1062.1	1062.1	1062.1	1062.1	1062.1
19	*	131.89	1264.0	1264.0	1264.0	1264.0	1264.0	1264.0	1264.0	1264.0
18	*	125.04	1465.9	1465.9	1465.9	1465.9	1465.9	1465.9	1465.9	1465.9
17	*	118.19	1528.7	1528.7	1528.7	1528.7	1528.7	1528.7	1528.7	1528.7
16	*	111.34	1462.6	1462.6	1462.6	1462.6	1462.6	1462.6	1462.6	1462.6
15	*	104.49	1396.5	1396.5	1396.5	1396.5	1396.5	1396.5	1396.5	1396.5
14	*	97.64	1330.4	1330.4	1330.4	1330.4	1330.4	1330.4	1330.4	1330.4
13	*	90.79	1264.3	1264.3	1264.3	1264.3	1264.3	1264.3	1264.3	1264.3
12	*	83.94	1198.3	1198.3	1198.3	1198.3	1198.3	1198.3	1198.3	1198.3
11	*	77.09	1132.2	1132.2	1132.2	1132.2	1132.2	1132.2	1132.2	1132.2
10	*	70.24	1066.1	1066.1	1066.1	1066.1	1066.1	1066.1	1066.1	1066.1
9	*	63.39	1000.0	1000.0	1000.0	1000.0	1000.0	1000.0	1000.0	1000.0
8	*	56.54	933.9	933.9	933.9	933.9	933.9	933.9	933.9	933.9
7	*	49.69	867.8	867.8	867.8	867.8	867.8	867.8	867.8	867.8
6	*	42.84	801.7	801.7	801.7	801.7	801.7	801.7	801.7	801.7
5	*	35.56	731.4	731.4	731.4	731.4	731.4	731.4	731.4	731.4
4	*	27.84	656.9	656.9	656.9	656.9	656.9	656.9	656.9	656.9
3	*	20.12	582.5	582.5	582.5	582.5	582.5	582.5	582.5	582.5
2	*	15.01	533.1	533.1	533.1	533.1	533.1	533.1	533.1	533.1

****

cylindrical tube rod no. 3
surface no. 1 of 1

simulation time = .00 seconds

conducts heat to channels 4 0 0 0 0 0
and azimuthally to surfaces 1 and 1

geometry type = 2
no. of radial nodes = 3

****

rod node no.		axial location (in.)	* outside surface heat flux (b/h ft2)	h.t. mode	**** temperatures (deg f) **** wall	vapor	liquid *	* inside surface **** temperatures (deg f) **** liquid	vapor	wall	h.t. mode	heat flux (b/h-ft1) *
24		162.72	.0000E+00		521.00	.00	.00			521.00		.0000E+00
23	*	159.29	.0000E+00		521.00	.00	.00			521.00		.0000E+00
22	*	152.44	.0000E+00		521.00	.00	.00			521.00		.0000E+00
21	*	145.59	.0000E+00		521.00	.00	.00			521.00		.0000E+00
20	*	138.74	.0000E+00		521.00	.00	.00			521.00		.0000E+00
19	*	131.89	.0000E+00		521.00	.00	.00			521.00		.0000E+00
18	*	125.04	.0000E+00		521.00	.00	.00			521.00		.0000E+00
17	*	118.19	.0000E+00		521.00	.00	.00			521.00		.0000E+00
16	*	111.34	.0000E+00		521.00	.00	.00			521.00		.0000E+00
15	*	104.49	.0000E+00		521.00	.00	.00			521.00		.0000E+00
14	*	97.64	.0000E+00		521.00	.00	.00			521.00		.0000E+00
13	*	90.79	.0000E+00		521.00	.00	.00			521.00		.0000E+00
12	*	83.94	.0000E+00		521.00	.00	.00			521.00		.0000E+00
11	*	77.09	.0000E+00		521.00	.00	.00			521.00		.0000E+00
10	*	70.24	.0000E+00		521.00	.00	.00			521.00		.0000E+00
9	*	63.39	.0000E+00		521.00	.00	.00			521.00		.0000E+00
8	*	56.54	.0000E+00		521.00	.00	.00			521.00		.0000E+00
7	*	49.69	.0000E+00		521.00	.00	.00			521.00		.0000E+00
6	*	42.84	.0000E+00		521.00	.00	.00			521.00		.0000E+00
5	*	35.56	.0000E+00		521.00	.00	.00			521.00		.0000E+00
4	*	27.84	.0000E+00		521.00	.00	.00			521.00		.0000E+00
3	*	20.12	.0000E+00		521.00	.00	.00			521.00		.0000E+00
2	*	15.01	.0000E+00		521.00	.00	.00			521.00		.0000E+00
1		13.75	.0000E+00		521.00	.00	.00			521.00		.0000E+00

****

1 heat slab results date 1998 0803 time 00:0 0:00

**** Test 31504 Bundle Rod 7x7 ****

****

heat slab no. 1 (wall)

simulation time = .00 seconds
fluid channel on inside surface = 4
fluid channel on outside surface = 0
geometry type = 3
no. of nodes = 3

****

rod node no.	axial location (in.)	outside surface heat flux (b/h ft2)	h.t. mode	**** temperatures (deg f) **** wall	vapor	liquid	inside surface **** temperatures (deg-f) **** liquid	vapor	wall	h.t. mode	heat flux (b/h-ft1)
23	159.29	.0000E+00		521.00			.00	.00	521.00		.0000E+00
22	152.44	.0000E+00		521.00			.00	.00	521.00		.0000E+00
21	145.59	.0000E+00		521.00			.00	.00	521.00		.0000E+00
20	138.74	.0000E+00		521.00			.00	.00	521.00		.0000E+00
19	131.89	.0000E+00		521.00			.00	.00	521.00		.0000E+00
18	125.04	.0000E+00		521.00			.00	.00	521.00		.0000E+00
17	118.19	.0000E+00		521.00			.00	.00	521.00		.0000E+00
16	111.34	.0000E+00		521.00			.00	.00	521.00		.0000E+00
15	104.49	.0000E+00		521.00			.00	.00	521.00		.0000E+00
14	97.64	.0000E+00		521.00			.00	.00	521.00		.0000E+00
13	90.79	.0000E+00		521.00			.00	.00	521.00		.0000E+00
12	83.94	.0000E+00		521.00			.00	.00	521.00		.0000E+00
11	77.09	.0000E+00		521.00			.00	.00	521.00		.0000E+00
10	70.24	.0000E+00		521.00			.00	.00	521.00		.0000E+00
9	63.39	.0000E+00		521.00			.00	.00	521.00		.0000E+00
8	56.54	.0000E+00		521.00			.00	.00	521.00		.0000E+00
7	49.69	.0000E+00		521.00			.00	.00	521.00		.0000E+00
6	42.84	.0000E+00		521.00			.00	.00	521.00		.0000E+00
5	35.56	.0000E+00		521.00			.00	.00	521.00		.0000E+00
4	27.84	.0000E+00		521.00			.00	.00	521.00		.0000E+00
3	20.12	.0000E+00		521.00			.00	.00	521.00		.0000E+00
2	15.01	.0000E+00		521.00			.00	.00	521.00		.0000E+00

****

1 lateral drift results date 1998 0803 time 00:0 0:00

case 0 **** Test 31504 Bundle Rod 7x7 ****

****

simulation time = .00000 seconds summary for gap 1 connecting channel 3 to channel 4

axial range (in.)	crossflows (lb/sec) liquid	vapor	entrained	velocities liquid	vapor	entrained	pressure diff. pii pjj	void fraction ii	jj	flow area
13.8- 16.3	.00	.00	.00	.00	.00	.00	.000	1.0000	1.0000	.034
16.3 24.0	.00	.00	.00	.00	.00	.00	.000	1.0000	1.0000	.105
24.0- 31.7	.00	.00	.00	.00	.00	.00	.000	1.0000	1.0000	.105
31.7- 39.4	.00	.00	.00	.00	.00	.00	.000	1.0000	1.0000	.105
39.4- 46.3	.00	.00	.00	.00	.00	.00	.000	1.0000	1.0000	.093
46.3- 53.1	.00	.00	.00	.00	.00	.00	.000	1.0000	1.0000	.093
53.1- 60.0	.00	.00	.00	.00	.00	.00	.000	1.0000	1.0000	.093
60.0- 66.8	.00	.00	.00	.00	.00	.00	.000	1.0000	1.0000	.093

66.8 73.7	.00	.00	.00	.00	.00	.00	.000	1.0000	1.0000	.093
73.7- 80.5	.00	.00	.00	.00	.00	.00	.000	1.0000	1.0000	.093
80.5- 87.4	.00	.00	.00	.00	.00	.00	.000	1.0000	1.0000	.093
87.4- 94.2	.00	.00	.00	.00	.00	.00	.000	1.0000	1.0000	.093
94.2 101.1	.00	.00	.00	.00	.00	.00	.000	1.0000	1.0000	.093
101.1-107.9	.00	.00	.00	.00	.00	.00	.000	1.0000	1.0000	.093
107.9-114.8	.00	.00	.00	.00	.00	.00	.000	1.0000	1.0000	.093
114.8 121.6	.00	.00	.00	.00	.00	.00	.000	1.0000	1.0000	.093
121.6 128.5	.00	.00	.00	.00	.00	.00	.000	1.0000	1.0000	.093
128.5-135.3	.00	.00	.00	.00	.00	.00	.000	1.0000	1.0000	.093
135.3-142.2	.00	.00	.00	.00	.00	.00	.000	1.0000	1.0000	.093
142.2-149.0	.00	.00	.00	.00	.00	.00	.000	1.0000	1.0000	.093
149.0 155.9	.00	.00	.00	.00	.00	.00	.000	1.0000	1.0000	.093
155.9 162.7	.00	.00	.00	.00	.00	.00	.000	1.0000	1.0000	.093

1 injection boundary conditions date 1998 0803 time 00:0 0:00

case 0 **** Test 31504 Bundle Rod 7x7 ****

****

simulation time = .00000 seconds

channel no.	node no.	wginjt lbm/sec	wlinjt lbm/sec	hginjt btu/lbm	hlinjt btu/lbm

```
*************************************************************************
*                         new time domain reached                       *
*  minimum    maximum    time       long      short    graphics   dump  *
*   time       time     domain      edit      edit      edit            *
*   step       step      end      interval  interval  interval  interval*
*                                                                       *
* 2.000E 04 1.500E 02 5.000E+02 5.000E+00 8.000E+02 1.000E+00 8.000E+02 *
*************************************************************************
```

time step ratio = 1.000E+00

```
* * * * *  saved graphics data at time     .0000 * * * * * * * * * * * *
* * * * *  saved graphics data at time     .9868 * * * * * * * * * * * *
* * * * *  saved graphics data at time    1.9918 * * * * * * * * * * * *
* * * * *  saved graphics data at time    2.9968 * * * * * * * * * * * *
* * * * *  saved graphics data at time    4.0018 * * * * * * * * * * * *
```

D.3 Sub-Channel Model Input Deck

```
            0
            0            0.0
         .001             5           40
        1     ****** Sub-Channel Model of RBHT 7x7 Bundle ******
    1   1
      40.0    1169.77        0.0     .46667      124.       0.0      .9999
1.0
air             .0001
    2   18
    1.0681.5875  0.0  0.0    1
   23    1   0
    2.13621.175  0.0  0.0    3
   23    1   0   23    2    0   23    3    0
    3.0681.5875  0.0  0.0    2
   23    2   0   23    4    0
    4.13621.175  0.0  0.0    3
   23    3   0   23    5    0   23    7    0
    5.13621.175  0.0  0.0    4
   23    4   0   23    5    0   23    6    0   23    8    0
    6.0681.5875  0.0  0.0    2
   23    6   0   23    9    0
    7.08741.083  0.0  0.0    2
   23    7   0   23   10    0
    8.08741.083  0.0  0.0    3
   23    8   0   23   10    0   23   11    0
    9.08741.083  0.0  0.0    3
   23    9   0   23   11    0   23   12    0
   10.0275.4339  0.0  0.0    1
   23   12   0
   11.4920 1.01  0.0  0.0    1
    3   13   0
   12.6150 1.01  0.0  0.0    2
    3   13   0    3   14    0
   13.50941.775  0.0  0.0    1
    3   14   0
   14.27242.350  0.0  0.0    2
    3   15   3    3   15    4
   15.34052.938  0.0  0.0    5
    3   15   3    3   15    4    3   16    7    3   16    8    3   16    9
   16.28973.683  0.0  0.0    3
    3   16   7    3   16    8    3   16    9
   175.60710.69  0.0.9026    2
    3    0  15    3    0   16
   186.2803.5001.616  0.0    0
    3   16
    1    1      20.1220.496  0.5  0.0    0    0  1.0    1    3
   1.  0.0
    2    2      30.1220.496  0.5  0.0    0    0  1.0    0    4
   1.  0.0
    3    2      40.1220.496  0.5  0.0    0    0  1.0    1    7
   1.  0.0
    4    3      50.1220.496  0.5  0.0    0    0  1.0    2    8
   1.  0.0
    5    4      50.1220.496  0.5  0.0    0    0  1.0    0    6
   1.  0.0
    6    5      60.1220.496  0.5  0.0    0    0  1.0    5    9
   1.  0.0
    7    4      70.122.3915  0.5  0.0    0    0  1.0    3   -1
   1.  0.0
```

```
  8    5     80.122.3915  0.5  0.0    0    0  1.0    4   -1
 1.   0.0
  9    6     90.122.3915  0.5  0.0    0    0  1.0    6   -1
 1.   0.0
 10    7     80.1000.496  0.5  0.5    0    0  1.0    0   11
 1.   0.0
 11    8     90.1000.496  0.5  0.5    0    0  1.0   10   12
 1.   0.0
 12    9    100.100.3915  0.5  0.5    0    0  1.0   11   -1
 1.   0.0
 13   11    120.9920.744  0.0  0.0    0    0  1.0    0   14
 1.   0.0
 14   12    131.4880.496  0.0  0.0    0    0  1.0   13    0
 1.   0.0
 15   14    150.1220.744  0.5  0.0    0    0  1.0    0   16
 2.   0.0
 16   15    160.1220.496  0.5  0.0    0    0  1.0   15    0
 3.   0.0
 18
  1    2    1    2    2    1    2    4    3    3    5    2
  4    5    2    4    6    4    5    4    3    5    8    7
  6    6    4    6    9    8    7   10    5    8   10    5
  8   11    6    9   11    6    9   12    9   10    8    7
 11    9    8   12   12    9
  4    5    1    0
  1    1    2      4.0
 17   14   15   16                  17
  2    3    2     2.875
 14    1    2    3                  17
 15    4    5    6                  17
 16    7    8    9   10             17
  3   10   22     2.51  5
  2      2.51   3     7.72   5      7.72    6      6.85   23      6.85

  1   11                            14
  2   11                            14
  3   11                            14
  4   12                            15
  5   12                            15
  6   12                            15
  7   13                            16
  8   13                            16
  9   13                            16
 10   13                            16
  4    3    2         4.0
 11   18                             1    2    3
 12   18                             4    5    6
 13   18                             7    8    9   10
  5    1    1         4.0
 18   18                            11   12   13
 18
235
  7    8    1    1    1    1    1    0    0    0
1.2    2    1    2    3    4    5    6    7    8    9   10
1.2    5    1    2    3    4    5    6    7    8    9   10
1.2    8    1    2    3    4    5    6    7    8    9   10
1.2   11    1    2    3    4    5    6    7    8    9   10
1.2   14    1    2    3    4    5    6    7    8    9   10
1.2   17    1    2    3    4    5    6    7    8    9   10
1.2   20    1    2    3    4    5    6    7    8    9   10
1.2   23    1    2    3    4    5    6    7    8    9   10
  1    8   10    1       1.4     .2952      1.5     1.984
```

```
    2     5     8    11    14    17    20    23
    1          0.5    1     1     2     1     3     1
    2          1.0    2     2     3     2     4     1     5     1
    3          0.5    3     3     5     2     6     1
    4          1.0    4     2     5     4     7     1     8     1
    5          1.0    5     3     6     2     8     2     9     1
    6          0.5    6     3     9     2    10     1
    7         0.75    7     2     8     4
    8         0.75    8     3     9     4
    9         0.75    9     3    10     2
   10         0.50   10     3
    8    10     4     3     3    10     6    31     1
    1     1     1     2       0.05         1.        1.0         0.     1    0.
    1  .125
    2     1     1     2       0.05         1.        1.0         0.     1    0.
    1   .25     2   .25
    3     1     1     2       0.05         1.        1.0         0.     1    0.
    1  .125     2   .25     3  .125
    4     1     1     2       0.05         1.        1.0         0.     1    0.
    2   .25     4   .25
    5     1     1     2       0.05         1.        1.0         0.     1    0.
    2   .25     3   .25     5   .25     4   .25
    6     1     1     2       0.05         1.        1.0         0.     1    0.
    3  .125     5   .25     6  .125
    7     1     1     2       0.05         1.        1.0         0.     1    0.
    4   .25     7   .25
    8     1     1     2       0.05         1.        1.0         0.     1    0.
    4   .25     5   .25     8   .25     7   .25
    9     1     1     2       0.05         1.        1.0         0.     1    0.
    5   .25     6   .25     9   .25     8   .25
   10     2     0     2       0.05         1.        0.0         0.     1    0.
    6  .125     9   .25    10  .125
    1     3      0.496    0.496        1.0    7                  0.        90.0
    2     3      0.496    0.496        1.0    8                  0.        90.0
    3     3      0.496    0.496        1.0    9                  0.        90.0
    4     3      0.537    0.287        1.0   10                  0.        90.0
    1     9     0     4
    1     2     3     4     5     6     7     8     9
     13.75      822.0    121.75     1600.     157.75      858.0     168.76
858.0
    2     1     0     4
   10
     13.75      372.0    121.75      645.0    157.75      383.0     168.76
383.0
    3     0     4     4
   -1    -2    -3    -4
     13.75      322.0    121.75      482.0    157.75      327.0     168.76
327.0
    1     1    -1    20     0          1.0         1.0         1.0         1.0         1.0
    1     2     4     2     1     2     4     2     1     2     4     2     3     5     9
 7
    3     7     9     5

    2     2    -1    20     0          1.0         1.0         1.0         1.0         1.0
    3     5     9     7     2     1     2     4     3     7     9     5     8    12    18
16
    6    10    13    10

    3     3    -1    20     0          1.0         1.0         1.0         1.0         1.0
    6    10    13    10     5     3     7     9     5     9     7     3    11    14    22
19
   11    19    22    14
```

```
      4     4     2    19     0           1.0          1.0          1.0          1.0          1.0
      8    12    18    16     7     3     5     9     8    16    18    12    17    21    -1
11
     14    22    19

      5     5     2    19     0           1.0          1.0          1.0          1.0          1.0
     11    14    22    19    10     6    10    13    12    18    16     8    20    25    -2
15
     23    26    23

      6     6     3    18     0           1.0          1.0          1.0          1.0          1.0
     15    23    26    23    14    11    19    22    14    22    19    11    24    27    -3
24
     -3    27

      7     7     4    13     0           1.0          1.0          1.0          1.0          1.0
     17    21    -1    16     8    12    18    17    -1    21    20    25    -2

      8     8     4    13     0           1.0          1.0          1.0          1.0          1.0
     20    25    -2    19    11    14    22    21    -1    17    24    27    -3

      9     9     5    12     0           1.0          1.0          1.0          1.0          1.0
     24    27    -3    23    15    23    26    25    -2    20    28    -4

     10    10     6     8     0           1.0          1.0          1.0          1.0          1.0
     28    -4    27    24    -3    27    -3    24

     -1
        .374        .8        .374        .496
     -2
        .374        .8        .100        .496        0.0        0.0        .8
.374

     -3
        .374        .8        .100        .496        0.0        0.0        .8
.374

     -4
        .374        .8        .100        .496        0.0        .248       .8
.374

     -5
        .374        .8        .100        .496        0.0        .248       .8
.374

     -6
        .374        .8        .100        .496        0.0        .248       .8
.374

      9     3
      1 hrod      .374        0.0     4     0
      1     2.0675   0.0     1     3  .045   1.0     3     2.0465   0.0     3     1.0280
0.0
      2 tube      .375        .209    1     0
      3     1  .083   0.0
      3 wall      .496        .250    1     0     0
      3     1  .250
     10     3
      1    12      528.8                              Inco
        212.        .111       9.09      392.        .121       10.04
        572.        .131      10.98      752.        .141       11.93
```

```
     932.        .151     12.88     1112.      .166    13.82
    1292.        .178     14.77     1472.      .191    15.72
    1652.        .204     16.66     1832.      .216    17.61
    2012.        .229     18.56     2192       .241    19.50
  2   14        119.2                            BN
     212.      .16587     67.37      392.    .22015    63.87
     572.      .26264     60.28      752.    .29590    56.74
     932.      .32194     53.19     1112.    .34233    49.65
    1292.      .35829     46.10     1472.    .37078    42.56
    1652.      .38057     39.01     1832.    .38822    35.47
    2012.      .39421     31.92     2192.    .39891    28.37
    2372.      .40259     24.83     2552.    .40546    21.28
  3   10        528.8                           Mon
      70.        .100    10.083      200.      .107    11.333
     400.        .114    13.000      600.      .117    14.833
     800.        .120    16.500     1000.      .125    18.333
    1200.        .132    20.000     1400.      .141    21.833
    1600.        .157    23.500     1800.      .186    25.167
 11    1    25
  1    4
   13.75           .5    121.75       1.5    157.75        .5    157.76
0.0
     0.0           1.      17.5      .921      35.0     .8704      52.5
.8326
     70.         .803      87.5     .7755     105.0     .7512     122.5
.7302
    140.         .714     157.5     .6973     175.0     .6837     192.5
.6710
    220.         .652     255.0     .6332     290.0     .6167     325.0
.6017
    360.         .588     395.0     .5769     430.0     .5656     465.0
.5562
    500.         .547     535.0     .5444     570.0     .5304     605.0
.5243
   1000.         .002
  13    2    0    1    0    0
   3    3
  0.0       0.0  0.1      1.01500.      1.0
  17    1    2    1    0  .0321610   95.3047      40.0
 124.  1.0.9999.0001

  18    4    1    0    0     ,  40. 1169.7685      40.0
 124.  1.0.9999.0001

  14    5    0    0    0    0    0    0
   0
   0

 300    0    0
       .00001        .00110         0.2          1.0    99000.0
          .19          50.0       100.0         50.0          0
       .00001        .00200        50.0          1.0    99000.0
         25.0          50.0       100.0          5.0          0
      -.00001        .00100       300.0          1.0    99000.0
          5.0           5.0       100.0          5.0          0
        -.001
```